THE UNIVERSITY OF ADELAIDE

NUMERICALLY ROBUST LOAD FLOW TECHNIQUES IN POWER SYSTEM PLANNING

by

Alberto J. Sarnari

A thesis submitted for the degree of

Doctor of Philosophy

in

School of Electrical and Electronic Engineering

Faculty of Engineering, Computer and Mathematical Sciences

January 2019

Supervisors:

Dr Rastko Živanović

Dr Said Al-Sarawi

Contents

CONTENTS I
LIST OF FIGURES V
LIST OF TABLES VII
DECLARATION OF AUTHORSHIP VIII
ABSTRACT X
ACKNOWLEDGEMENTS XII
LIST OF PUBLICATIONS XIV
ABBREVIATIONS XV
SYMBOLS XVII
CHAPTER 1: INTRODUCTION 1
1.1. Voltage stability 1
1.2. Contingency evaluation 1
1.3. Preventive versus emergency indicators 2
1.4. Voltage stability analysis 4
1.5. Review of recently proposed load flow methods 5
1.5.1. Robust Padé approximants 6
1.5.2. DFT-Padé 7
1.6. Conclusions 7
CHAPTER 2: LITERATURE REVIEW 10
2.1. Introduction 10
2.2. Plain Newton-Raphson 11

2.2.1. Newton-Raphson equations 12
2.3. Improvements in the Newton-Raphson power flow algorithm 14
2.3.1. Starting point 15
2.3.2. Solutions to ill-conditioned power systems 17
2.3.3. Multiplication parameter 18
2.3.4. Power flow in rectangular coordinate system 20
2.3.5. Dealing with multiple load-flow solutions 21
2.3.6. Low voltage solutions 23
2.3.7. Proximity to voltage stability limit 24
2.3.8. Homotopy methods 28
2.3.9. Continuation power-flow methods 29
2.4. Non-iterative methods 31
2.4.1. The holomorphic load flow method (HELM) 32
2.4.2. Quadratic approximations 34
2.5. Conclusions 35
CHAPTER 3: ROBUST PADÉ APPROXIMATION FOR HELM 37
3.1. Introduction 39
3.2. Bus-voltage representation through Taylor series expansion 40
3.2.1. Bus voltage Taylor series coefficients [86] 41
3.2.2. Padé rational functions 42
3.3. The Rational approximation Algorithm 42
3.3.1. Defect and ill-posed Padé approximation 43
3.3.2. Removal of spurious poles via SVD-based Padé approximation 44
3.4. Simulation study 46
3.5. Conclusions 50

CHAPTER 4: DFT-PADÉ MATHEMATICAL FOUNDATIONS.....52
4.1. Introduction.....54
4.2. Mathematical foundations of the DFT-Padé load-flow method 54
4.2.1. Roots of unity on the unit disk.....55
4.2.2. When the radius of convergence is different from 1.....57
4.2.3. Interpolation by harmonic polynomials 57
4.2.4. How to reconstruct an aperiodic curve: Fourier Series and Transforms 57
4.3. Application to load-flow problem.....59
4.3.1. Nodal equations.....61
4.3.2. Computational process 63
4.3.3. Conclusions.....65
CHAPTER 5: DFT-PADÉ APPLICATION.....67
5.1. Introduction.....69
5.1.1. Application to 14-bus system 69
5.1.2. Two-bus system study.....73
5.1.3. IEEE 30-bus system test case 77
5.2. Improvements over the plain N-R method and comparison with the continuation power flow approach.....79
5.2.1. Application to a 7-bus network 80
5.2.2. Performance comparison 82
5.2.3. Critical bus determination.....85
5.3. Comparison with the holomorphic embedding load-flow method (HELM).....88
5.3.1. IEEE 14-bus system 89
5.3.2. IEEE 118-bus system 90
5.4. Flexible AC transmission system (FACTS) and high voltage direct current transmission (HVDC) 91

5.5. Conclusions 95

CHAPTER 6: CONCLUSION AND FUTURE WORK 98

BIBLIOGRAPHY 102

List of Figures

Figure 1-1: Pre- and post-contingency P-V curves. 3

Figure 1-2. Active power vs. absolute voltage curves for different power factors..... 5

Figure 1-3 Thesis structure..... 9

Figure 2-1. Seven-bus system: Newton-Raphson vs HELM. 33

Figure 2-2. Bus 3 voltage stability limit, N-R vs HELM comparison.....33

Figure 4-1: P-V curve for load bus at constant power factor 59

Figure 5-1. Circle of complex active power values.....70

Figure 5-2. Voltage complex absolute values. 70

Figure 5-3. Fourier series coefficients. 71

Figure 5-4. Taylor series coefficients.....71

Figure 5-5. Estimation of series' convergence radius.....72

Figure 5-6. Padé and Taylor approximations to branch solutions. 72

Figure 5-7. Singularities of the Padé rational function. 73

Figure 5-8. Two bus system: load base-line values in MW and Mvar.....74

Figure 5-9. Two-bus branch solutions. 75

Figure 5-10. Zeros and poles of the Padé rational function (3.9).....75

Figure 5-11. Bus No. 30 comparison of three methods. 78

Figure 5-12. 7-bus network. 81

Figure 5-13. 7-Bus network – |V3| vs P6. 82

Figure 5-14. Radius of Convergence. 87

Figure 5-15. Poles and zeros of the Padé rational function. 88

Figure 5-16. Bus 14: HELM and DFT-Padé methods, HV branch comparison.....89

Figure 5-17. Bus 118: HELM and DFT-Padé methods HV branch comparison.....91

List of Tables

Table 3-1: Poles and zeros of Padé approximant. 49

Table 5-1. Rational function singularities. 73

Table 5-2. Comparison of Voltage Stability Limits. 74

Table 5-3. Voltage stability limits via HELM and DFT-Padé methods. 76

Table 5-4. Bus No. 3 characteristic parameters, DFT-Padé method. 80

Table 5-5. MATPOWER continuation power flow parameters and values 81

Table 5-6. Continuation Power Flow time performance parameters 83

Table 5-7. Time performance comparison: D-P, N-R and CPF. 83

Table 5-8. Time performances using systems contingencies. 85

.Table 5-9. 14-bus network - PQ buses ordered by criticality.....87

Table 5-10. 30-bus network - PQ buses ordered by criticality.....87

Table 5-11. Weakest buses in14-bus system. 87

Table 5-12. Weakest buses in 30-bus system. 87

Table 5-13. Bus 14: HELM and DFT-Padé voltage stability limits comparison. 89

Table 5-14. Bus 118: HELM and DFT-Padé voltage stability limits comparison. 90

Declaration of Authorship

I certify that this work contains no material that has been accepted for the award of any other degree or diploma in my name, in any university or other tertiary institution and, to the best of my knowledge and belief, contains no material previously published written by another person, except where due reference has been made in the text. In addition

I certify that no part of this work will, in the future, be used in a submission in my name, for any other degree or diploma in any university or other tertiary institution without the prior approval of the University of Adelaide and where applicable, any partner institution responsible for the joint-award of this degree.

I give permission for the digital version of my thesis to be made available on the web via the University's digital research repository, the Library catalogue, the Australasian Digital Thesis Program (ADTP) and through web search engines, unless permission has been granted by the University to restrict access for a period of time.

I acknowledge the support I have received for my research through the provision of an Australian Government Research Training Program Scholarship.

_____ _____ 21/01/2019

Signature Date

Abstract

Since deregulation of the electric power industry, investment in the sector has not kept up with demand. State grids were interconnected to form vast power networks, which increased the overall system's complexity. Conventional generation sources have, in some cases, closed under financial stress caused by the growing penetration of renewable sources and unfavourable government measures. The power system must adapt to a more demanding environment to that for which it was conceived. This thesis investigates the robustness of planning and simulation study tools for the determination of bus-voltages and voltage stability limits. It also provides an approach to obtain greater certainty in the determination of voltages where conventional methods fail to be deterministic.

Two complementary methods for determining the collapse voltage are developed in this thesis. The first method applies Robust Padé approximations to the holomorphic embedding load flow method; while the second method uses the Newton-Raphson numerical calculation method to obtain both high and low voltage solution branches, and voltage stability limits of power system load buses. The proposed methods have been implemented using MATLAB and been demonstrated through a number of IEEE power system test cases.

The robust Padé approximation algorithm improves the reliability of solutions of load flow problems when bus-voltages are presented in Taylor series form by converting the series into optimised rational functions. Differences between the classic Padé approximation algorithm and the new robust version, which is based on singular value decomposition (SVD), are described. The new robust approximation method can determine an optimal rational function approximation using the coefficients of a Taylor series expansion. Consequently, the voltage collapse points, as well as the steady-state voltage stability margin, can be calculated with high reliability. Voltage collapse points (i.e. branching points) are identified by using the locations of poles/zeros of a rational function approximation. Numerical examples are devised to illustrate potential use of the proposed method in practical applications.

Use of the Newton-Raphson method, combined with the discrete Fourier transform and robust Padé approximation, enables the calculation of the voltage stability limits and both the high and low voltage solution branches for the load buses of a power system. This can work to a great advantage of existing N-R based software users, as problems of initial guess, multiple solutions and Jacobian matrix conditioning when operating close to the voltage collapse point are avoided. The findings are assessed by comparisons with conventional Newton-Raphson, the holomorphic embedding load flow method, and continuation power flow method.

This thesis contains a combination of conventional and publication formats, where some introductory materials are included to ensure that the thesis delivers a consistent narrative. For this reason, the first two chapters provide the required background information, research gap identification and contributions, whilst other chapters are written to provide more detailed work that has not yet been published or to summarise the research outcomes and future research directions. Furthermore, publications are listed in their publication formats, complete with statements of the authors' contributions.

Acknowledgements

My most sincere gratitude goes to Dr Rastko Živanović for conveying his power system vision, allowing me to tackle this investigation with confidence and enthusiasm. His depth of knowledge and understanding of key issues were the foundation of my growth in the research field. For this, I consider myself very fortunate.

To the same extent, I feel grateful to Dr Said Al-Sarawi, who was supportive and provided continuous guidance in the most diverse of topics related to the candidature, reviewing draft papers and thoroughly commenting on them is just one of his many skills. Diligent, determined and focused, he taught me critical skills so that I could research with both passion and a positive attitude.

My gratitude goes to the University of Adelaide for the postgraduate research scholarship that allowed me to tackle this long-term endeavour and learn the researcher's skills that otherwise would have been unattainable.

My appreciation goes to Dr Melissa Tacy for allowing me to attend Pure Math: Complex Analysis III classes and tutorials and Dr Javen Qinfeng Shi for the Scientific Computing classes and tutorials.

I am also very thankful to Qirui Li from Arizona State University who patiently provided the information about non-iterative methodology that I used to assess my results.

My appreciation goes to Dr Wen Soon, Head of the School of Electrical and Electronic Engineering and Dr Withawat Withayachumnankul, Postgraduate Coordinator, for their support and guidance.

I appreciate David Vowels' comments and discussion of my journal paper.

Many thanks to Alison-Jane Hunter for her editing services.

I am appreciative of the CaRST group and Director for their comprehensive courses that help shape the researcher's outlook and formation.

To my family, my wife Flora who is an unconditional supporter and friend: THANK YOU. Also, my gratitude goes to my children for their interest and encouragement.

Lastly, but not least, to my life-long friends from Firmat'71, my deepest appreciation for their affection and companionship, and, why not, my daily laughs. It also goes to my colleague P. Baridón for the book in reference [1].

I offer my gratitude also for the memory of my parents, Tito and Amelia, and for their unfailing, unconditional love, which has shaped my character.

List of Publications

Journal article

A. J. Sarnari and R. Živanović, and Said Al-Sarawi, “Augmenting Load Flow Software for Reliable Steady-State Voltage Stability Studies", *International Journal of Electrical Power & Energy Systems,* for printing.

Conference articles

A. J. Sarnari and R. Živanović, "Robust Padé approximation for the holomorphic embedding load flow," in *2016 Australasian Universities Power Engineering Conference (AUPEC)*, 2016.

A. J. Sarnari and R. Živanović, "Reliable steady state voltage stability limit estimation using Newton-Raphson-based method," in *2017 Australasian Universities Power Engineering Conference (AUPEC)*, 2017.

Abbreviations

Acronym	Description
CPF	Continuation power flow.
CPFLOW	Load-flow software based in the continuation power flow method
DFT	Discrete Fourier transform
DFT-Padé or D-P	Load-flow method based on Discrete Fourier Transform and Padé approximants to obtain both, load bus P-V curve and VSL
FFT	Fast Fourier transform as used to obtain power series coefficients
HV	High voltage: pertaining to absolute voltage values on the top branch of the P-V curve
HELM	Holomorphic embedding load flow method
HEE	Holomorphic error embedding
IEEE	Institution of Electrical and Electronic Engineers
LV	Low voltage: pertaining to absolute voltage values on the bottom branch of the P-V curve
MLP	Maximum loading point
MSHEM	Multi-stage holomorphic embedding
N-R	Newton-Raphson
ODE	Ordinary differential equation
OM	Optimal multiplier
PV	Generator bus
P-V	Curve of active power versus voltage absolute value for a Load bus
RPA	Robust Padé approximations

SNBP	Saddle-node bifurcation point (or voltage stability limit)
SQE	Scalar quadratic equation
SRM	Simple robust method
SSR	Sum of the square residuals
SVD	Singular value decomposition
V-Q	Curve of bus absolute voltage versus reactive power
VAF	Volt-Ampere function
VSL	Voltage stability limit

Symbols

Symbol	Description
Chapter 2	
$\boldsymbol{y}$	Vector of scheduled active and reactive power
$\boldsymbol{f}(\boldsymbol{x})$	Vector of calculated power
$\boldsymbol{x}$	Vector of state variables: bus voltage angle δ, and bus voltage absolute value V
N	Number of nodes or buses in the power system
$\|V_i\|$	Absolute voltage value for bus i
δ_i	Voltage angle for bus i
Y_{ik}	admittance of the transmission line between buses i and k absolute value
θ_{ik}	Admittance angle of the transmission line between buses i and k
$P_i(x)$	Bus i calculated active power
$Q_i(x)$	Bus i calculated reactive power
$\boldsymbol{F}(\boldsymbol{x}^{(j)})$	Vector of power residuals for iteration j
$\boldsymbol{J}^{(j)}$	Jacobian matrix at iteration j
N	Number of nodes in the network
$\|\boldsymbol{J}\|$	Norm of the Jacobian matrix in the Euclidean sense of length
K	Size of the condition number of the Jacobian matrix
$\|\sigma_{max}\|$	Maximum eigenvalue of the Jacobian matrix
$\|\sigma_{min}\|$	Minimum eigenvalue of the Jacobian matrix
$\eta^{(j)}$	Multiplication parameter at iteration j
$\left\|\boldsymbol{F}(\boldsymbol{x}^{(j)})\right\|$	m-norm of the vector of residuals at iteration j

$\left\|\sum_{h,l} \frac{\partial^2 F(x^{(j)})}{\partial x_h \, \partial x_l} \Delta x_h \, \Delta x_l\right\|$	is the m-norm of the second derivative of the vector of residuals multiplied by the vectors of corrections twice at iteration j
$F_C^{(j)}$	Cost function, function to be minimised (at iteration j)
$\mu^{(j)}$	Optimal multiplier
V_i	Voltage phasor at bus i
I_i	Current injected at bus i
z_{i0}	Impedance between buses i and 0 (reference)
t	Homotopy parameter
$\boldsymbol{Y_{s0}}$	Vector of base generation and loads
$\boldsymbol{Y_D}$	Vector of generation and loads' direction of change
$\boldsymbol{Y_s(t)}$	Vector of resulting loads and generation
Δt_j	Step change in the homotopy parameter
$\boldsymbol{g(x)}$	Vector of initial power residuals function - CPF
$\boldsymbol{P^{inj}}$	Vector of injected active power - CPF
$\boldsymbol{Q^{inj}}$	Vector of injected reactive power - CPF
$\boldsymbol{P_{target}^{imj}}$	Vector of target injected active power - CPF
$\boldsymbol{Q_{target}^{inj}}$	Vector of target injected reactive power - CPF
λ	Continuation parameter

Chapter 3

z	Complex parameter or variable
$V_k(z)$	Voltage at bus k expressed in Taylor series expansion.
Y_{ik}	Admittance of transmission line between buses i and k
S_i^*	Bus i apparent power conjugate
N	Set of network buses in the power system

r	Reference bus / Slack bus
$\mathrm{c}_{\mathrm{s}}^{[\mathrm{k}]}$	Taylor series coefficient of order s for bus k
$d_s^{*[i]}$	Taylor series coefficient conjugate for bus i of order s
$a_0 \dots a_m$	Numerator polynomial coefficients order zero to order m
$\boldsymbol{a}$	Vector of numerator polynomial coefficients
$b_0 \dots b_n$	Denominator polynomial coefficients order zero to order n
$\boldsymbol{b}$	Vector of denominator polynomial coefficients
$O(z^{m+n+1})$	Truncation error for rational function of degrees m, n
$f(z)$	Meromorphic function in the complex domain
$r_{m,n}$	Set of rational functions of degrees m, n
$p(z)$	Rational function numerator polynomial
$q(z)$	Rational function denominator polynomial
δ	Defect of the Padé rational function.
μ	Best possible order of numerator polynomial.
ν	Best possible order of denominator polynomial.
$\|c\|$	2-norm of vector of coefficients $\boldsymbol{c}$
tol	Specified tolerance (problem dependent)

Chapter 4

$f(z)$	Analytic or meromorphic function interpolated in the roots of unities $\{z_k\}$ in the disk D_R
D_R	Open disk of radius $R > 1$, domain where f is analytic
R	Radius of the domain D_R
$p(z)$	Unique polynomial interpolant of function $f(z)$ in the complex domain
k	Coefficient order of variable order
c_k	Power series coefficient of order k

z^k	Power series complex variable of order k
n	Number of roots of unity where f is sampled
$\{z_k\}$	Set of interpolating points at the roots of unity
S	Unit disk where the Cauchy integral applies
j	Imaginary unit
ζ	Integration variable of the Cauchy integral
D_ρ	Disk where $f(z)$ is analysed
ρ	Radius $\rho < R$
$O(\rho^{-k})$	Size of the bounded approximation error
f_k	Value of function $f(z)$ when applied to point z_k
c_i^n	Taylor coefficient of order (degree) i calculated for n roots of unity using Trapezoidal rule
i	$i = 1, 2, \ldots$
τ	Scalation factor for values of $\|z\| > 1$
$f(t)$	Periodic function of period T defined in the real domain, where t can be thought of as time.
T	Period of $f(t)$
$e^{j2\pi kt/T}$	Exponential function of order (period multiple) k and fundamental frequency $1/T$
$\hat{f}(k)$	Alternative notation for Fourier or harmonic coefficient c_k
$\hat{f}(s)$	Fourier transform in the frequency domain s
$\boldsymbol{F}[m]$	Value of the discrete Fourier transform (DFT) for point m in vector $\boldsymbol{F}$.
$\|V(P)\|$	Absolute value of the voltage function at active power P
h_k	Coefficient of Taylor series of order k
P	Variable representing active power values
P_c	Base-line active power centre of the series

r	Estimated radius of convergence of the power series
θ	Angle between sampling points in the complex domain circle of radius r
N	Number of sample points
l	Specific sample point, $l = 0, \ldots, N-1$
$\overline{\lvert V(\theta_l)\rvert}$	Complex bus voltage modulus at the point θ_l
δ	Bus voltage angle
$\boldsymbol{Vr}$	Vector of bus voltage active components
$\boldsymbol{Vi}$	Vector of bus voltage reactive components
$\boldsymbol{rY}$	Matrix of bus admittances
$\boldsymbol{iY}$	Matrix of bus susceptances
$\bar{\boldsymbol{I}}_{\boldsymbol{C}}$	Vector of bus injected currents based on complex voltage magnitude
$\bar{\boldsymbol{I}}_{\boldsymbol{Cr}}, \bar{\boldsymbol{I}}_{\boldsymbol{Ci}}$	Vector of active and reactive components of $\bar{I}_C$ respectiely
$\boldsymbol{S_c}, \boldsymbol{P_c}, \boldsymbol{Q_c}$	Vectors of bus apparent, active and reactive powers
$\boldsymbol{S^{sch}}$	Vector of scheduled apparent power

Chapter 1: Introduction

The criticality of power system operation has been brought to the fore by the many incidents happening in the industry over many decades, and it is now even more critical as dependency on electricity is ever increasing. Taking society back to pre-electricity times would be unthinkable. Tools have been developed to assess the health of the grid at any given time. In this chapter, an overview of some of the most commonly used health checking mechanisms and grid state evaluation are presented. The heavy dependence on any method used will make any shortcomings all the more apparent, i.e., the underpinning mathematical models are exposed to the full scope of the variables' domain. What follows is an overview of such dependency, which will be even more evident through the literature review in Chapter 2.

1.1. Voltage stability

The electric power industry world-wide has become increasingly concerned with voltage instability and collapse [2]. This concern is based on several recent incidents. Static analysis can be used effectively to determine security margins and identify network limitations. To deal with voltage stability related problems effectively, industry needs analytical tools, planning, operating guidelines and protection schemes [3].

Among the lines of defence against voltage collapse, the real time assessment of voltage security in control centres is an important aspect, alongside complementary automatic protection devices. The traditional approach has been the establishment of off-line secure operating limits, to be monitored by on-line operators.

1.2. Contingency evaluation

The purpose of contingency evaluation is to assess the system robustness at a given operating point with respect to credible contingencies and design normal countermeasures, including secondary voltage control and reactive power compensation.

The contingency evaluation can be classified into static and time simulation methods [4]. Static methods are usually based on load flow equations. Time simulation methods offer some advantages, including higher accuracy. However, its disadvantages are the large number of parameters and models needed. Some parameters may not be accurate, and also large computation resources are required. Time simulation methods are based on differential equations describing both transient and long-term dynamics.

1.3. Preventive versus emergency indicators

Preventive voltage stability indicators aim to assert the robustness of the system under normal operating conditions. Emergency indicators warn the operator after serious disturbances that the system may become unstable or that an insufficient security margin remains [4]. The concept of an emergency state before collapse is closely related to long-term voltage instability, where the system degradation takes some time to develop, e.g. a few minutes. Nothing similar would exist for transient angle and transient voltage instability, which are faster than they can be perceived by standard control centre measurements. Two different approaches are envisaged to devise emergency indicators. The first one consists of building these indicators off-line. The second one takes advantage of the time available during long-term instability. Some of the indicators in use are [4]:

- System topology, especially the status of important transmission lines, and sources of reactive and real power,
- Indicators that dynamic sources of reactive power have reached their limits or are near to their limits of capacity, and
- Heavy loading or overloading of transmission or generation.

These indicators are often combined to predict voltage collapse conditions and require reliable, fast communication to bring information from different parts of the power network. However, emergency voltage indicators have received comparatively less attention.

Sometimes, the power grid is under serious strain due to a diverse number of factors such as insufficient generation before contingencies, increased peak demand, renewables penetration, etc. [5-7]. Multiple solutions are devised to overcome such

adversities [8-10]. Also, if a system's conditions are close to critical loading, numerical problems may be encountered during conventional load flow calculations using the Newton-Raphson method [3], so new approaches to tackle the power flow problem with more reliable tools [11-13] are needed. Power system analysts are still searching for the ideal index. Circumstances vary widely from utility to utility, both in electrical characteristics and in affordable means [14]. Loss of equilibrium is the basic instability mechanism most observed for voltage collapses in the time frame of a few minutes. This kind of dynamics can be analysed with static indices [14]. This gives space to the load-flow software that needs to solve the Jacobian matrix many times to obtain a full picture of the network state. However, dynamic phenomena like oscillatory instability require a different approach. An outstanding aspect of the test results, encompassing these static indices, is the relevance of contingencies, i.e. a single outage is comparable to a 10% load increase, or more, confirming the fact that a clear majority of voltage collapses have been triggered by contingencies, as per Figure 1-1.

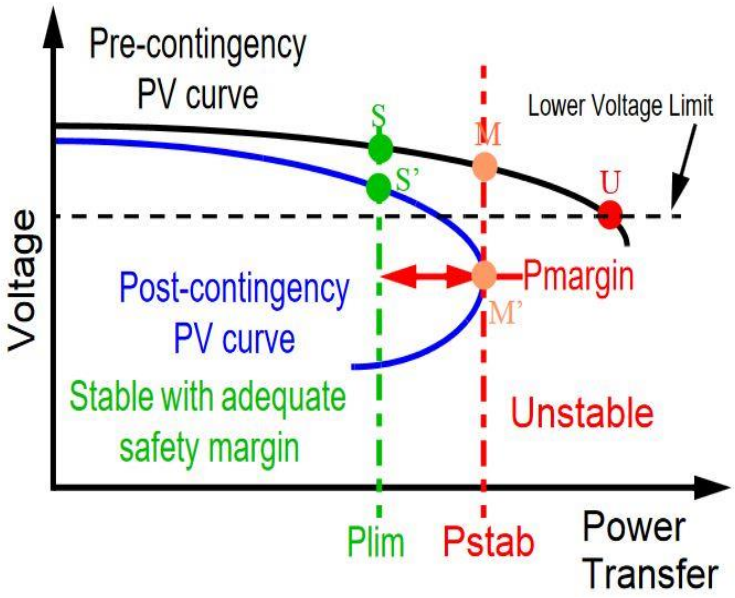

Figure 1-1: Pre- and post-contingency P-V curves.
Operating point "U" is unstable and leads to voltage collapse. Point "M" is marginally stable. Operating point "S" is stable even after the contingency [15].

The two curves represent the bus P-V characteristic pre-contingency (black) and post-contingency (blue), such as the loss of a transmission line. If the bus voltage is close to the lower standard limit (operating point U), then the bus will suffer voltage collapse, i.e.,

voltage will be zero or an inadmissible low value. The marginally stable situation arises when operating point M becomes M' after the contingency (or its vicinity), which corresponds to a load designated as Pstab. On the other hand, if the active load Plim is such that it corresponds to an operating point S, the bus will ride over the contingency whilst remaining at an acceptable voltage level. This operating point is then within an adequate safety margin.

As the risk of voltage collapse increases, the system becomes increasingly stressed. A satisfactory voltage stable state can be characterized as having a minimum post contingency security margin and having the ability to retain that margin to a foreseeable peak load. In terms of the indices, this means that the post contingency threshold should not be crossed [14]. The post contingency index value can be determined by extensive off-line simulation and prevent the system from undergoing voltage collapse if a second contingency occurs. This approach can give warnings hours in advance and allows operators to take either preventive or remedial action [14].

1.4. Voltage stability analysis

The two methods that are widely used for network stability analysis are the $P-V$ and $V-Q$ curves. These curves determine the steady-state stability limits [16]. $P-V$ curves are also useful for conceptual analysis and studies of radial systems. The method can be used for large networks where P is the total load in the area and V is the voltage at a representative bus [16].

The power consumed by loads varies with the voltage and frequency. For a specified load demand, the equation defining P will form a curve on the $P-V$ space and will intercept the $V(P,Q)$ curve at one or more points. These points are possible operating points for a given demand. When the demand changes, the intersection points move on the surface forming the network $P-V$ characteristic [17]. Figure 1-2 shows a P-V curve for varying power factors [18] without operating points.

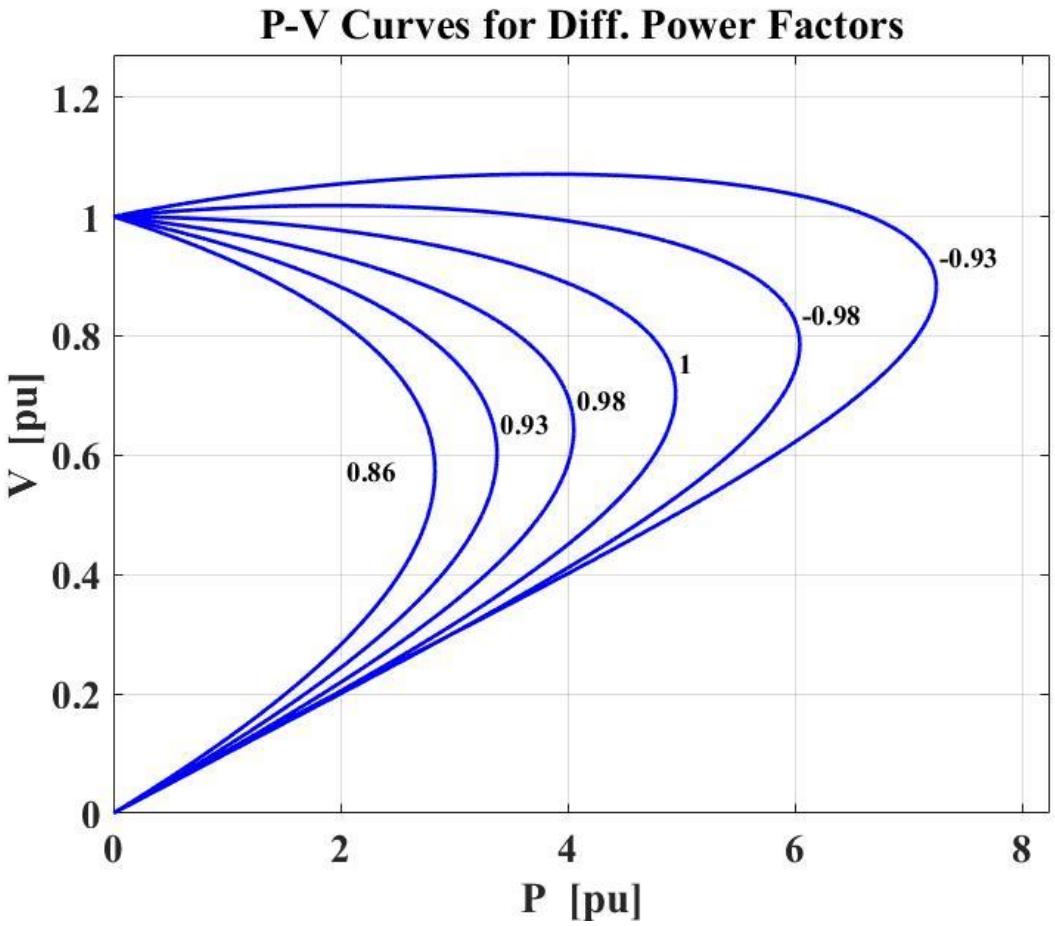

Figure 1-2. Active power vs. absolute voltage curves for different power factors.

A typical modern power system is a high-order multivariable process whose dynamic response is influenced by a wide array of devices with different characteristics and response rates. Voltage stability refers to the ability of a power system to maintain steady voltages at all buses in the system after being subjected to a disturbance from a given initial operating condition. Voltage collapse is the process by which the sequence of events accompanying voltage instability leads to a blackout or abnormally low voltages in a significant part of the power system.

1.5. Review of recently proposed load flow methods

The Load Flow methods based on the analytic continuation principle and rational function approximations have reached a great degree of accuracy in determining load flow states [11]. This is also true for the points near voltage collapse, which are the most difficult to compute as they lie at the nose of the active power - voltage curve (i.e. PV-

curve) where the system of equations to solve become ill-conditioned. These methods use a bus-voltage representation based on a Taylor series expansion in the complex domain. To ensure the accuracy of the calculated voltage at points close to voltage collapse, the Taylor series is converted into a rational function to extend the radius of convergence of the series. These rational functions are the Padé approximants. They can reconstruct a complete solution branch using approximation at a single point [11, 12].

The Holomorphic Embedding Load Flow method (HELM) has overcome problems that exist in traditional load flow methods [11-13] . Iterative methods like Newton-Raphson (N-R) and all its variations [11, 12], as used in the power industry today, can have limitations for the study of steady-state voltage stability, as described in [19], Section II of [11] and Section IV of [12]. Changes in current practices, including new software suites, are unlikely, as HELM has not been in the public domain for long. Its serious use may be limited and may involve a relatively large outlay of capital to fully deploy and replace existing iterative-based tools.

1.5.1. Robust Padé approximants

The aim of this thesis is to improve HELM and present a tool that can produce the same results, working within the Newton-Raphson (N-R) environment. Details about N-R can be found in text books like [20, 21]. This novel algorithm uses the discrete Fourier transform and Padé rational function, or DFT-Padé (D-P). The direct methods of calculating Padé approximants by using coefficients of a Taylor series may not be the most computationally efficient [22], therefore in this thesis a novel method based on the Singular Value Decomposition (SVD) is explored. The new method is able to find a robust and optimal rational function fit. It should be noted that classic direct methods of constructing the Padé approximants could have some problems from a practical implementation point of view. For example, degeneracies of the approximation may occur in which the numerator and denominator have less than the allowed degree. This leads to several entries in the Padé table being identical, some of them matching the Taylor series of the function being approximated to less than the expected order [23]. In this thesis, the application of the SVD-based Padé approximation technique, and a corresponding numerical algorithm, are

proposed. Robust Padé approximants go a long way towards eliminating the problems associated with the classic Padé approximant constructor.

1.5.2. DFT-Padé

In this thesis, an alternative method based on the use of existing N-R software and the application of the Discrete Fourier Transform is proposed to find the loading range of each load bus in the system and their voltage stability limit. As will be shown below, minor modifications to the Jacobian matrix may be needed to satisfy the mathematical requirements of the method. This approach will give power system planners, using Newton-Raphson, the same advantages as non-iterative load flow methods possess.

As in the holomorphic embedding method, the bus-voltage representation is done through a truncated Taylor series, whose coefficients are found by the application of the discrete Fourier transform to the complex absolute voltage values extracted from the Newton-Raphson method. Robust Padé approximations are then used to extend the radius of convergence of the resulting Taylor series (polynomial). The rational function thus found has two inherent properties, i.e., a) it extrapolates the voltage solution branch, and b) it approximates the voltage stability limits through the intersection of the high voltage (HV) and low voltage (LV) branches of the $P-V$ curves, or through its inner singularities.

1.6. Conclusions

From the above discussion, it can be seen that the load flow method plays a key role in the planning and operation of the power grid, and that new methods have emerged to overcome the reliability issues of conventional methods.

A review of improvements to the conventional load flow based on the Newton-Raphson algorithm (N-R) across the last decades are presented in the literature review in Chapter 2. In that chapter, it is shown that the method's shortcomings have been identified in many papers and proposed solutions have been provided by their authors. It should be noted that only selected articles focused around the typical issues have been chosen and presented.

An examination of robust load flow techniques, which lie at the core of this thesis, are explained in the remaining chapters.

Chapter 3, “Robust Padé Approximations for HELM”, provides a brief description of HELM and its improvement via RPA. This enhancement is based on the exact determination of numerator’s and denominator’s degree for the univocal resolution of the rational function that will represent the bus-voltages. This chapter is the conference article by A. J. Sarnari and R. Živanović, "Robust Padé approximation for the holomorphic embedding load flow," given at the 2016 Australasian Universities Power Engineering Conference (AUPEC), 2016, pp. 1-6.

Chapter 4, “DFT-Padé mathematical foundations”, sets the basis of the D-P method. Its salient components are examined, and the combined numerical accuracy of the algorithm is demonstrated:

- Bus-voltages are sampled using the values of active power represented in the unit circle of the complex domain applying the N-R algorithm. This is a mathematical artifice that is required by the tools used to find the voltage representation through power series coefficients.
- Trigonometric polynomials are obtained to form the bus voltage truncated power series using discrete Fourier transform (DFT).
- The trapezoidal rule is the approach taken to solve the Fourier integrals.
- The numerical adequacy of the trapezoidal rule is justified for its geometric convergence properties.

The method implementation has been presented in the conference article by A. J. Sarnari and R. Živanović, "Reliable steady state voltage stability limit estimation using Newton-Raphson-based method," in *2017 Australasian Universities Power Engineering Conference (AUPEC)*, 2017, pp. 1-6.

Chapter 5, “DFT-Padé applications” shows the applicability of the DFT-Padé method for different power systems and the analysis and use of its key parameters (power series radius of convergence and tolerance for the determination of the power series coefficients). Comparison with plain N-R, HELM and continuation power flow are presented, as well as time performance, weak bus determination and applicability to

networks with FACTS and HVDC. The main part of this chapter belongs to the submitted journal article by A. J. Sarnari, R. Živanović, and Said Al-Sarawi, "Augmenting Load Flow Software for Reliable Steady-State Voltage Stability Studies", *International Journal of Electrical Power & Energy Systems,* submitted 09/07/ 2018.

Chapter 6, "Conclusions and future work" presents reflections on every chapter and a summary conclusion of the benefits of using the Padé-DFT method, including the fact that N-R users can take advantage of the same results as the non-iterative HELM method provides. Additional research work for future improvement to the presented DFT-Padé method is also described. The structure of the thesis is summarised in Figure 1-3.

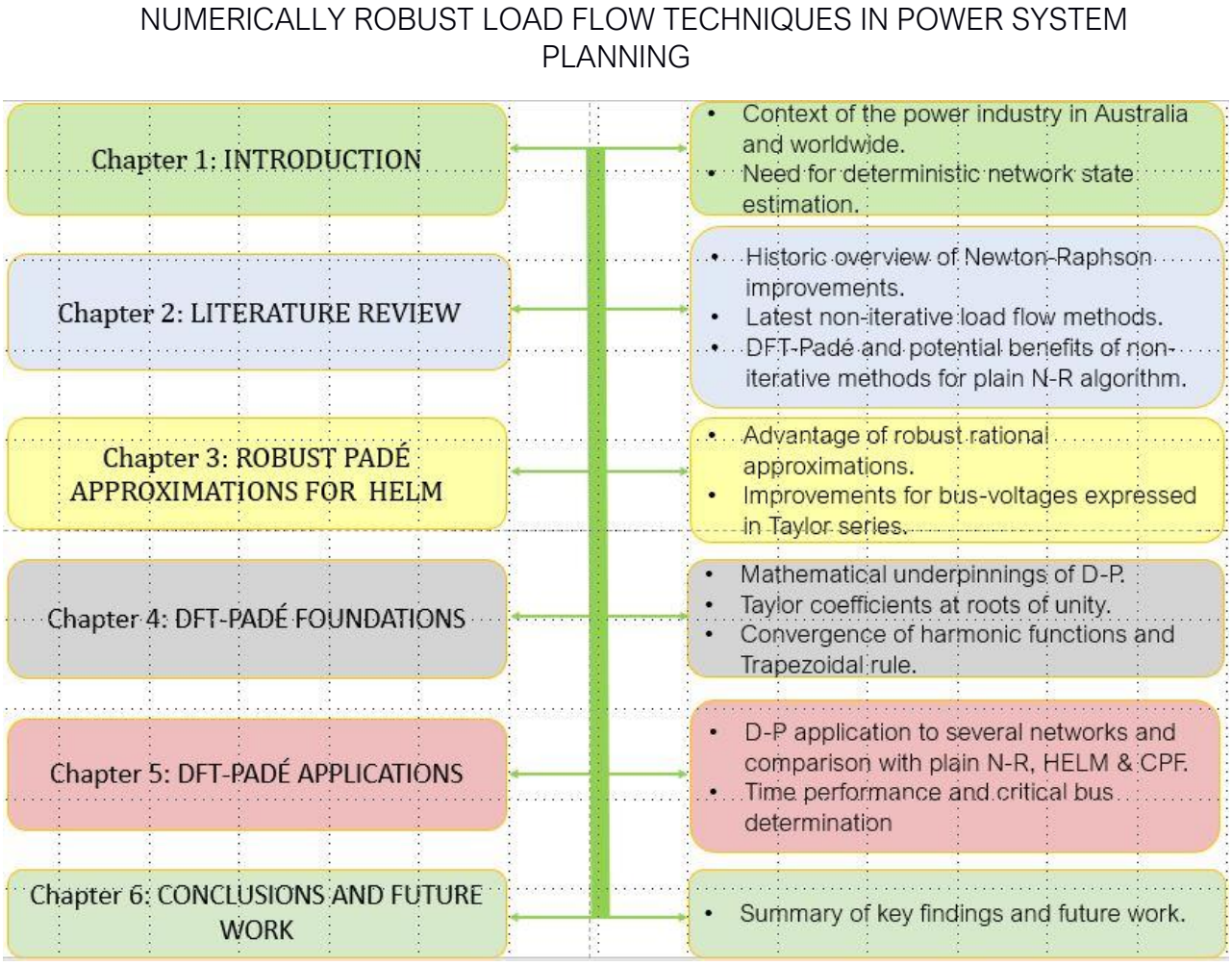

Figure 1-3 Thesis structure
Chapter titles and content summary

Chapter 2: Literature Review

2.1. Introduction

Solving load flow problems is a prerequisite for the dependable operation of a power grid. The information thus obtained is used to tackle a variety of analyses and processes, i.e., expansion planning, voltage stability analysis, outage scheduling, contingency analysis, etc. They rely on the effectiveness of load-flow solvers [24].

Iterative methods have been used in power systems to determine load flows for many decades. Newton-Raphson has been the algorithm of choice since the 1960s. For the most part, N-R is a reliable algorithm. However, that may not be the case when the grid starts to be heavily loaded.

Many alternative techniques have been developed to overcome the deficiencies presented by the iterative load flow methods, i.e., multiple solutions, starting points, Jacobian matrix conditioning, convergence problems, and ill-conditioned systems. Stating the obvious, if Newton-Raphson yielded the correct answer for every generation and load demand situation, then the variety of alternative solutions would never have appeared. The present chapter will focus on the attempts to resolve those limitations, and how the solutions have matured through time.

Much has been written about voltage stability in the last two decades. The approach has been varied from a) variations to existing iterative methods, (b) an assorted quantity of stability indices applicable to static and dynamic power system states, as well as planning tools, to c) new power flow algorithms and software.

Some important evaluations have already taken place for (b) in [25] and [26],

Among the more recent power flow methods that are not based on iterative algorithms are the Holomorphic Embedding Load Flow [11-13] and Quadratic approximation based on Hermite-Padé approximants [26, 27].

The improvements to iterative methods, principally Newton-Raphson, include modifications to the basic algorithm [28] (followed by many others as summarised in Section 2.3). These improvements also include variations to Newton's method, incorporating Gaussian elimination in Brown's method [29, 30], use of the second-order term of the Taylor series [31] to improve convergence, modifications to N-R to solve ill—conditioned systems [32] [33] ,or presenting the method in complex form [34] to include distribution systems under asymmetrical operating conditions. Continuation Power Flow formulation remains well conditioned around the critical point referred to as the voltage stability limit (VSL), can calculate the voltage stability index and identify areas prone to voltage collapse [35, 36], and it is arguably the most frequently used technique to date. This brief overview names a range of contributions in different directions.

2.2. Plain Newton-Raphson

What follows is a discussion about modifications to N-R, and added methods, that have been developed to enhance the load flow results, which aim at satisfying the requirements of network operators in an environment of high complexity due to extended power grids, as well as maximisation of the infrastructure resources.

The Newton-Raphson method was introduced in 1961 and was shown to have very good convergence properties in comparison with contemporary methods [37]. B. Stott, in his 1974 review of load-flow calculation methods [38], refers to previous work [39] wherein more than 200 "respectable" publications in English had already been produced. One of the early drivers for change was the availability of increased computer capacities. Y-matrix methods took advantage of the low memory requirements, while Z-matrix methods had better convergence properties. In N-R, each bus power function is approximated by its tangent hyperplane, built with a Jacobian matrix and multiplied by the vector of angles and voltage differences of two consecutive iterations. Its convergence is quadratic and takes 4 to 5 iterations when the solution point is near. Polar or rectangular coordinates can be used. Stott also mentions the decoupled Newton methods based on the loose connection between active power and voltage magnitude, on the one hand, and reactive power and voltage angle on the other. This approximation simplifies the Jacobian matrix. However, although it may be faster than the full Newton method, it sacrifices

accuracy. Several other methods and variations are also discussed. As it was seen back then that the non-uniqueness of the load-flow solution is an important issue as well as the advantages of sparse matrix factorisation.

2.2.1. Newton-Raphson equations

The method is based on representing the system's apparent power approximation (to the scheduled power) via Taylor series expansion, for which an initial estimation of bus voltages and voltage angles are provided. The algorithm entails the successive recalculation of voltages and angles until the linearised model of the apparent power is within an agreed tolerance of the actual (scheduled) power [21]. If power is expressed in megawatts, an acceptable tolerance could be 10^{-04}. When the iterations converge, the voltages and angles are very accurate.

The vectors scheduled power $\boldsymbol{y}$, calculated power $\boldsymbol{f(x)}$, and state variables $\boldsymbol{x}$ are shown in (2.1) for an N bus system. The power functions used to compare with the scheduled power are as per (2.2), where V_i and δ_i are the voltage and angle of the bus in question, and $|Y_{ik}|$ and θ_{ik} are the admittance's absolute value and angle of the transmission line between buses i and k. It is to be noted that bus 1 is the slack bus, used as the reference, and is therefore not part of the system [21].

$$\boldsymbol{y} = \begin{bmatrix}\mathbf{P}\\ \mathbf{Q}\end{bmatrix} = \begin{bmatrix}P_2\\ \vdots\\ P_N\\ Q_2\\ \vdots\\ Q_N\end{bmatrix};\ \boldsymbol{f(x)} = \begin{bmatrix}\mathbf{P(x)}\\ \mathbf{Q(x)}\end{bmatrix} = \begin{bmatrix}P_2(x)\\ \vdots\\ P_N(x)\\ Q_2(x)\\ \vdots\\ Q_N(x)\end{bmatrix};\ \boldsymbol{x} = \begin{bmatrix}\boldsymbol{\delta}\\ \mathbf{V}\end{bmatrix} = \begin{bmatrix}\delta_2\\ \vdots\\ \delta_N\\ V_2\\ \vdots\\ V_N\end{bmatrix}. \tag{2.1}$$

$$\begin{aligned} P_i(x) &= |V_i| \sum_{k=2}^{N} |Y_{ik}|\,|V_k|\, cos(\delta_i - \delta_k - \theta_{ik}),\\ Q_i(x) &= |V_i| \textstyle\sum_{k=2}^{N} |Y_{ik}|\,|V_k| sin(\delta_i - \delta_k - \theta_{ik}). \end{aligned} \tag{2.2}$$

The system of equations (2.2) is nonlinear and its solution requires an approximation method. Newton-Raphson uses the two first terms of the Taylor series expansion

(discarding the higher order ones, assuming they are very small) to represent (2.2), in a single dimension that is [20]:

$$y_i \cong f_i(x_i^{(0)}) + (\frac{\partial f_i}{\partial x})^{(0)}\Delta x_i^{(0)}, \tag{2.3}$$

where f_i is the active and/or reactive power function of (2.2) evaluated at $x_i^{(0)}$, the initial estimate of the state variables, which are normally $V_i(0) = 1$, and $\delta_i(0) = 0$, also known as a "flat start". In general, $\Delta x = x^{(j+1)} - x^{(j)}$, where x^j is the value of x at iteration j. Rearranging (2.3) with this in mind,

$$x_i^{(j+1)} \cong x_i^{(j)} + [(\frac{\partial f_i}{\partial x_i})^{(j)}]^{-1}[y_i - f_i(x^{(j)})]. \tag{2.4}$$

Writing the terms of (2.4) in vector and matrix form, where

$$\boldsymbol{x}^{(j)} = \begin{bmatrix}\boldsymbol{\delta}^{(j)}\\ \mathbf{V}^{(j)}\end{bmatrix}, \text{ and } \boldsymbol{F}(\boldsymbol{x}^{(j)}) = \mathbf{y} - \boldsymbol{f}(\boldsymbol{x}^{(j)}) = \left(\begin{bmatrix}\mathbf{P}\\ \mathbf{Q}\end{bmatrix} - \begin{bmatrix}\mathbf{P}(\boldsymbol{x}^{(j)})\\ \mathbf{Q}(\boldsymbol{x}^{(j)})\end{bmatrix}\right), \tag{2.5}$$

$$\boldsymbol{J}^{(j)} = (\frac{\partial \boldsymbol{f}}{\partial \boldsymbol{x}})^{(j)} = \begin{bmatrix} \frac{\partial P2}{\partial \delta 2} & \cdots & \frac{\partial P2}{\partial \delta N} & \frac{\partial P2}{\partial |V2|} & \cdots & \frac{\partial P2}{\partial |VN|} \\ \vdots & & & \vdots & & \\ \frac{\partial PN}{\partial \delta 2} & \cdots & \frac{\partial PN}{\partial \delta N} & \frac{\partial Pn}{\partial |V2|} & \cdots & \frac{\partial PN}{\partial |VN|} \\ \frac{\partial Q2}{\partial \delta 2} & \cdots & \frac{\partial Q2}{\partial \delta N} & \frac{\partial Q2}{\partial |V2|} & \cdots & \frac{\partial Q2}{\partial |VN|} \\ \vdots & & & \vdots & & \\ \frac{\partial QN}{\partial \delta 2} & \cdots & \frac{\partial QN}{\partial \delta N} & \frac{\partial QN}{\partial |V2|} & \cdots & \frac{\partial QN}{\partial |VN|} \end{bmatrix}^{(j)}, \tag{2.6}$$

$\boldsymbol{F}(\boldsymbol{x}^{(j)})$, the right-hand side equation of (2.5), is called the vector of residuals, and (2.6) is known as the Jacobian matrix (at iteration j).

Using (2.3), (2.5) and (2.6), the correction vector, $\Delta \boldsymbol{x}^{(j)}$ for iteration j, can be expressed as

$$\Delta \boldsymbol{x}^{(j)} = \boldsymbol{x}^{(j+1)} - \boldsymbol{x}^{(j)} = \boldsymbol{J}^{(j)^{-1}}\boldsymbol{F}(\boldsymbol{x}^{(j)}). \tag{2.7}$$

It is worth mentioning that the Jacobian is presented in its general form in (2.6). The amount and type of unknown variables change with the bus type. For each voltage-controlled bus the $|V|$ is already known, and the function $Q(x)$ is not needed, therefore they can be removed from the system of equations. As a result, the Jacobian matrix is of the order $(2N-2-m) * (2N-2-m)$, where N is the number of power system nodes, " $*$ " is the multiplication operator, and m is the number of PV buses. This can be clearly seen if (2.6) and (2.7) are written as

$$\begin{bmatrix}\Delta P\\ \Delta Q\end{bmatrix} = \begin{bmatrix}J_{11} & J_{12}\\ J_{21} & J_{22}\end{bmatrix}\begin{bmatrix}\Delta\delta\\ \Delta|V|\end{bmatrix}, \tag{2.8}$$

where

$$J_{11} = \left[\frac{\partial P(x)}{\partial\delta}\right], \quad J_{12} = \left[\frac{\partial P(x)}{\partial|V|}\right], \quad J_{21} = \left[\frac{\partial Q(x)}{\partial\delta}\right], \; J_{22} = \left[\frac{\partial Q(x)}{\partial|V|}\right], \tag{2.9}$$

and the iteration number is omitted. J_{11}, J_{12}, J_{21} and J_{22} are the Jacobian submatrices. For $N-1$ known ΔP (rows), there will be $N-1$ unknown $\Delta\delta$ columns, defining the size of $J_{11} = (\mathrm{N}-1) * (\mathrm{N}-1)$, and applies to $\mathrm{PQ} + \mathrm{PV}$ buses. PQ and PV represent the sets of load and voltage-controlled buses. For J_{12} there will be $\mathrm{PQ} + \mathrm{PV}$ buses of known ΔP (rows), and there will be PQ buses of unknown $\Delta\delta$ (columns), making the size of $J_{12} = (\mathrm{N}-1) * (\mathrm{N}-1-\mathrm{m})$. For J_{21} there will be PQ number of known ΔQ (rows) and $\mathrm{PQ} + \mathrm{PV}$ buses of unknown $\Delta\delta$ (columns), which make the size of $J_{21} = (\mathrm{N}-1-\mathrm{m}) * (\mathrm{N}-1)$. Then, for J_{22} there will be PQ number of known ΔQ (rows), and PQ buses of unknown $\partial|V|$ (columns) making the size of $J_{22} = (\mathrm{N}-1-\mathrm{m}) * (\mathrm{N}-1-\mathrm{m})$. The generators' reactive power is checked at the end of each iteration when reactive power limits are taken into account. If limits are exceeded then the bus type is changed to PQ, and its reactive power set to the maximum (or minimum) limit.

2.3. Improvements in the Newton-Raphson power flow algorithm

The following list shows some of the most important aspects of the proposed improvements to the N-R method that have been taking place since the early 1970s:

- Starting points: this addresses the fact that convergence can be compromised if the initial guess is not close enough to the actual solution (an innate limitation of this iterative method).
- Solutions to ill-conditioned power systems: this condition refers to how sensitive the solution of a problem is to changes in the input data. Round-off errors in successive calculations make the solution of some problems unstable and is also known as ill-conditioning [40].
- Multiplication parameter: this is perhaps the most exploited mathematical artifice [41] that has been perfected to make N-R a more reliable algorithm.
- Rectangular coordinates: one of its initial advantages is that it uses the exact number of terms in the Taylor series approximation.
- Multiple load flow solutions: this is one of the problems encountered early on when systems get close to the stability limit. Figures 2-1 and 2-2 depict N-R convergence to these possible values.
- Low voltage solution: this can also be seen as part of the previous problem. It is also shown in Figs. 2-1 and 2-2. There is a HELM approach to this problem as well as a DFT-Padé one, as described below.
- Proximity to voltage stability limit: Jacobian matrix conditioning is one of the problems faced by the N-R algorithm for convergence at this particular point as it becomes singular. Also treated by many, due to its key importance.
- Homotopy methods: this is another numerical algorithm where a difficult problem is embedded in an easier one [42]. This algorithm succeeded when formulated as continuation power flow.
- Continuation power flow [41]: this is a specific case of homotopy, based on the predictor-corrector method.

2.3.1. Starting point

In 1971, a basic non-iterative load-flow was outlined in "Effective starting process for Newton-Raphson load flows" [43] to obtain starting values for the N-R method. It is well-known for its reliance on the initial guess in numeric applications, and it is used to solve ill-conditioned cases. The approximation to those values is done in two steps: a) voltage angles are calculated using DC load-flow, and b) the voltage magnitudes are calculated

directly using those angles. The process takes advantage of several assumptions that simplify the set of equations. The processing time corresponds to half of one conventional N-R iteration. The tests of the method accelerate the convergence and makes it more accurate by two or three orders of magnitude. Other uses are also mentioned, they include: facilitating pinpointing problems caused by erroneous data, detection of split networks which otherwise would render non-convergence, and quick AC power-flow approximations.

The authors of "Starting algorithm and modification for Newton-Raphson load-flow method" [44] propose an algorithm that provides good starting values for the system variables. They calculate the Jacobian matrix once, disregard the weak links $\partial P/\partial|V|$ and $\partial Q/\partial\theta$, and take the values of the bus-voltage and angle based on two functions defined by minimal values of the couplings' sensitivity matrices. Applying this method also implies taking some of the second order terms of the Taylor series expansion of the load flow equation. The method has better convergence than B. Stott's [43] and N-R in several tests carried out over four different networks. This convergence is also achieved in fewer iterations than conventional N-R. The method could easily be programmed into existing N-R software. The authors claim this method of generating starting values delivers better results than any other methods known to them.

The authors investigate homotopy-based techniques applied to the power flow problem using the N-R method with poor starting points in reference [24], and obtain robust results tested on 1200-bus, 2500-bus and 46000-bus networks. Previous works first solved the "easy" DC power flow to get the starting points and then solved the "hard" AC power flow but did not give robust outcomes [45, 46]. The two first techniques the authors tried, injenction homotopy and phase homotopy, did not give satisfactory performance because the solutions were attracted to near null voltage magnitudes. A third approach included preferences such that the solutions were inclined to voltages near one per unit in magnitude. This magnitude homotopy approach outperformed both Newton-Raphson and line search Newton-Raphson.

2.3.2. Solutions to ill-conditioned power systems

A quadratic convergent Newton-like method that employs Gaussian elimination is proposed in [30], which does not solve all power system equations simultaneously as in the N-R algorithm.

It presents results for the 11-, 13- & 43-bus systems, where other iterative methods did not converge. This method was developed by mathematician K. M. Brown.

A problem is defined as ill-conditioned when the solution changes widely to small input variations and can be well characterised by the condition number K. For a symmetric positive definite Jacobian matrix $[\boldsymbol{J}]$, it can be stated as:

$$K = \|\boldsymbol{J}\| * \|\boldsymbol{J}^{-1}\| \; = \; K([\boldsymbol{J}^T\boldsymbol{J}])^{1/2} = \; (^{|\sigma_{max}|}/_{|\sigma_{min}|})^{1/2}. \qquad (2.10)$$

This is a Euclidean matrix norm expressed by $|\sigma_{max}|$ and $|\sigma_{min}|$ real and positive eigenvalues. If the condition number is greater than the decimal precision of the computer, then the problem cannot be solved. The key aspect of Brown's formulation is to change the $[\boldsymbol{J}]$ matrix to a transverse upper triangular one using Gaussian elimination with triangular pivoting to lessen roundoff errors [47]. The condition number of this new matrix is much smaller than Newton's Jacobian, and therefore the approach can resolve systems that the conventional N-R could not resolve.

In "Continuous Newton's method for power flow analysis" [48] the author tackles ill-conditioned power flow problems aiming at the stability of the numerical method if the starting point is within the region of attraction of the solution. The technique used is the Runge-Kutta RK4 formula to approximate the voltage solution. It is shown that the vector continuous Newton's method is analogous to a set of ordinary differential equations (ODE). The set of equations is similar to Davidenko's homotopy method. These facts allow the use of Runge-Kutta formulas to solve the load-flow problem. The formulation of ODE can be solved by the Euler method where its parameter matches the optimal multiplier in robust N-R methods. It outperforms the simple robust method (SRM) and Iwamoto's method in terms of the number of iterations when tested on 1254-bus UCTE system. The computational burden also improves that of Iwamoto's, but it is below the SRM.

2.3.3. Multiplication parameter

In [28] the load-flow steady-state stability problem is framed as a periodic stability (as opposed to self-oscillation in the system caused by automatic control not properly tuned). A parameter η (2.11) that multiplies the inverse of the Jacobian is proposed.

$$\boldsymbol{x}^{(j+1)} = \boldsymbol{x}^{(j)} + \eta^{(j)}[(\frac{\partial \boldsymbol{f}}{\partial \boldsymbol{x}})^{(j)}]^{-1}\boldsymbol{F}(\boldsymbol{x}^{(j)}). \tag{2.11}$$

This parameter, less or equal to one, is a function of the norm of the vector of residuals and its second derivative with respect to the state variables (2.12).

$$\eta^{(j)} \propto \left\|\boldsymbol{F}(\boldsymbol{x}^{(j)})\right\| \left\|\sum_{h,l} \frac{\partial^2 \boldsymbol{F}(\boldsymbol{x}^{(j)})}{\partial x_h\, \partial x_l} \Delta x_h\, \Delta x_l\right\|,^{-1} \tag{2.12}$$

where $\left\|\boldsymbol{F}(\boldsymbol{x}^{(j)})\right\|$ is the m-norm of the vector of residuals, and $\left\|\sum_{h,l} \frac{\partial^2 \boldsymbol{F}(\boldsymbol{x}^{(j)})}{\partial x_h\, \partial} \Delta x_h\, \Delta x_l\right\|$ is the m-norm of the second derivative of the vector of residuals multiplied by the vectors of corrections twice.

This algorithm ensures convergence provided the Jacobian is not zero. The stability limit is achieved by increasing the system load in decreasing steps, where the previous result is the initial condition of the following system's resolution. As the load approaches the limit, the value of the parameter and the Jacobian tend to zero. The limit can be determined by the change in sign of the Jacobian. To achieve this, the authors suggest two different methods, according to the type of change in the system. Jacobian divergence is avoided, and strained buses can be identified. The number of iterations to obtain the stability limit, in five load steps, increases from, say, four to eight.

An Optimal Multiplier is proposed in [32]. The method never diverges and can resolve ill-conditioned systems. It uses the nonlinear programming formulation, where the cost function (2.13) is defined using the least squares method. The method makes use of the third term of the Taylor series expansion in the load flow equation in rectangular

coordinates. A factor, $\mu^{(j)}$ in (2.13) that minimises the cost function in a least squared sense is calculated, using the Cardan's formula, and applied to the correction vector $\Delta x^{(j)}$ at each iteration j, where $2 * (N - 1)$ is the number of equations.

$$F_C^{(j)} = \frac{1}{2}\sum_{k=1}^{2*(N-1)} [y_k - f_k(x^{(j)} + \mu^{(j)}\Delta x^{(j)})]^2. \quad (2.13)$$

Convergence is found when the cost function becomes zero, as in the 11-bus system example, or stays at some positive value, as in the 43-bus system. It took nine iterations in both cases to determine convergence or otherwise. Details of these two bus systems can be found in [30].

Another technique based on the minimization of the sum of the square of the residuals using Newton's polar form is nondivergent and is presented in [49]. It also points to potential problems like incorrect data usage by allocating the highest mismatch at the overloaded bus. This method entails reaching the critical point of the volt-ampere function (VAF) (2.14) at each iteration.

$$VAF(V) = \sum_{i=1}^{N} [-2V_i I_i + \frac{V_i^2}{z_{i0}} + \frac{1}{2}\sum_{k=1}^{N} \frac{(V_i - V_k)^2}{z_{ik}}] \quad (2.14)$$

where V_i and I_i are the phasors' voltage and current at bus i, z_{i0} and z_{ik} are the line impedances between buses i and reference 0, and between buses i and k respectively. In this case, the optimal multiplier μ affects the correction vector ΔV, and is obtained from (2.15) and solving for it. Here, the voltage correction vector is calculated using rectangular coordinates and the exact Taylor formulation; the results are then converted to polar coordinates.

$$\frac{\partial VAF(V + \mu\nabla V)}{\partial \mu} = 0. \quad (2.15)$$

The resulting equation from (2.15) is scalar cubic in μ, and the smallest root is chosen to calculate the sum of square residuals (SSR). When tested on the 11-bus and 43-bus systems, the solutions are not obtained but the estimated solutions are nondivergent with

a minimum $SSR = 0.0001$ and $SSR = 1$ respectively. This routine can identify the overloaded bus by the highest mismatch, which is more consistent than the rectangular coordinate-based method.

2.3.4. Power flow in rectangular coordinate system

In 1977, a Newton-Raphson method [50] claimed to execute the load-flow many times faster than the polar coordinate version of the software, even though it took 1.5 as many iterations. Because of the quadratic nature of the nodal equations in rectangular coordinates, their Taylor representation is exact and takes only three terms. The third term is one half of the second partial derivative of the power functions with respect to each one of the state variables. The computing time is drastically reduced since the Jacobian matrix is treated as constant. However, no indication is given in relation to ill-conditioned systems.

In "Simplified Newton–Raphson power-flow solution" [51], the author presents a simplified version of the Newton–Raphson power-flow solution method, based on the current balance principle to formulate a set of nonlinear equations. Although there exist several powerful load-flow solvers based on the standard N-R method, their corresponding problem formulation is not simple due to the need to calculate derivatives in their Jacobian matrix. The proposed method employs nonlinear current mismatch equations instead of the commonly used power mismatches to simplify the overall equation complexity. A derivation of the Jacobian matrix's updating formulae is illustrated in comparison with those of the standard Newton–Raphson method. To demonstrate its use, a simple 3-bus power system was selected as a numerical example. The effectiveness of the proposed method was examined by computer simulations through five test systems: (1) a 5-bus test system, (2) a 6-bus test system, (3) the 24-bus IEEE test system, (4) the 30-bus IEEE test system and (5) the 57-bus IEEE test system. Its convergence and calculation times were observed carefully and compared with solutions obtained by the standard N-R load-flow method. The results show that the proposed N-R method takes less execution time than the standard method, with similar convergence characteristics.

In “A comparison of the optimal multiplier in polar and rectangular coordinates” [52] four methods are compared: the N-R algorithm with and without optimal multipliers (OM) using polar and rectangular coordinates. The paper concludes that the polar NR load flow with OM is the best method for both solvable and unsolvable load flow cases. The rectangular OM load flow by Iwamoto and Tamura [32] is the method used. For the polar OM load flow, the method developed by Castro and Braz [53] was chosen due to its comparative advantages, as demonstrated in [54]. The most significant drawback to the polar formulation is the presence of transcendental functions. These functions lead to an infinite number of terms in the Taylor expansion, which makes (2.4) an approximation rather than a strict equality as in the rectangular formulation. Also, the presence of sine and cosine in the polar load flow equations results in a more complex calculation of the second-order term needed to solve for the optimal multiplier. The greatest benefit of using the rectangular formulation results from the quadratic nature of the load flow equations when rectangular coordinates are used. Because all the state variables appear in quadratic terms in the equations, the third and higher order terms of the Taylor expansion are zero; which makes (2.4) hold with strong equality when the third term is included. This can lead to greater accuracy in the calculation of the rectangular formulation relative to the polar one. The extremely poor performance of the decoupled load flow in rectangular coordinates [55] also indicates that the rectangular formulation may not have as good a linearization as the polar formulation. The polar OM had fewer iterations than the rectangular OM, especially in unsolvable cases, where the rectangular OM took many more iterations before stopping the process, and also diverged more often. The authors endorse the use of polar coordinates when using an optimal multiplier to get faster responses and more robust results for any system condition or size.

2.3.5. Dealing with multiple load-flow solutions

Researchers and practitioners found that Newton-Raphson can converge to more than one voltage solution for a given bus load. The topic was discussed as early as 1975 by Klos and Kerner [56]. This is depicted in Figs. 2-1 and 2-2 from the insightful work of Baghsorkhi-Suetin [12].

A method for analysing multiple solutions was developed since more than one solution is possible due to the non-linearity of the load flow equations. According to [57] it is necessary to find all feasible solutions to those equations when analysing the power system's voltage stability. The authors propose a set of linearised equations to find the low and high voltage solutions of load buses for a given load. The positive (HV) or negative (LV) mode solutions, as named by the authors, are given according to the selection of initial values. The power transfer is maximum when both solutions coincide. There are also two reactive power and angle solutions for PV buses. The number of combinations of modes is 2^N (without counting the reference bus). When the active power for bus i, P_i , is greater than the maximum value, then the correction ∇V_i becomes a complex number, effectively determining the voltage stability limit for that bus and the given system conditions under this linearised model.

A pair of solutions obtained using the N-R method is related to voltage instability in power systems. The authors of [58] discovered that the convergent characteristic of the N-R load flow in rectangular coordinates has a unique linearity. It tends to converge straight towards a pair of multiple solutions when they are closely located to each other. They belong to the high voltage and low voltage solution branches. Their proximity indicates a near-coalescence, which is the voltage stability limit of the P-V curve. They also minimise the cost function, cubic in nature, that delivers 3 roots, and they must be real numbers for the system to have the two close solutions. The optimal multiplier, as described in [32], is the first one of those roots, and the proposed method uses the third root to find the second convergent voltage value. It was successfully tested in ill-conditioned systems. The remarkable aspect of this approach is that its convergence is very fast, and therefore suitable for on-line applications.

Voltage stability assessment using the energy method has been used in [59] to determine a voltage security measure in closed form by integrating the power mismatch between the low and high voltage solutions. A key aspect of the energy function is that it can determine the correct low voltage solution to use in the voltage security measure. As generation and load move towards voltage collapse, the amount of low voltage solutions decreases until there is only one at the point of maximum active power. For a load increasing scenario, the energy measures will decrease, however, this is not constant in

all areas (the group of buses) of the system since this measure can change rates for different areas. Combining the rates of change with the energy values would signal the proximity of the system's voltage collapse to operators.

A method to approximate the closest loadability limit (CLL), in the local sense, is proposed in [60] from a pair of multiple load flow results, i.e., the low voltage and the operating solutions to localise the nearest (Euclidean norm) loadability limit, assuming that the loads and generations are increased in the worst direction. Right and left eigenvectors from the zero eigenvalue of the Jacobian matrix are used to identify the weak areas in the power system. This follows the work in [61]. The voltage collapse is then obtained by increasing load and generation in the worst direction. The midpoint between the HV and LV solutions is the loadability limit where the Jacobian becomes singular; and this holds regardless of the distance between both solutions. The conditions for the approximation in [60] are that the operating point is near the voltage collapse and the Jacobian matrix is symmetrical. The approximations to the loadability limits are then compared with exact ones calculated using [62] and [63]. The maximum error found using test systems, from 5/6/14/30/57-bus systems, was 6%. The computation time reported for these approximations corresponded to one iteration of the power flow, while the exact results required 100 power flow solutions.

2.3.6. Low voltage solutions

Low voltage solutions could be considered as a subset of multiple load-flow solutions, but they stimulate interest of their own. Iba et al found that two voltage solutions, HV and LV, could be found when the bus approaches its stability limit; hence that limit lies half way between the two solutions [58]. Others discuss how the stability limit can be found where the two solutions coalesce: details are given below. Indeed, this is one of the approaches taken by DFT-Padé, to find the bus-voltage stability limits.

An improved method to calculate the low voltage solution using state space search is presented in [64]. The method does so in polar coordinates which would make it easier to integrate to existing load flow software. It can always obtain an initial value leading to a low voltage solution regardless of its distance to the stable HV solution. The method is state space search-based and is also able to detect a lack of both convergence and

divergence. It develops step size optimisation from a second order Taylor representation of the power functions, and an optimisation factor that minimises the quadratic function of power mismatches in the direction of the state variable increments. As a result, an initial value for voltage and its angle are obtained. The optimised step change allows the load flow calculations to approach the LV solution initial estimate and the LV solution. The maximum loading point (MLP) and proximity index are also obtained.

An auxiliary gradient to obtain the low voltage of load buses is proposed in [65]. It shows how the stability points are worked out for the related gradient systems, which are also the solutions to the low voltage load flow. Following others, the authors argue that an indication of voltage collapse proximity is given by fewer LV solutions for any given bus load. The collapse happens when the critical LV solution coalesces with that of the HV. The method finds the critical LV solution by keeping on searching if the one found coalesces with another LV solution, which is the difference from previous state-space search methods. The authors also found few cases of non-convergence to either an LV or an HV solution. They see the method as being reliable and promising, with more research required to find the critical LV solution, as well as the existence of more than one stable load flow solution.

The Step Size of the Newton Raphson Method [66] finds the low voltage solution at the maximum loading point of a system using scalar quadratic equations (SQE) to determine the optimal multiplier. In this work, it is shown that the optimal multiplier is the closest to an indicator based on the SQE, overcoming problems from previous step size methods that are based on the smallest optimal multiplier. The SQE indicator is the singularity point of the P-V curve. This optimal multiplier gets the correct LV solution from all possible ones at the maximum loading point.

2.3.7. Proximity to voltage stability limit

The uncertain solutions, including Jacobian singularity, that may be found by the Newton-Raphson algorithm when the system loading approaches the stability limit, prompted researchers to devise methods to overcome this hurdle. Some of them are shown below since the papers written on this topic is vast.

The voltage instability proximity index (VIPI) proposed in [67] predicts the voltage instability based on multiple power flow solutions. It states that despite voltage collapse being a dynamic event, the static qualities are also relevant. Several indices are compared including a) the number of iterations in power flow calculations, b) transmission losses, c) variations in bus voltages with respect to variations in the reactive load, d) the quantity of multiple load flow solutions, e) the determinant of the Jacobian matrix, f) convergence rate, and g) the proposed index VIPI, defined by the angle between the node-specification vector and the singular vector in the space of the node-specification. The authors concluded that power losses, determinant of the Jacobian and VIPI, are well suited to determine voltage collapse. The last two are rather sensitive to generators' reactive power limits. Weak buses can be identified by a sensitivity defined as the bigger of the VIPI variations, with respect to active and reactive power variations. VIPI needs only two solutions to be worked out. When systems are overloaded, they produce these two solutions only. Their selection is essential and is achieved using [68]. The authors acknowledge that further research, through case studies, is required to establish the effectiveness of the index.

In "Towards a theory of voltage collapse in electric power systems" [69], the authors frame the loss of equilibrium of the load flow when the system approaches the voltage collapse, within the saddle-node bifurcation. A dynamic mechanism to describe the voltage progression towards saddle node bifurcation is used. Other authors have discussed the nature of voltage collapse, whether static or dynamic. This work is based around Sotomayor's Dynamic Systems. Despite the simplification of the model that encompasses the key mechanisms of voltage collapse, the authors feel that it is a robust candidate to explain the phenomenon.

In "Power system steady-state stability and the load-flow Jacobian" [70], an association between the conventional static load flow, from the linearised model and the system dynamic model, is attempted. Both sets of equations attempt to solve the system in three Jacobian matrices. The zero value of the standard Jacobian is associated with the maximum load transfer of the system, coinciding with the other authors in this assessment. If the Jacobians were not singular, then the steady-state stability would be given by the eigenvalues of the dynamic state Jacobian, where the system could be

critically unstable if the real part of one eigenvalue was zero. For the analysis of voltage instability and collapse, the singularity of the Jacobian matrix would be relevant if the system should be close to its maximum power transfer.

In “An energy-based security measure for assessing vulnerability to voltage collapse” [71], a security measure or distance to voltage collapse is developed based on the power system dynamic model and energy functions, taking into account the non-linearities caused by generators’ var limits. Bifurcation analysis, dynamics of the load, as well as Jacobian singularity from the load flow equations are also considered. It is recognised that voltage collapse is not preceded by large disturbances, nor a loss of transient stability, but rather by the gradual increase of the general system load. The authors adopt a dynamic model where the voltage depends on the active power demand and they call it the energy function instead of the Lyapunov function, where the original model is extracted from that, using the notion of the closest unstable equilibrium. Low voltage results and the associated energy differences from the high voltage results can be related to areas of vulnerability. As the system gets loaded up, the number of solutions decreases until only one remains, thus reducing the computational effort. The method requirements entail a load flow solution, apart from the current load point results, and an assessment of the energy function for each weak bus. The method was still being developed and the authors deemed it required more research in some areas.

In “Cascaded voltage collapse” [72], voltage collapse is seen as a series of dynamic phenomena that start at the weakest bus and expand to other weak buses nearby. Transients at generators are ignored for these tests, as they tend to disappear much more quickly than those found at the loads. These tests are conducted in two stages: first, the load flow is solved for motor loads. A disturbance is considered in the second stage, where the motor slips are taken into consideration. Then, the power flow is recalculated for the new set of loads. The change in speed of the motor and the voltage drop could be controlled by switching capacitors at this point. It is noted that the system could be recovered after the voltage dip into the low voltage region. The dynamic voltage stability is characterised as a local phenomenon. After testing systems with motor loads, it is concluded that voltage collapse starts in the weak bus and gradually expands to other

weak buses. It is also concluded that it is not always unstable to operate in the lower voltage area of the P-V curve, subject to the dynamic behaviour or the load in question.

In “Point of Collapse Methods Applied to AC/DC Power Systems” [73], the authors present an addition to the point of collapse (PoC) method developed for AC systems. They use the bifurcation theory of nonlinear systems [42] to find an estimate of the loadability margin of a power system. Hopf bifurcations [42] are suitable when the dynamics of high voltage direct current transmission (HVDC) are considered. Important instabilities happen when the Jacobian of the system is singular, however the PoC method is robust to the saddle-node bifurcations that can be produced. It uses a transient stability model for near static voltage evolution, and voltage and frequency load models. The HVDC model employs two types of controls. The authors take advantage of the fact that both the power flow Jacobian and the Jacobian of the linearised dynamic system at the balance point have zero eigenvalues. Obtaining these eigenvalues allows the system to find the singularities or points of maximum loading. The PoC method uses a specific technique to find a suitable starting point for the eigenvectors that will allow the N-R to converge to the desired bifurcation, namely, the power flow Jacobian undergoes several iterations of the inverse power method [40]. Whilst it is reasonably accurate, its efficacy is not guaranteed. The method produces a P-V curve of the systems buses, with the number of equations being twice as many as for conventional N-R, and the solution times being around 10 to 20 times those of conventional load flows.

In “New methods for computing a closest saddle node bifurcation and worst case load power margin for voltage collapse” [62], an index of voltage collapse is defined as the distance of the current load to the closest bifurcation point, or worst case load margin, using the proposed iterative and direct methods. These methods rely on both static and dynamic models of the power system. The iterative method obtains the maximum load of the system based on the worst case when the load increase direction is unknown. The direct method uses the load flow equations in an estimated direction of load increase, the corresponding Jacobian and its left eigenvector at the point of critical loads. It can be applied to the whole system, to a set of buses, or to an individual bus. The worst-case power margin is convenient when the direction of load increase is undefined, and it assists the load power margin. Sensitivities, as a function of the distance to the bifurcation points,

can also be derived and assist in determining what loads should be shed. It was reported in [60] that the direct method may have problems with finding suitable initial estimates. However, it is proposed that the iterative method can be used to find the exact solution.

In "Computation of maximum loading points via the factored load flow" [74], a quick algorithm is presented to find the maximum loading point of a network by executing binary searches between viable and unviable power flow cases. The factored load flow (FLF) method has a modified set of equations such that the iterative process converges quadratically and its region of attraction around the solution point is much wider. This allows the method to converge from initial points that are remote from the result. Therefore, it requires less iterations to converge. It will also reach for results in the complex domain when there are none in the real domain. It does so by making the starting point complex by adding a small imaginary part. The maximum loading point is sought in two steps: first, by solving the base load problem, then generation and load are multiplied by an increasing scalar until the method finds a solution with a significant imaginary part. This unviable result, together with the last viable one, form a gap that is shrunk through binary search. The method was tested against continuation power flow (CPF) and point of collapse (PoC) methods in various cases up to 2383 buses, showing a faster convergence in all cases. Unlike competing methods, the number of steps is independent of the network size. The other remarkable fact is that it needed an average of 3.1 iterations per step (network resolution) despite most of them being close to voltage collapse.

2.3.8. Homotopy methods

Homotopy methods are based on continuous mapping from a starting point to an end point (or continuous deformation). In other words, first a simple problem whose solution is easy to obtain is specified, then a path is defined between such a solution and the one that is hard to solve. This technique is particularly useful when a "flat start" may not be as good an option as an initial guess [35]. If $\boldsymbol{F}(\boldsymbol{x}) = 0$ is the difficult problem to solve, i.e. the bus-voltage near the stability limit, and $\boldsymbol{G}(\boldsymbol{x}) = 0$ is the easy problem to solve, i.e., the network is lightly loaded, then the homotopy equation can be given by (2.16).

$$\boldsymbol{H}(\boldsymbol{x}, \lambda) = \lambda \boldsymbol{F}(\boldsymbol{x}) + (1 - \lambda)\boldsymbol{G}(\boldsymbol{x}), \qquad 0 \leq \lambda \leq 1 \tag{2.16}$$

beginning at $\lambda = 0$ with the simple problem and hopefully finishing at $\lambda = 1$ with the difficult one [42].

In "Calculation of Critical Loading Condition with Nose Curve Using Homotopy Continuation" [75], the authors use a Newton-Raphson based method to calculate the critical load and to determine the nose of the P-V curve, overcoming the singularity problems of the Jacobian matrix. The Newton-Raphson is solved with a homotopy parameter t that affects generation and loads linearly as per $Y_s(t) = Y_{s0} + tY_D$, where Y_{s0} is the base load and Y_D the direction of change. The homotopy continuation method is used to choose the step change $\Delta t_j = t_j - t_{j-1}$. Both sides of the curve can be obtained using [58], but two different procedures are used according to the system loading condition, since [58] may not find a solution if the HV and LV solutions are far apart, which is the case for base loadings. Four systems are tested: Klos-Kerner's 11-bus, 233, 118 and 469-bus systems. The P-V curve for some of the buses in each system is drawn, and the critical loading point is reached within ten steps, showing the robustness of the method.

The "Numerical polynomial homotopy continuation method locates all the power flow solutions" [76]. It embeds the load flow equations in the complex domain. The solution converges to the real domain at the end of the homotopy path. The method makes use of polynomial equations that guarantee to find all the solutions at the expense of high computational cost, finding its limit in perhaps 15 buses.

"Improving the robustness of newton-based power flow methods to cope with poor initial points" [24] is a homotopy-based technique applied to the power flow problem using the Newton-Raphson method with poor starting points. Details of the method can be read on page 15 under Starting point subsection. This homotopy approach outperforms N-R and line search N-R.

2.3.9. Continuation power-flow methods

Continuation power flow is a method that ensures the correct bus voltage values are obtained at the nose of the P-V curve, since convergence problems and the Jacobian singularity of plain N-R can compromise those results [77]. This method encompasses

the following process: a) predictor steps, b) parameterisation, c) corrector steps, and d) step length control. The predictor step gives an estimate of the state variables for the corrector step to find the correct result. The step size is the distance between two successive solutions. As the P-V curve trace approaches the critical solution or maximum bus loading, the Jacobian matrix becomes singular. It is here where the continuation parameter also becomes unsuitable. Then, arc length parameterisation is used to overcome this problem. Local parameterization [35, 78] allows not only the added load parameter λ, but also the state variables to be used as continuation parameters.

In "Continuation power flow: a tool for stead-state stability analysis" [79], the authors present a method to track the P-V curve around the maximum loading point accurately, without being affected by either convergence problems or the Jacobian matrix singularity. As a by-product of the calculations, a voltage stability index and weak bus indicator are also obtained. The weak bus is determined by the greatest change in bus voltage in respect of the whole system's active load change, where the bus voltage differentials are obtained from the tangent vector calculated in the predictor step, and the total active load change is proportional to the load parameter λ. The authors also use the inverse of the weakest bus determination for its maximum active load, as the system voltage stability index. According to this load scenario, the total reactive power change can also be used in the index determination. The results were demonstrated using diverse scenarios of the 30-bus New England grid that had been used by other authors for research into voltage stability.

In "CPFLOW: a practical tool for tracing power system steady-state stationary behaviour due to load and generation variations" [36], a form of software applying the continuation method is described. It works with fully modelled power systems and avoids ill-conditioning by a) treating the parameter λ as a state variable, b) introducing the arc length as a new parameter that combines with the step size, providing an additional constraint, c) applying this constraint to all load buses forming part of the Jacobian matrix. These constraints make a set of equations that is well-conditioned at any point of the P-V curve. CPFLOW uses two type of predictors for computational efficiency: first, the tangent method, then, the secant method. It uses N-R in the corrector step. A step length control

is also included, such that the step is longer where the P-V curve is flat and shorter where the change of voltage is greater. It handles up to 12,000 buses in its original release.

There are many CPF packages available from the Internet; some of them are open source that can be used for testing and research. Amongst others, the list includes PSSE [80], PowerWorld [81], PSAT [82], PST [83] and MATPOWER [84]. MATPOWER was used for verification and comparison purposes in Chapter 5, modelling a 7-bus network where it serves as a benchmark against results obtained using the developed DFT-Padé method. To determine the steady state loading limit, the basic power flow equation [84]:

$$g(x) = \begin{bmatrix} P(x) & - & P^{inj} \\ Q(x) & - & Q^{inj} \end{bmatrix} = 0, \tag{2.17}$$

is system of N nonlinear equations, with $g(x), x \in R^n$. By adding a continuation parameter λ and one more equation to the system, x can be traced by varying λ. The resulting system $f(x, \lambda) = 0$, has $\mathrm{N} + 1$ dimensions.

$$f(x, \lambda) = g(x) - \lambda b = 0, \tag{2.18}$$

where $\mathrm{x} \equiv (\theta, \mathrm{V_m})$, and b is a vector of power transfer given by:

$$b = \begin{bmatrix} P^{inj}_{target} & - & P^{inj}_{base} \\ Q^{inj}_{target} & - & Q^{inj}_{base} \end{bmatrix}, \tag{2.19}$$

where the target power can be approximated to the voltage stability limit, or any other greater than the base-line value, specifying the stoppage parameter at “NOSE”. For the curve to trace the LV branch, then “FULL” needs to be specified instead. Application details are given in Chapter 5.

2.4. Non-iterative methods

There are two non-iterative, novel approaches, explained below, that overcome the limitations of N-R.

- HELM: the bus voltages are represented by Taylor approximations whose coefficients are obtained by a successive convolution process until the number of coefficients is reached or their relative differences converge.
- Quadratic approximation: Bus voltages are also represented by a truncated Taylor series, whose coefficients are part of a system of quadratic equations obtained by the application of singular value decomposition (VSD). The HV and LV branches are then obtained by applying the quadratic formula whose determinant will yield the branching points (or voltage stability limits).

2.4.1. The holomorphic load flow method (HELM)

Trias, in 2012 [11], promised to overcome N-R shortcomings, i.e. starting points in the region of attraction, multiple solutions and Jacobian singularity when the system approaches voltage collapse. This is vital, particularly for online applications where the physical model, which is accurate, must be solved one hundred percent of the time. The proposed method takes the nodal equations to the complex domain where it is embedded in a larger problem, which is easier to solve. The method consists of finding the bus voltages in a Taylor series (or truncated polynomials) whose coefficients are unravelled by a recursive process that finishes when either a desired amount or tolerance is reached. Linear systems are solved at each step of the way. One of the key points is the determination of the germ of the analytic function. Such germ will allow to start the recursive process. The working out of the germ will have a bearing on the “strength” of the obtained power series. So far, the limitation would be the radius of convergence of the series, such that it could cover all possible solutions. The only way to ensure that is to resort to the analytic continuation property of some functions in the complex domain. The Padé rational functions (Padé approximants) can guarantee maximal analytical continuations.

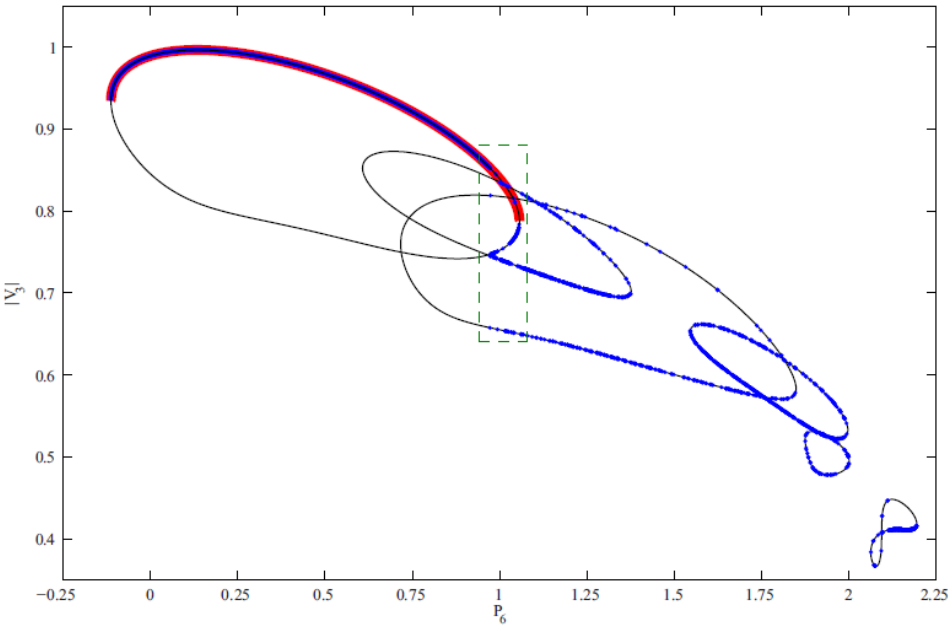

Figure 2-1. Seven-bus system: Newton-Raphson vs HELM.
N-R (blue), HELM (red) [12].

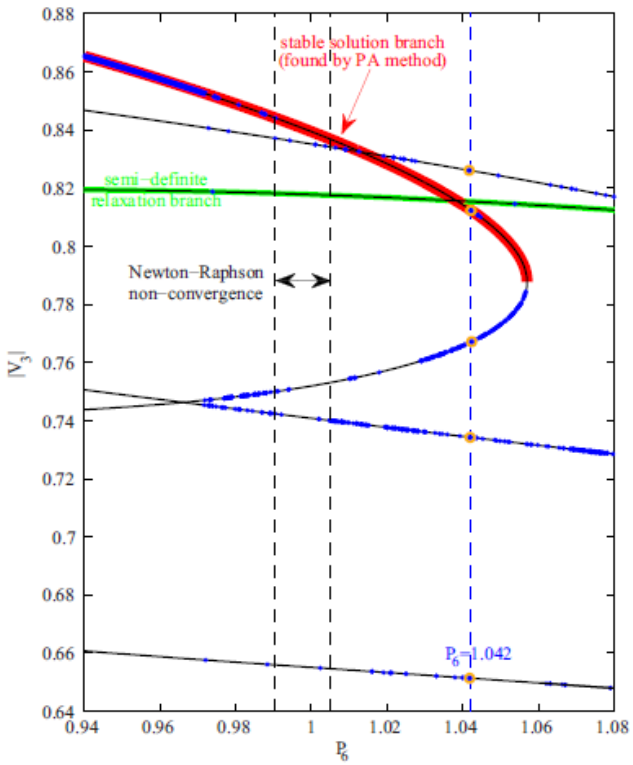

Figure 2-2. Bus 3 voltage stability limit, N-R vs HELM comparison.
Inset from Fig. 2-1. Voltage $|\boldsymbol{V_3}|$as a function of P6. N-R (blue), HELM (red) [12].

That is, the limit of these approximants are the branching points that will determine the voltage stability limit of the system or buses in question. Some of its basic equations are

presented in the next chapter, “Robust Padé approximations for the Holomorphic embedding load flow method”.

In “Embedding the AC power flow with voltage control in the complex plane: the case of analytic continuation via Padé approximants” [12], the authors show how the holomorphic idea can be applied to a complex variable fixed in its modulus, as is the case of generator buses where the voltage magnitude is set. An interesting 7-bus example, Fig. 5-12, demonstrates the unpredictability of N-R before the voltage stability limit, where load bus 3’s absolute voltage $|V_3|$ is drawn as a function of generator bus 6’s active power P_6, acting as free parameter, see Fig. 2-1. Past $P_6 = 0.973\ pu$ N-R (the blue trace) finds physically unrealisable branches, whereas HELM, taking advantage of Padé approximants (the red trace), finds solutions on the HV branch only. Fig. 2-2 shows the details of the inset around the voltage stability limit.

This clearly depicts the multiple solutions found by the iterative method, where a low voltage branch gets some of the convergences, making uncertain the coalescence of both branches to determine the VSL. The green trace belongs to the convergence of the semi-definite relaxation method that is also discussed in [12].

In “Multi-stage holomorphic embedding method for calculating the power-voltage curve” (MSHEM) [85], a HELM method that is based on predictor-corrector steps is proposed to avoid precision issues, as reported in [26]. A HELM that uses physical germs to yield the Taylor series is required to calculate the next point on the curve as the predictor step. The step length is chosen such that a predetermined error with the actual curve is reached. The corrector step uses the holomorphic error embedding (HEE) to join the incorrect power flow solution to the accurate one when close to the nose of the P-V curve. MSHEM reached the nose of the New England 39-bus network in 3 steps when tested against CPF, employed as a benchmark, which took 228 steps.

2.4.2. Quadratic approximations

In “Continuation via quadratic approximation to reconstruct solution branches and locate singularities in the power flow problem” [27], it is demonstrated how quadratic

approximants of the Hermit-Padé type [22] have better performance than Padé approximants, since their structure resembles that of the nodal equations.

It was found in "Exploration of a scalable holomorphic embedding method formulation for power system analysis applications" [26] that the quadratic approximants can get the solution to the required tolerance using fewer terms than Padé approximants when using the correct coefficient polynomial orders. It was observed, through many structured trials, that the combination of those polynomial orders was system dependent. It was also observed that up to 32% fewer terms of the quadratic approximants were needed, compared with those of Padé's, as the loads of the 14-bus and 118-bus test systems were increasing.

2.5. Conclusions

Since the use of the Newton-Raphson (N-R) method became widespread, limitations were identified, and improvements were devised to overcome application problems. A diverse number of approaches were taken to overcome such limitations. Starting points or initial guesses of the iterative algorithm were some of the first to be identified. As with the other approaches to solve ill-conditioning, multiple solutions, proximity to voltage collapse singularity, etc, have all matured along the way as new research and improvements were realised. One of the most successful approaches is the continuation power flow (CPF), which is taken as a benchmark when new improvements or algorithms are tested. To this day, it is, perhaps, the most successful of the N-R related methods.

The use of new mathematical instruments like complex analysis has opened a new window to more robust approaches to solve the load-flow problems, giving birth to non-iterative methods such as HELM and quadratic approximations. Non-iterative methods have come to light to avoid the shortcomings of their iterative counterparts. HELM was introduced to the public in 2012 and has had many contributors making the algorithm more robust and reliable. Subsequently, Hermit-Padé quadratic approximations have been implemented to solve the load flow problem with remarkable success, though they are not yet fully explored.

The proposed DFT-Padé method brings together both approaches, N-R and the use of additional approximation algorithms, based on complex analysis which provides highly reliable convergence. In this context, the D-P method is developed and promises to give similar results to those of HELM but in the N-R environment, so N-R users can reap the benefits of non-iterative techniques.

Chapter 3: Robust Padé Approximation for HELM

A. J. Sarnari and R. Živanović, "Robust Padé approximation for the holomorphic embedding load flow," in *2016 Australasian Universities Power Engineering Conference (AUPEC)*, 2016. DOI: 10.1109/AUPEC.2016.7749303

Statement of Authorship

Title of Paper	Robust Padé Approximation for the Holomorphic Embedding Load Flow (HELM).
Publication Status	☑ Published ☐ Accepted for Publication ☐ Submitted for Publication ☐ Unpublished and Unsubmitted w ork w ritten in manuscript style
Publication Details	A. J. Sarnari and R. Živanović, "Robust Padé approximation for the holomorphic embedding load flow," in *2016 Australasian Universities Power Engineering Conference (AUPEC)*, 2016, pp. 1-6.

Principal Author

Name of Principal Author (Candidate)	Alberto J. Sarnari		
Contribution to the Paper	Developed ideas, wrote corresponding MATLAB scripts, performed simulations, analysed data, wrote manuscript, and acted as corresponding author.		
Overall percentage (%)	65		
Certification:	This paper reports on original research I conducted during the period of my Higher Degree by Research candidature and is not subject to any obligations or contractual agreements with a third party that would constrain its inclusion in this thesis. I am the primary author of this paper.		
Signature		Date	04 Nov 2018

Co-Author Contributions

By signing the Statement of Authorship, each author certifies that:

i. the candidate's stated contribution to the publication is accurate (as detailed above);

ii. permission is granted for the candidate in include the publication in the thesis; and

iii. the sum of all co-author contributions is equal to 100% less the candidate's stated contribution.

Name of Co-Author	Rastko Živanović		
Contribution to the Paper	Supervised work development reviewed and assessed manuscript.		
Signature		Date	21 January 2019

Name of Co-Author			
Contribution to the Paper			
Signature		Date	

Please cut and paste additional co-author panels here as required.

3.1. Introduction

The Load Flow methods, based on the analytic continuation principle and rational function approximations, have reached a great degree of accuracy in determining load flow states [11]. This is also true for the points near voltage collapse, which are most difficult to compute as they lie at the nose of the active power - voltage curve (i.e. the P-V curve). These methods use a bus-voltage representation, based on a Taylor series expansion in the complex domain. To ensure the accuracy of the calculated voltage at points close to voltage collapse, the Taylor series is converted into a rational function that extends its radius of convergence. These particular rational functions are the Padé approximants [22]. They provide a greater radius of convergence, as compared with the power series (i.e. Taylor expansion). They can reconstruct a complete solution branch in a complex plane using approximation at a single point.

The direct methods of calculating Padé approximants by using the coefficients of a Taylor series may not be the most computationally efficient [22], Section 2.1. Therefore, in the following sections, a novel method based on Singular Value Decomposition (SVD), which is able to find robust and optimal rational functions, is explored. It should be noted that classic direct methods of constructing the Padé approximants could have some practical problems; for example, degeneracies of the approximation may occur in which the numerator and denominator have less than the allowed degree, and this leads to several entries in the Padé table being identical, some of them matching the Taylor series of the function being approximated to less than the expected order [23]. Another complication is that in the presence of computational rounding errors, Padé approximants are subject to the appearance of spurious pole-zero pairs or "Froissart doublets" in arbitrary locations that prevent the expected efficient point-wise convergence [23].

From here on, an application of the SVD-based Padé approximation technique is proposed, alongside the corresponding numerical algorithm that goes a good way towards eliminating the problems associated with a classic Padé approximant constructor.

This topic is developed as follows: the section "Bus-voltage representation through Taylor series expansion" gives an overview of HELM, nodal equations with holomorphic

embedding in the complex parameter *z*, the importance of the germ, the convolution process to obtain the power series coefficients and their conversion into rational functions. The section "The rational approximation algorithm" describes the ill-conditioning and spurious-poles problems of the Padé approximation algorithm and gives an insight as to how to overcome them by using the SVD algorithm. Under "Simulation studies", comparisons of the classic (diagonal) Padé with the Robust Padé algorithm are shown, as well as the advantages of using Robust Padé in practical applications.

3.2. Bus-voltage representation through Taylor series expansion

As was introduced by Trias in [11], the Holomorphic Embedding Load Flow (HELM) method is based on representing the bus-voltages through a Taylor power series. In practice, a derived polynomial is used, whose coefficients' order is determined by the required bus-voltage approximation accuracy. The Taylor expansions are obtained by writing the following nodal equations, where the bus-voltages are expressed as a function of a complex variable z:

$$\sum_{k \in N} Y_{ik}\, V_k(z) = \frac{z S_i^*}{V_i^*(z^*)}, \forall\, i \in N - r, \tag{3.1}$$

where

$$\mathrm{V_k(z)} = \sum_{\mathrm{s=0}}^{\infty} \mathrm{c_s^{[k]}\, z^s}. \tag{3.2}$$

$V_k(z)$ in (3.2) is the voltage of the bus *k* in the set of all *N* buses. The slack bus *r* is used as the reference. The constants $c_s^{[k]}$ in (3.2) are the coefficients of order *s* for the bus *k* power series approximation. These voltage functions are holomorphic, and thus it is possible to guarantee an accurate approximation in the high voltage arc of the P-V curve, even in the critical area of voltage collapse, where iterative methods are not reliable [11, 12]. Introducing embedding parameter z and formulating the nodal equation (3.1) will permit computation of the coefficients of the Taylor expansions (3.2) for all bus-voltages at a point (i.e. a reference condition), called a germ solution.

3.2.1. Bus voltage Taylor series coefficients [86]

Combining (3.1) and (3.2), and introducing

$$\frac{1}{V_i^*(z^*)} = \sum_{s=0}^{\infty} d_s^{*[i]} z^s, \tag{3.3}$$

we obtained the following expression:

$$\sum_{k\in N} Y_{ik} \left(\sum_{s=0}^{\infty} c_s^{[k]} z^s\right) = z S_i^* \left(\sum_{s=0}^{\infty} d_s^{*[i]} z^s\right). \tag{3.4}$$

The first coefficients of Taylor expansions (3.2) are obtained by making the embedding variable $z = 0$,

$$\sum_{k\in N} Y_{ik}\, c_0^{[k]} = 0. \tag{3.5}$$

The $\mathrm{d_s^{*[i]}}$coefficients of the expansion representing $\frac{1}{\mathrm{V_i^*(z^*)}}$ can be obtained from the convolution formula:

$$1 = V(z)V^{-1}(z) = \left(\sum_{s=0}^{\infty} c_s^{[k]} z^s\right)\left(\sum_{s=0}^{\infty} d_s^{[k]} z^s\right). \tag{3.6}$$

So, at $z = 0$, we have $\mathrm{d_0^{*[k]}} = 1/\,\mathrm{c_0^{[k]}}$.

By taking the derivatives of (3.4) and (3.6) with respect to z and then making $z = 0$, we find the equations that will allow us to obtain successive coefficients for $c_s^{[k]}$and $d_s^{[k]}$:

$$\sum_{k\in N} Y_{ik}\, c_s^{[k]} = S_i^*\, d_{s-1}^{*[i]}, \text{ and} \tag{3.7}$$

$$d_s^{[i]} = -\frac{\sum_{t=0}^{s-1} c_{s-t}^{[i]}\, d_t^{[i]}}{c_0^{[i]}}. \tag{3.8}$$

We will have the Taylor series (3.2) for each bus when the desired orders of c coefficients have been computed. However, the radius of convergence of the polynomials (3.2) may not be large enough to ensure the correct bus-voltages' extrapolation to branch

points. The HELM method suggests the use of the Padé approximants to ensure maximal analytical continuation and extrapolation of P-V curves up to branch points. (i.e. voltage collapse points) [11]. Further information and discussion about HELM can be found in [87, 88].

3.2.2. Padé rational functions

From (3.2), $\mathrm{V}(\mathrm{z})$ for any bus can be represented as

$$\sum_{s=0}^{\infty} c_s z^s = \frac{a_0+a_1z+a_2z^2+\cdots+a_mz^m}{b_0+b_1z+b_2z^2+\cdots+b_nz^n} + O(z^{m+n+1}). \tag{3.9}$$

Normally b_0 in (3.9) is chosen to be 1. The remaining $\mathrm{m}+\mathrm{n}+1$ unknowns must fit the power series through the orders $1, \mathrm{z}, \mathrm{z}^2, \ldots, \mathrm{z}^{\mathrm{m+n}}$ [22]. By cross multiplying (3.9) we get:

$$\begin{aligned}&(b_0 + b_1z + \cdots + b_nz^n)(c_0 + c_1z + \cdots)\\ &= a_0 + a_1z + \cdots + a_mz^m + O(z^{m+n+1}).\end{aligned} \tag{3.10}$$

The coefficients of z^{m+1} to z^{m+n} of the cross product on the left-hand side will be equated to zero, and (3.10) can be expressed as the system of linear equations.

3.3. The Rational approximation Algorithm

Zeros and poles of the rational approximants (3.9) tend to accumulate on the branch cuts of the bus-voltage function in the load flow problem [11]. Therefore, their values and pattern of appearance, as the approximant order increases, may be used as indicators of voltage collapse proximity. Zero-pole distributions of the Padé approximants show the analytic structure of the bus-voltage functions and confirm the general pattern of the voltage stability margin [12]. The concentration of zeros and poles of the diagonal Padé approximant defines the closest common branch point of the bus-voltage function. This branch point is given by Fabry's theorem as the following ratio: $\lim_{\mathrm{s}\to\infty} \frac{\mathrm{c_s}}{\mathrm{c_{s+1}}}$, where $\mathrm{c_s}$ and $\mathrm{c_{s+1}}$ are consecutive coefficients of a bus-voltage power series (3.2). The rational function obtained from the bus-voltage Taylor series also helps determine the safe operating

margin by computing the distance between the operating point and the location of the closest zeros and poles [12, 27].

3.3.1. Defect and ill-posed Padé approximation

Equation (3.10) can be written as [22]:

$$p(z) = V(z)q(z) + O(z^{m+n+1}), \tag{3.11}$$

The numerator polynomial of the rational function approximation of $V(z)$ is

$$p(z) = a_0 + a_1 z + a_2 z^2 + \cdots + a_m z^m, \tag{3.12}$$

and its denominator

$$q(z) = b_0 + b_1 z + b_2 z^2 + \cdots + b_n z^n, \tag{3.13}$$

where the "big O" is the order of the first non-zero term in the difference $V(z) - \frac{p(z)}{q(z)}$.

Normalization is usually done by a coefficient condition such as $\mathrm{b}_0 = 1$, whereupon what remains in (3.11) is a system of linear equations that may be highly ill-conditioned or singular. Instead, we can normalize by using the condition $\|\mathbf{b}\| = 1$, where $\|\mathbf{b}\|$ is the 2-norm vector of the coefficient vector $\mathbf{b}$ [89]. This normalization will help eliminate problems of singularity and ill-conditioning [23]. The Padé approximation is ill-posed if the rational function, which represents the Taylor polynomial of the bus-voltage expressed with degrees m and n, of $p(z)$ and $q(z)$ respectively, has a defect $\delta > 0$. The defect is defined as

$$\delta = min\{m - \mu, n - v\}. \tag{3.14}$$

In exact arithmetic, the degrees μ and v are defined, such that $\mu \leq m$ and $v \leq n$, and match $f(z)$ as far as possible [23]. The reason is that an arbitrarily small perturbation could fracture the block, forcing the rational function approximation to match the bus-voltage function to a higher order than before. For details see [90, 91].

3.3.2. Removal of spurious poles via SVD-based Padé approximation

How can a pole-zero pair be spurious? The formal definition of spurious poles is given in [92]. In the simplest case, we assume $f(z)$ is a meromorphic function in the complex plane *C*, and we consider the behaviour of $f(z) - r_{mn}$, where $r_{mn} = \frac{p(z)}{q(z)}$, as $m, n \to \infty$. It could be expected that for a compact set, disjointed from the poles of $f(z)$, the supremum norm of $f(z) - r_{mn}$ should converge to zero. However, this does not happen in general. The Padé approximants $\mathrm{r_{mn}}$ can have poles in arbitrary locations in *C*, and as $m, n \to \infty$. Although the residues of these poles will decrease, they may never disappear entirely. In fact, it may even happen that the diagonal type of the Padé approximants to a fixed entire function $f(z)$ have so many spurious poles that the sequence of approximants is unbounded at every nonzero point in the complex plane [23].

Arbitrary small perturbations in the Taylor series coefficients (i.e. rounding errors) could lead to cases where the rational function approximation will match the bus-voltage power series to a higher degree [1, 90]. As a rule of thumb, approximately n decimal places of accuracy are lost in the calculation of an $[m/n]$ approximant by direct solution of the linear system. This means that approximately *n* extra decimal places of precision are required for the data coefficients $c_{m-n+1}, c_{m-n+2}, \dots, c_{m+n}$ than is expected of the solution coefficients $b_0, b_1, \dots, b_n$ [22].

If the equations are rank degenerate, caused by m and n being bigger than they should be, there is a multiplicity of solutions. Conversely, if the equations appear numerically to have a full row rank n, there is no problem and the solution is said to be unique [22]

A central feature of the Robust Padé algorithm is that it removes spurious poles (i.e. Froissart doublets) as a by-product of the use of numerical ranks computed with the SVD [23]. This algorithm also produces the absolute value of the residue for each pole, which can suggest how to distinguish genuine from spurious values, introduced by rounding errors.

The system of equations (3.10) can be written in the following matrix form:

$$\begin{bmatrix} a_0 \\ a_1 \\ \vdots \\ a_n \\ \vdots \\ a_m \\ \hline a_{m+1} \\ \vdots \\ a_{m+n} \end{bmatrix} = \begin{bmatrix} c_0 & & & \\ c_1 & c_0 & & \\ \vdots & & \ddots & \\ c_n & c_{n-1} & \cdots & c_0 \\ \vdots & \vdots & & \vdots \\ c_m & c_{m-1} & \cdots & c_{m-n} \\ \hline c_{m+1} & c_m & \cdots & c_{m+1-n} \\ \vdots & \vdots & \ddots & \vdots \\ c_{m+n} & c_{m+n-1} & & c_m \end{bmatrix} \begin{bmatrix} b_0 \\ b_1 \\ \vdots \\ b_n \end{bmatrix}, \tag{3.15}$$

where,

$$\begin{bmatrix} a_{m+1} \\ \vdots \\ a_{m+n} \end{bmatrix} = \begin{bmatrix} 0 \\ \vdots \\ 0 \end{bmatrix}. \tag{3.16}$$

Normalisation is typically done by setting a coefficient $b_0 = 1$, so a system of linear equations (3.15) may be highly ill-conditioned or singular. Instead, following [89], we normalize using the condition $\|\mathbf{b}\| = 1$, where $\|\cdot\|$ is the 2-norm vector. This normalisation will help eliminate problems of singularity and ill-conditioning [23].

Vector $\mathbf{b}$ values, of $q(z)$ polynomialsin (3.11), are obtained by solving the system below the dotted line in (3.15)

$$0 = \tilde{\boldsymbol{C}}\boldsymbol{b}, \tag{3.17}$$

where for known m and n,

$$\tilde{\boldsymbol{C}} = \begin{bmatrix} c_{m+1} & c_m & \cdots & c_{m+1-n} \\ \vdots & \vdots & \ddots & \vdots \\ c_{m+n} & c_{m+n-1} & & c_m \end{bmatrix}. \tag{3.18}$$

Applying the SVD to $\tilde{\mathbf{C}}$, the following factorization is obtained:

$$\tilde{\boldsymbol{C}} = \boldsymbol{U}\boldsymbol{\Sigma}\boldsymbol{V}^T, \tag{3.19}$$

where U is $(n \times n)$ and unitary matrix, V, is $(n+1) \times (n+1)$ also unitary matrix, and $\boldsymbol{\Sigma}$ is an $n \times (n+1)$ real diagonal matrix with diagonal entries $\sigma_1, \sigma_2, \ldots, \sigma_n \geq 0$. If $\sigma_n > 0$, then

$\widetilde{\boldsymbol{C}}$ has rank n, and the final column of $\boldsymbol{V}$ provides a unique nonzero null vector $\boldsymbol{b}$ of $\widetilde{\boldsymbol{C}}$ up to a scale factor. This null vector defines the coefficients of the polynomial q [23]. If $\sigma_n = 0$, $\widetilde{\boldsymbol{C}}$ must have rank $\rho < n$ with zero singular values $\sigma_{\rho+1} = \cdots = \sigma_n = 0$. Then $\widetilde{\boldsymbol{C}}$ has a rank ρ and the defect of the rational function is at least $(n - \rho)$, and we can reduce the degree of the q polynomial from n to ρ, and the degree of the p polynomial from m to $m - (n - \rho)$ [23]. The resulting algorithm will produce a unique Padé approximant in a minimal degree representation. More details of the algorithm are presented in [23].

Recapping the matrix work to find the coefficients a and b of $p(z)$ and $q(z)$ in (3.11): once the σ singular values are calculated in (3.19) and those smaller than the specified tolerance (they are considered to be zero) are discarded. Then, the matrix of (3.15) is reformulated using the first ρ coefficients of the voltage power series $V(z)$. Therefore, the last $(n - \rho)$ columns and rows of the original matrix will disappear. This process is repeated until all singular values σ remain above the specified tolerance value. In other words, only the linearly independent columns of (3.15) are left [27]. The values of vector $\boldsymbol{b}$ are then extracted from the last column of matrix $\boldsymbol{V}$ (3.19), which are the least square solutions [27]. The values of vector $\boldsymbol{a}$ are then calculated using (3.15) above the line.

The Robust Padé algorithm also caters for noisy data, whether intrinsic to the data or rounding errors: it treats singular values as zero if they are less than a specified tolerance computed as $tol * \|\boldsymbol{c}\|$, where $c = [c_0, \ldots, c_{m+n}]^T$ is the vector of power series coefficients, and tol is the problem dependent parameter. Rounding errors or other perturbations commonly introduce Froissart doublets, which do not reflect genuine information about the specific function. The algorithm presented removes such an effect by reducing the degrees of m and n to optimal values.

3.4. Simulation study

To compare the classical Padé approximation algorithm and the robust version based on the SVD, we selected a 3-bus power system as presented in [12] and shown in Figure 3-1.

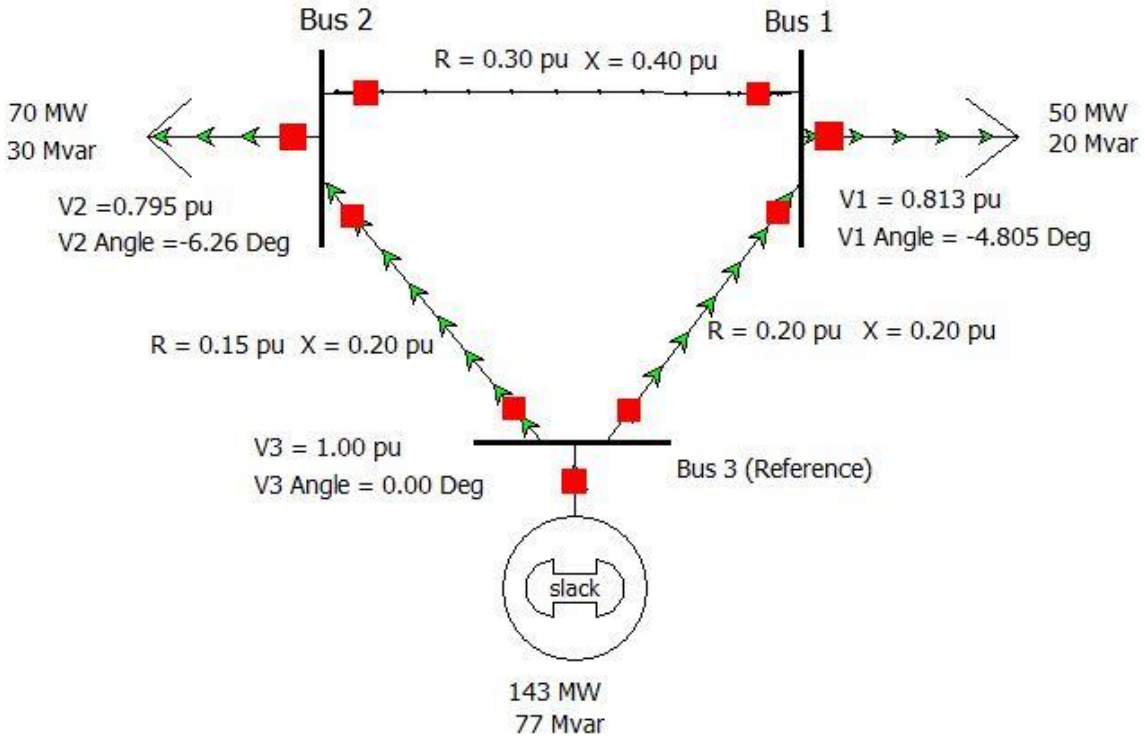

Figure 3-1. 3-bus system for the analysis of bus 1 state variables
Drawing obtained from PowerWorld [81].

The following Figures, 3-2 and 3-3, show the rate of convergence of the bus 1 voltage power series constructed at a nominal loading condition, and the locations of poles and zeros of the resulting classic (diagonal) Padé rational function, respectively. The voltage power series has been constructed with 201 coefficients, consequently the diagonal Padé approximant has 100 poles and 100 zeros. The poles (crosses) and zeros (small circumferences) in Figure 3-3, that lie concentrically around the zero point, cancel one another out. They are the Froissart doublets as defined in [93]. The embedding parameter used in this approximation was the active power at bus 1. The Robust Padé algorithm has been used to determine the poles and zeros of the rational function for bus 1 voltage.

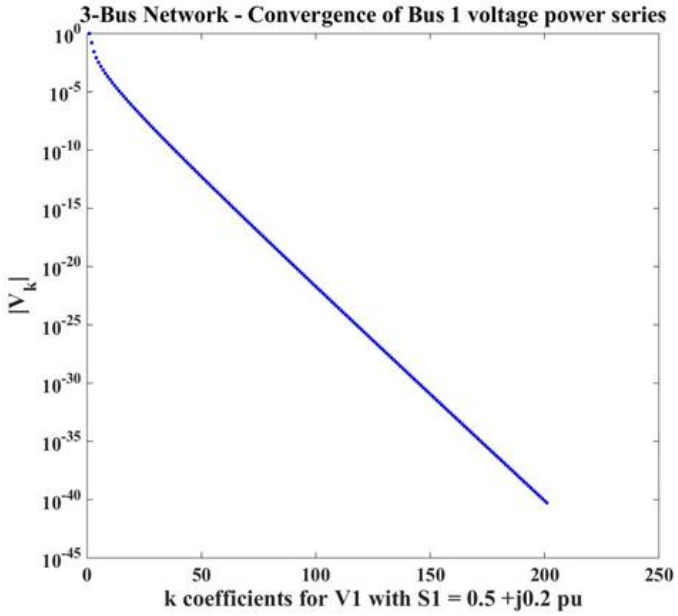

Figure 3-2. Convergence of 201 power series coefficients.
$|V_1|$ bus 1 voltage at base load using HELM [86].

The rational function approximation with nine poles and nine zeros will approximate the voltage function for bus 1 at the given base load. Critical poles and zeros are shown in Figure 3-4, and all 9 values are listed in Table 3-1.

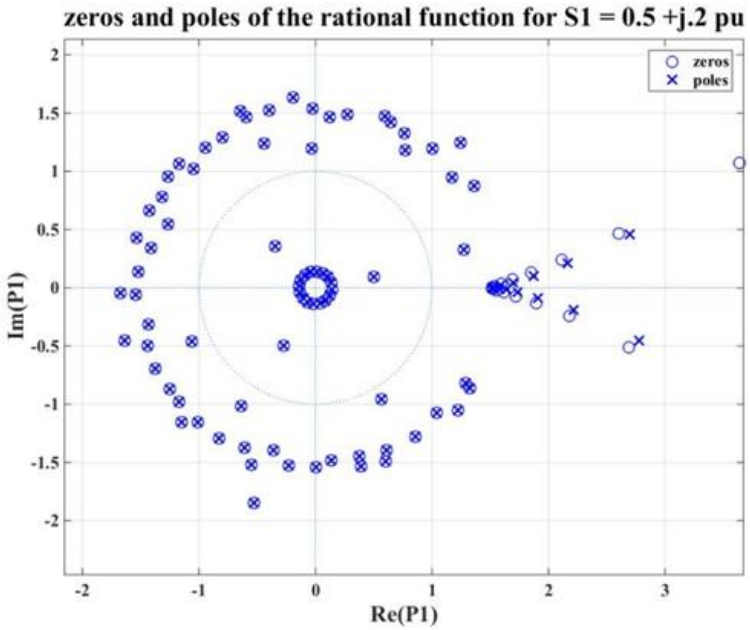

Figure 3-3: Poles and zeros of the rational function.
Padé direct method. No. of coefficients = 201, 100 poles and 100 zeros

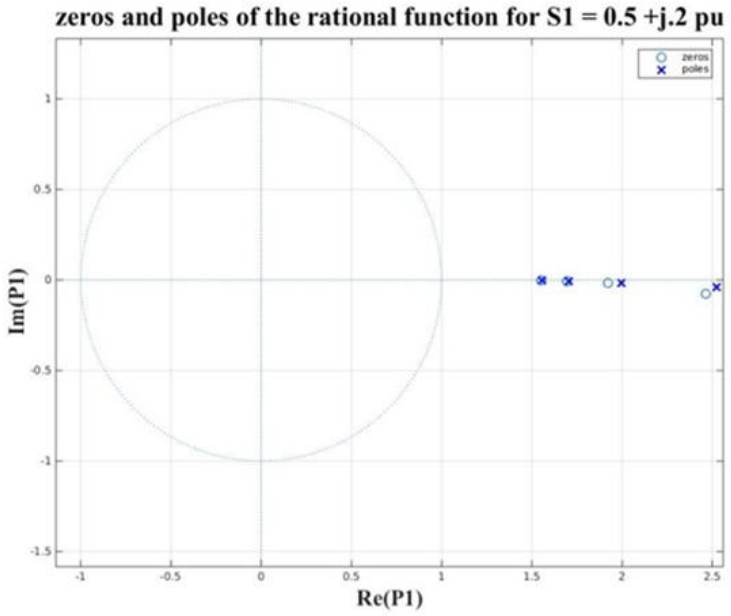

Table 3-1: Poles and zeros of Padé approximant. Voltage at bus 1, including stability limit.

-39.1511 -13.2294i
22.2097 -40.3922i
12.6390 - 2.6372i
5.8175 - 0.4208i
3.5440 - 0.1167i
2.5243 - 0.0407i
1.9947 - 0.0152i
1.7051 - 0.0052i
1.5567 - 0.0011i

Branching point at p = 1.5567

Figure 3-4: Nine poles and zeros using Robust Padé for the 3-bus system.

Figure 3-5 shows the application of analytic continuations (i.e. extrapolations of bus 1 voltage magnitudes vs bus loads at fixed power factors), by using the rational function with 9 poles and zeros, when varying the active power at bus 1 in the range p = -2 to 1.56. A power value of 0.5 is the germ value of the analytic function used to calculate the function approximation, well away from the convergence radius of the power series [11].

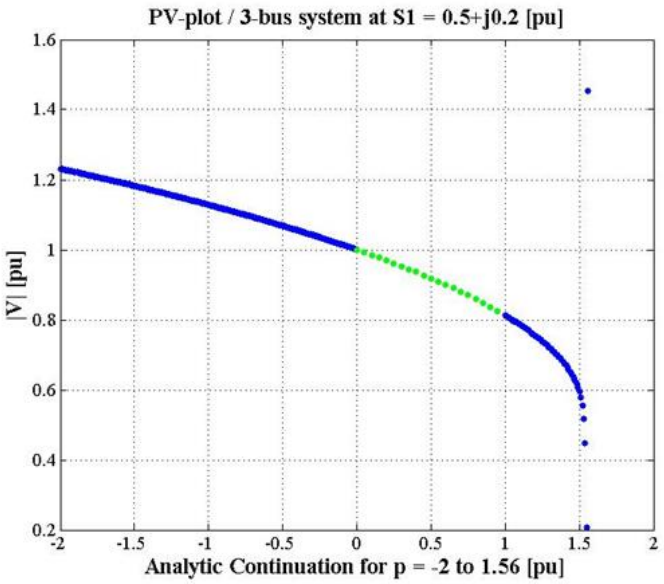

Figure 3-5: $|\mathbf{V_1}|$ voltage analytic continuation vs active power p at bus 1

It can be seen in Figure 3-5 that the nose of the PV-curve is at the value given by the zero closest to the origin in Fig. 3.4, i.e. p = 1.5567, which is the approximation to the voltage stability limit.

Another way of finding the maximum power transfer is doing binary searches varying the parameter $\mathbf{z}$ in the rational function until the boundary is reached, after which the power balance equations are not maintained as per the HELM formulations presented in [13]. This active power limit is sometimes called saddle-node bifurcation point where the $\frac{\mathrm{dV}}{\mathrm{dP}} \rightarrow \infty$. If Newton-Raphson was used to solve the load flow, its Jacobian matrix would be singular. In practice, this matrix normally becomes ill-conditioned before reaching the vertical tangent point to the P-V curve. Saddle node refers to the turning point of the P-V curve, see Figs 1-1 and 1-2, where the low voltage branch meets the high voltage branch. The term is used to characterise the behaviour of solutions in differential equations [42] (dynamic systems).

The other type of voltage collapse, called-limit induced bifurcation can take place when the generator reactive power reaches its limit, (and not typified by the singularity of the Jacobian matrix in the Newton-Raphson algorithm) [94]. The determination of this limit acquires even more significance when it is far from the saddle-node bifurcation point. A HELM method to determine the limit-induced bifurcation is presented in [26], and also discussed in [95].

3.5. Conclusions

Steady-state voltage stability margin approximations can be reliably determined using the inner-most zero/pole location of the rational function of all bus-voltages in a power system. In this chapter, it has been shown how the classic algorithms for constructing Padé approximations in the HELM load flow algorithm can be ill-posed. As a result of using such a method, the degrees of the rational approximation numerator and denominator are greater than physically required and such representation becomes very sensitive to any type of noise, including round-off errors. It has also been shown how the application of the SVD algorithm can solve the problem of ill-posed equations. The SVD-based Robust Padé approximation algorithm can determine reliably the exact rank of the problem and

will avoid multiple solutions and remove all spurious poles from the rational function approximation.

Chapter 4: DFT-Padé mathematical foundations

A. J. Sarnari and R. Živanović, "Reliable steady state voltage stability limit estimation using Newton-Raphson-based method," in *2017 Australasian Universities Power Engineering Conference (AUPEC)*, 2017. DOI: 10.1109/AUPEC.2017.8282450

Statement of Authorship

Title of Paper	Reliable Steady State Voltage Stability Limit Estimation using Newton-Raphson-based Method
Publication Status	☑ Published ☐ Accepted for Publication ☐ Submitted for Publication ☐ Unpublished and Unsubmitted work written in manuscript style
Publication Details	A. J. Sarnari and R. Živanović, "Reliable steady state voltage stability limit estimation using Newton-Raphson-based method," in *2017 Australasian Universities Power Engineering Conference (AUPEC)*, 2017, pp. 1-6.

Principal Author

Name of Principal Author (Candidate)	Alberto J. Sarnari		
Contribution to the Paper	Developed ideas, wrote corresponding MATLAB scripts, performed simulations, analysed data, wrote manuscript, and acted as corresponding author.		
Overall percentage (%)	65%		
Certification:	This paper reports on original research I conducted during the period of my Higher Degree by Research candidature and is not subject to any obligations or contractual agreements with a third party that would constrain its inclusion in this thesis. I am the primary author of this paper.		
Signature		Date	17 January 2019

Co-Author Contributions

By signing the Statement of Authorship, each author certifies that:

i. the candidate's stated contribution to the publication is accurate (as detailed above);

ii. permission is granted for the candidate in include the publication in the thesis; and

iii. the sum of all co-author contributions is equal to 100% less the candidate's stated contribution.

Name of Co-Author	Rastko Živanović		
Contribution to the Paper	Supervised work development reviewed and assessed manuscript.		
Signature		Date	21 January 2019

Name of Co-Author			
Contribution to the Paper			
Signature		Date	

Please cut and paste additional co-author panels here as required.

4.1. Introduction

This chapter discusses the mathematical foundations and technicalities to make possible the use of the Newton-Raphson (N-R) method combined with the discrete Fourier transform and Robust Padé approximation (DFT–Padé) to obtain the high voltage (HV) solution branch for load buses, as well as the voltage stability limit of a power system. This is of potentially great advantage to existing N-R based software users because the problem of Jacobian matrix singularity at the voltage collapse point is avoided.

In the next two chapters, an alternative method based on the use of the existing Newton-Raphson (N-R) algorithm and the application of the Discrete Fourier Transform (DFT) to find the loading range of each load bus in the system and their saddle-node bifurcation points (SNBP) is proposed. As will be shown below, minor modifications to the Jacobian matrix may be needed to satisfy the mathematical requirements of the method. In addition to N-R based load flow software, the proposed method integrates the tool that finds the best approximation to the solution branch of load buses using rational functions of the Robust Padé type [96].

4.2. Mathematical foundations of the DFT-Padé load-flow method

The following discussion is based on the works of Živanović [27], Trefethen, Austin, Kravanja [97], Trefethen and Weideman [98], and Curtiss [99]. These works encompass the approximation of analytic or meromorphic functions sampled at the roots of unity in the unit disk. In this case, the functions in question are the bus voltages expressed first as Taylor series and then as Fourier series, whose coefficients are calculated by the trapezoidal rule and the Discrete Fourier Transform, using the Fast Fourier Transform (FFT). These algorithms provide accurate solutions when the problems at hand can be defined within the constraints of the algorithms' applicability, as will be shown below.

First, the advantages of sampling the voltage function to be approximated by a polynomial (truncated Taylor series) at the roots of unity, or at a circle where the radius is bigger or smaller than 1. Then, what happens, in terms of convergence properties when those approximants are constructed using harmonic functions. Lastly, what behaviour is

expected when the coefficients of those harmonic functions are obtained using the Trapezoidal rule. These are the three main pillars of the DFT-Padé method that justify its robustness. Equations are presented, and the nodal equations are revisited under the lights of the method, and its computational process is described step by step.

4.2.1. Roots of unity on the unit disk

The following explanation refers to the bus-voltage function which is to be approximated using tools of complex analysis and starts with a generic example where the function domain is an open disk.

It is assumed that a function $f(z)$, analytic in the open disc D_R with radius $R > 1$, can be approximated for any value of the z in the disk $\{z \in C : |z| < R\}$. The approximation technique used is the power series or truncated polynomial and then its conversion to rational interpolation for its improved convergence properties [97]. The available information is a set of sampled values $\{f_k\}$ of the actual functions at n roots of unity points $\{z_k\}, 0 < k < n-1$ and $z_k = e^{2\pi jk/n}$, where j is the imaginary unit.

The polynomial interpolation approaches $f(z)$ by $p(z)$, where $p \in P_{n-1}$ (the set of polynomials of degree less or equal to $n-1$) is the unique polynomial interpolant of f at the roots or unity $\{z_k\}$. If the Taylor series is used,

$$p(z) = \sum_{k=0}^{\infty} c_k z^k , \tag{4.1}$$

and the coefficients c_k are defined in the unit disk S using the Cauchy integral:

$$(2\pi i)^{-1} \int_S (\zeta - z)^{-1} f(\zeta) d\zeta . \tag{4.2}$$

If f is defined within a disk D_ρ and $\rho < R$, the uncertainty in the determination of the coefficients according to Cauchy's estimate is

$$|c_k| = O(\rho^{-k}), k \to \infty. \tag{4.3}$$

Truncating the series to $n-1$ degree, the resulting polynomial can be written as

$$p_{n-1}(z) = \sum_{k=0}^{n-1} c_k z^k \,, \tag{4.4}$$

and for any z within D_ρ the error is given by

$$|f(z) - p_{n-1}(z)| = O((|z|/\rho)^n), n \to \infty. \tag{4.5}$$

Given that $|z| < \rho$, the error in the approximation is very small. The Taylor polynomial coefficients can be calculated through the Fast Fourier Transform (FFT) with MATLAB notation:

$$\boldsymbol{c} = FFT(f_k)/n. \tag{4.6}$$

Where the trapezoidal rule is applied to (4.2) n times simultaneously to calculate the $\boldsymbol{c}$ vector of Taylor coefficients in reverse order (highest degree first). The trapezoidal rule has geometric convergence (4.5) for analytic functions, and its natural place of application is to integrals defined over circles in the complex domain, for instance, $z = e^{j\theta}$, where j is the imaginary unit. The Taylor coefficients can then be defined by the following approximation:

$$c_i^n = \frac{1}{n} \sum_{k=1}^{n} z_k^{-i} f_k, \; i = 0, 1, 2, \ldots, n-1 \,, \tag{4.7}$$

where there are n roots of unity $z_k = e^{2\pi jk}$ that define the coefficient c_i^n of order (degree) i. Polynomial interpolants in the roots of unity are maximally convergent [97]. The geometric convergence of (4.5) reflects the fact that the accuracy increases exponentially with the number of roots of unity used. It can also be said that calculating the c_i^n Taylor coefficient is equivalent to evaluating the derivative of ith order at $z = 0, f^i(0) = i!\, c_i^n$ (or other value-centred series). The same convergence rate applies to the calculation of the derivatives using the trapezoidal rule. If the Taylor series is not centred at 0, the contour integral will not have a pole at 0 but at ζ, according to (4.2), where $|\zeta| < 1$.

4.2.2. When the radius of convergence is different from 1

If the sampling of f happens on a disk of radius $R > 1$ then the convergence rate improvement is $O((1/R)^n)$. Convergence could be accelerated even further if the complex variable z is scaled by a factor $\tau < 1$, making it $O\left(\left(\frac{\tau}{R}\right)^n\right)$. However, there may be problems of ill-conditioning for floating-point arithmetic. They become increasingly evident when trying to compute higher order terms of the Taylor series. It has also been shown that an optimal choice of τ can eliminate ill-conditioning.

4.2.3. Interpolation by harmonic polynomials

A function defined within a certain complex domain of a smooth first derivative and sampled at $2n + 1$ points, can be replicated by a harmonic polynomial of maximum degree n that is uniquely determined and converges at an exponential rate. The interpolation to the continuous function is on the closed domain boundary, where the convergence ensues. If the choice of sampling points is on the roots of unity, the convergence is maximised [99].

4.2.4. How to reconstruct an aperiodic curve: Fourier Series and Transforms

A periodic function $f(t)$ of period T can be represented by Fourier series as

$$\sum_{k=-\infty}^{\infty} c_k e^{2\pi jkt/T} , \tag{4.8}$$

where k takes positive integers $1, 2, 3, \ldots$. These numbers can be associated with harmonic multiples of the fundamental frequency $k = 1$. t is the independent variable that can take the time dimension. c_k is the terms' coefficient that can be complex-valued. Each coefficient c_k is calculated using the following integral,

$$c_k = \hat{f}(k) = \frac{1}{T}\int_0^T e^{-2\pi jkt/T} f(t)dt , \tag{4.9}$$

with $\hat{f}(k)$ being its alternative notation.

If the function to be represented is not periodic, then $T \to \infty$, and the different harmonics k/T are replaced by the new variable s. Such coefficients are to be obtained by (4.10)

$$\hat{f}(s) = \int_{-\infty}^{\infty} e^{-2\pi jst} f(t)dt, \tag{4.10}$$

"periodising" $f(t)$ [100], that is, representing the aperiodic function with harmonic components. This process is known as the Fourier transform. It produces a continuum of frequencies and opens the doors to many possible applications. The inverse Fourier transform that will allow the recovery $f(t)$ is in (4.11)

$$f(t) = \int_{-\infty}^{\infty} e^{\mathrm{j}2\pi st} \hat{f}(s)ds, \tag{4.11}$$

The discrete Fourier transform (DFT) was born from the need to have a fast and efficient means to calculate the transform. Instead of thinking in terms of "sampled values", it can be thought of as a process that takes a vector of N numbers as inputs $\boldsymbol{f} = (f[0], f[1], \ldots, f[N-1])$ and returns another $N-tuple$ vector of numbers as outputs $\boldsymbol{F} = (F[0], F[1], \ldots, F[N-1])$ and defined by

$$\boldsymbol{F}[m] = \sum_{k=0}^{N-1} f[k]\, e^{-\mathrm{j}2\pi km/N}, m = 0, 1, 2, \ldots, N-1, \tag{4.12}$$

the $f[k]$ are the values of the f function at N different points of the domain where f is defined. The equation implies the addition of every function value multiplied by the inverse of the roots of unity at the corresponding power [100]. $k = 0$ would correspond to the direct current component of the frequency spectrum.

The computational complexity of the method in terms of floating-point operations is N^2 for an N points-based DFT. One of the decisive factors that made the practical Fourier so useful is the fast Fourier transform algorithm, a highly efficient way to calculate the DFT. The computation work involved in its calculation is approximately $N * logN$ arithmetic operations [101].

4.3. Application to load-flow problem

We look for the representation of the bus voltage, or its absolute value, as a function of the active power injected into the bus in question. Figure 4-1 shows such a representation which consists of three entities: the high voltage branch or stable solution is represented by the blue trace, the branching point, dot at the intersection, and low voltage branch or unstable solution is represented by the green trace [16, 17]. Conventional load-flow programs solve the bus-voltage for the given active power by an initial guess or point for each bus to start the iteration process.

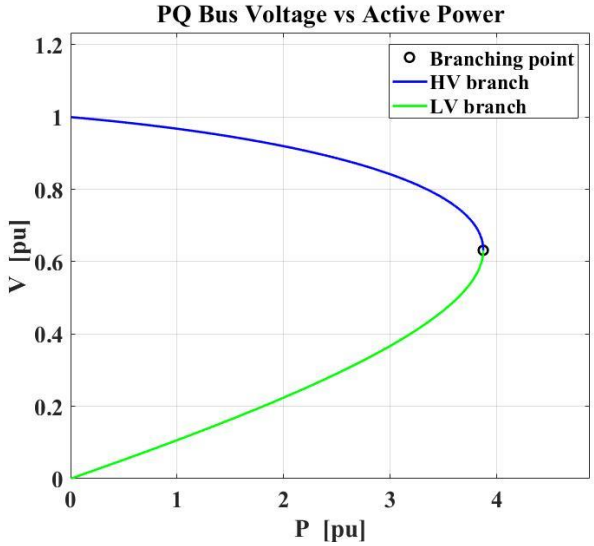

Figure 4-1: P-V curve for load bus at constant power factor

There are two voltage solutions for each value of active power within the range defined to the branching point, where there is only one solution and the voltage slope becomes vertical. The solution sought and starting point are usually close, so the process converges successfully.

The approach taken here considers the HV absolute value being approximated by a power series (4.13). Approximations to continuous functions on a bounded interval can get arbitrarily close when approximated by polynomials, according to Weierstras' theorem [102]:

$$|V(P)| = \sum_{k=0}^{\infty} h_k (P - P_c)^k. \tag{4.13}$$

This series expansion is an analytic function within its radius of convergence R, for $|P - P_c| < R$, where P can be any active power value within R, and P_c is its bus load. This assertion has a direct implication on the left-hand side (LHS) of (4.13) in terms of feasible voltage values for the system in question. Coefficients h_k of the series (4.13) are obtained by considering the bus active power *P* in the complex plane (4.7) and [27]:

$$P(\theta) = P_c + re^{j\theta}, \tag{4.14}$$

where r is selected so that P_c and the circular contour of $P(\theta)$ is within the radius of convergence R. It is shown by Walsh, Curtiss and others [97, 99] that the resulting polynomial obtained by (4.15) below, will have maximal convergence.

Replacing $P(\theta)$ in (4.13), a trigonometric series is obtained. This will allow us to obtain the Taylor series coefficients using the discrete Fourier transform (DFT):

$$\left|V(P_c + re^{j\theta})\right| = \sum_{k=0}^{\infty} h_k r^k e^{jk\theta}, \tag{4.15}$$

where, $\left|V(P_c + re^{j\theta})\right|$ is a 2π-periodic function or a Fourier series, whose coefficients are given by [100]:

$$h_k r^k = \frac{1}{2\pi}\int_0^{2\pi} \left|V(P_c + re^{j\theta})\right| e^{-jk\theta} d\theta. \tag{4.16}$$

These, $h_k r^k$, are scaled coefficients of the Taylor series given in (4.13). The h_k coefficients are numerically computed by approximating the integral (4.16) using the composite trapezoid rule [98] with *N* equidistant points $\theta_l = \frac{2\pi l}{N}$:

$$h_k = \frac{1}{r^k}\left[\frac{1}{N}\sum_{l=0}^{N-1} \left|V\left(P_c + re^{j\theta_l}\right)\right| e^{-jk\theta_l}\right], \tag{4.17}$$

where $l = 0, \ldots, N-1$. The expression between brackets [ ] is equivalent to the Discrete Fourier Transform (DFT) [100]. Computation of these *N* coefficients is possible using the Fast Fourier Transform (FFT) algorithm. The values $\left|V\left(P_c + re^{j\theta_l}\right)\right|$ are obtained through the Newton-Raphson method for every one of the resulting $(P_c + re^{j\theta_l})$. In other words,

these $\overline{|V(\theta_l)|}$ are samples of the voltage function in the complex domain. Once those voltage samples have been obtained, the approach is to compute consecutive FFTs of $N = 2^k$ points θ_l, for $k = 2, 3, 4, \ldots$ until the coefficients h_k converge within a given tolerance. So, the first round, *k* = 2 will give four h_k coefficients, then their convergence is tested. This process continues until convergence is achieved. This means that some of the coefficients of the last round may be below tolerance, and so they get trimmed. To make the algorithm manageable, the required number of sample points, $P(\theta_l) = P_c + re^{j\theta_l}$, is kept to a minimum, since each sample is a run of the N-R algorithm.

Recapping this load flow application equations and their correspondence with those of the mathematical concepts in subsection 4.2, the following can be said:

- The power series coefficients c_k of (4.1) correspond with the coefficients h_k of (4.13).

- The sampling of the voltage continuous function, $|V(P)|$ in (4.13) or $p(z)$ in (4.1), is done in z_k roots of unity, or $P(\theta) = P_c + re^{j\theta}$ (4.14), in a radius $r < R$ radius of convergence of the series. As can be seen, the complex active power is a mathematical artifice, as well as the voltage complex absolute value $\left|V(P_c + re^{j\theta})\right|$ in (4.15) as a result of the Fourier series representation. However, the FFT returns real coefficients for (4.13).

4.3.1. Nodal equations

Active and reactive power are real functions of real variables in conventional N-R, but they are a real function of complex variables as required by the D-P method. Nodal equations are written to preserve the integrity of the bus voltage complex absolute values as well as the complex expressions of the active and reactive power alike. These are mathematical artifices that return to their real values by virtue of the FFT for the final expression of the bus-voltage in Taylor series.

The voltages $\overline{|V(\theta_l)|}$ are complex values, indicated with a long dash, since they are the summation of the product by complex exponential functions (4.15), so is the active power $P(\theta)$ (4.14). Reactive power is also a complex magnitude $Q(\theta) = a * P(\theta)$. Factor $a =$

$\frac{base\ P}{base\ Q}$ is a scalar number. A 3-bus system is used as an example of an application. The bus currents, for such a model using MATLAB notation, are:

$$\begin{bmatrix} y_{11r}+jy_{11i} & y_{12r}+jy_{12i} & y_{13r}+jy_{13i} \\ y_{21r}+jy_{21i} & y_{22r}+jy_{21i} & y_{23r}+jy_{23i} \\ y_{31r}+jy_{31i} & y_{32r}+jy_{32i} & y_{33r}+jy_{33i} \end{bmatrix} * \begin{bmatrix} \overline{|V_1|}cos\delta_1 + j\overline{|V_1|}sin\delta_1 \\ \overline{|V_2|}cos\delta_2 + j\overline{|V_2|}sin\delta_2 \\ \overline{|V_3|}cos\delta_3 + j\overline{|V_3|}sin\delta_3 \end{bmatrix}, \quad (4.18)$$

where $y_{12r}+jy_{12i}$ is the admittance between buses 1 and 2, $\overline{|V_1|}$ is the voltage complex absolute value and δ_1 voltage angle for bus 1, making $\overline{|V_1|}cos\delta_1$ and $\overline{|V_1|}sin\delta_1$ the active and reactive components of the said voltage; "*" is the matrix multiplication sign. The expression of the resulting current for bus 1 is:

$$\bar{I}_{C1} = \begin{bmatrix} (y_{11r}\overline{|V_1|}cos\delta_1 - y_{11i}\overline{|V_1|}sin\delta_1) + & j(y_{11r}\overline{|V_1|}sin\delta_1 + y_{11i}\overline{|V_1|}cos\delta_1) + \\ (y_{12r}\overline{|V_2|}cos\delta_1 - y_{12i}\overline{|V_2|}sin\delta_2) + & j(y_{12r}\overline{|V_2|}sin\delta_2 + y_{12i}\overline{|V_2|}cos\delta_2) + \\ (y_{13r}\overline{|V_3|}cos\delta_3 - y_{13i}\overline{|V_3|}sin\delta_3) + & j(y_{13r}\overline{|V_3|}sin\delta_3 + y_{13i}\overline{|V_3|}cos\delta_3) \end{bmatrix}, \quad (4.19)$$

where $\bar{I}_{C1} = \bar{I}_{C1r} + j\bar{I}_{C1i}$ is the current phasor based on voltage complex absolute value split into its two components. The writing can be simplified and generalized by using vectorized MATLAB notation:

$$\bar{\boldsymbol{I}}_{\boldsymbol{C}} = (\boldsymbol{rY} * \boldsymbol{Vr} - \boldsymbol{iY} * \boldsymbol{Vi}) + j(\boldsymbol{rY} * \boldsymbol{Vi} + \boldsymbol{iY} * \boldsymbol{Vr}) \quad (4.20)$$

with the following descriptions:

$\bar{\boldsymbol{I}}_{\boldsymbol{C}}$	Vector of bus currents based on voltage complex absolute values.
$\boldsymbol{rY}, \boldsymbol{iY}$	Line conductance and susceptance matrices respectively.
$\boldsymbol{Vr}, \boldsymbol{Vi}$	Vectors of bus active and reactive voltage complex absolute values.

And their expressions from the example above are:

$$\boldsymbol{rY} = \begin{bmatrix} y_{11r} & y_{12r} & y_{13r} \\ y_{21r} & y_{22r} & y_{23r} \\ y_{31r} & y_{32r} & y_{33r} \end{bmatrix}, \boldsymbol{iY} = \begin{bmatrix} y_{11i} & y_{12i} & y_{13i} \\ y_{21i} & y_{21i} & y_{23i} \\ y_{31i} & y_{32i} & y_{33i} \end{bmatrix}, \tag{4.21}$$

for the line conductance matrix and line susceptance matrix. The bus active and reactive voltage absolute values are:

$$\boldsymbol{Vr} = \begin{bmatrix} \overline{|V_1|} cos\delta_1 \\ \overline{|V_2|} cos\delta_2 \\ \overline{|V_3|} cos\delta_3 \end{bmatrix}, \boldsymbol{Vi} = \begin{bmatrix} \overline{|V_1|} sin\delta_1 \\ \overline{|V_2|} sin\delta_2 \\ \overline{|V_3|} sin\delta_3 \end{bmatrix}. \tag{4.22}$$

The corresponding vector of the buses' apparent power can be expressed as:

$$\boldsymbol{S_C} = (\boldsymbol{Vr} + \boldsymbol{jVi}).* (\boldsymbol{I_{Cr}} + j\boldsymbol{I_{Ci}})^*, \tag{4.23}$$

Effecting the multiplication, the equation becomes:

$$\boldsymbol{S_C} = \boldsymbol{P_C} + \boldsymbol{jQ_C} = (\boldsymbol{Vr}.* \boldsymbol{I_{Cr}} + \boldsymbol{Vi}.* \boldsymbol{I_{Ci}}) + \boldsymbol{j}(\boldsymbol{Vi}.* \boldsymbol{I_{Cr}} - \boldsymbol{Vr}.* \boldsymbol{I_{Ci}}), \tag{4.24}$$

where $.*$ indicates the element to element product. The vector of residuals between the scheduled power and the calculated power from (2.5) above is:

$$\boldsymbol{misvect} = [(\boldsymbol{P^{sch}} - \boldsymbol{P_C}); (\boldsymbol{Q^{sch}} - \boldsymbol{Q_C})]^T. \tag{4.25}$$

As $\boldsymbol{P_c}$ and $\boldsymbol{Q_c}$ are complex values, their derivatives have to be separate, as shown in (2.6). In conventional N-R $\partial S/\partial\delta$ and $\partial S/\partial|V|$ are acceptable since the real part is the derivative of P and the imaginary part is the derivative of Q.

4.3.2. Computational process

The proposed method can be summarised in steps to show the computational process and its working sequence: 1) determining the equally spaced points in the roots of unity by applying (4.14) and the corresponding P active powers for a load bus; 2) calculating the voltage complex absolute values through N-R for each of the P points; 3) obtaining the corresponding power series coefficients using the fast Fourier transform; 4) verifying

the coefficients' tolerance with respect to each other; 5) repeating the above process, increasing the number of sampling points if there was no convergence; 6) obtaining the Padé approximants for the resulting power series; and 7) obtaining the LV solution, if required.

The details of the steps are as follows:

1. There will be four values of $l = 0, \ldots, 3, N = 4$, and $\theta_l = \frac{2\pi l}{N}$ if the process is started with $\mathrm{k} = 2$, (4.17), the polynomial initial order. This is convenient as the next set of sample points will be located in interleaving positions. See Figures 4-2 and 4-3.

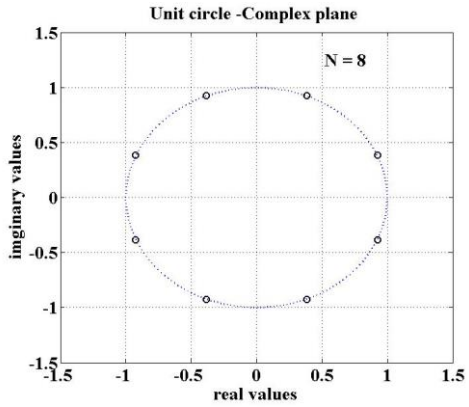

Figure 4-2. Eight Sample points.

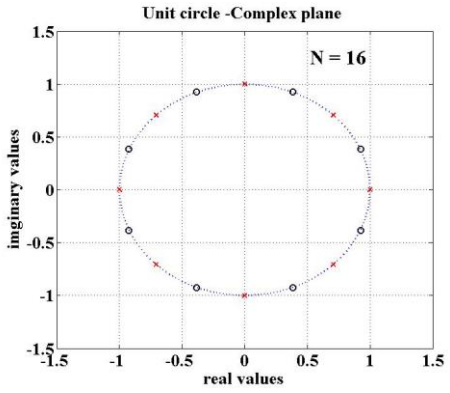

Figure 4-3. Sixteen interspersed sample points

The coefficients' tolerance needs to be decided, and 10^{-5} can be a good starting value. This value is related to the bus position in the network, as well as the network loading. The value of r is related to the radius of convergence of the series, a choice of $\mathrm{r} = 1$ is a sensible first approach. The power series radius of convergence, like the tolerance, will depend on the bus load and location in the network. So, as a choice guide, the bigger the relative load, the smaller the value of r, and, conversely, the bigger the tolerance choice (see 4.14 and 4.17).

2. The complex active power is calculated using $\mathrm{P}(\theta_l)$ (4.14) for each sampling point, with $\mathrm{P_c}$ equal to the bus base-line active power. The bus reactive power is then calculated keeping the original power factor, resulting in a complex value as well.

3. The bus voltage $\left|V(P_c + re^{j\theta_1})\right|$ is calculated using the N-R method for the apparent power $S\,(\theta_1)$ of the bus in question. The sequence cycles to cover each of the sampling points, while the load of the other buses remain at the baseline.
4. The set of $|V\,(P\,(\theta_1))|$ so obtained will be used to calculate the coefficient h_k of the power series (4.13) using the FFT. Their absolute values are then compared against their normalised tolerance.
5. The above process is repeated until a coefficient is smaller than the set tolerance. Coefficients smaller than the tolerance are discarded.
6. The power series (polynomial) so formed will be converted to a rational function using Robust Padé [96]. This Padé approximant will depict the whole HV branch of the P-V curve for the chosen bus, as it will be shown in the next chapter. The inner singularities of this approximant will be a very good estimate of the bus stability limit in terms of the feasible load range at a constant power factor. This is so in relation to the power system loading at the specific time of the bus in question's base-line load.
7. If a closer approximation to the bus voltage stability limit is required, it can be obtained at the intersection of the HV and LV solution branches. The LV branch can be obtained by using a small initial value at the start of the N-R iterations, for instance 0.4 [pu], to ensure that the bottom part of the PV curve is approximated. This will also be shown in the next chapter.

4.3.3. Conclusions

It has been shown that the Taylor series coefficients, in the complex domain, calculated via the Trapezoidal rule applying the FFT have geometric convergence (4.5) within their radius of convergence. Also, if the radius of the sampling circle is greater than 1, convergence improves. The it is a harmonic series extrapolated through function values obtained at the roots of unity, then fast convergence is also guaranteed.

The method's equations have been presented and their detailed applicability has been shown step by step. This includes the selection of the Taylor series radius of convergence and series coefficients tolerance, the use of N-R to obtain sampled voltage absolute

values, and how to obtain the LV solution branch to find a closer approach to the stability limit through its intersection with the HV solution branch.

Chapter 5: DFT-Padé application.

A. J. Sarnari and R. Živanović, and Said Al-Sarawi, “Augmenting Load Flow Software for Reliable Steady-State Voltage Stability Studies", *International Journal of Electrical Power & Energy Systems,* for printing.

Statement of Authorship

Title of Paper	Augmenting Load Flow Software for Reliable Steady-State Voltage Stability Studies.
Publication Status	☐ Published ☐ Accepted for Publication ☑ Submitted for Publication ☐ Unpublished and Unsubmitted w ork w ritten in manuscript style
Publication Details	A. J. Sarnari and R. Živanović, and Said Al-Sarawi, "Augmenting Load Flow Software for Reliable Steady-State Voltage Stability Studies", *International Journal of Electrical Power & Energy Systems,* submitted 09/07/ 2018.

Principal Author

Name of Principal Author (Candidate)	Alberto J. Sarnari		
Contribution to the Paper	Developed ideas, wrote corresponding MATLAB scripts, performed simulations, analysed data, wrote manuscript, and acted as corresponding author.		
Overall percentage (%)	65%		
Certification:	This paper reports on original research I conducted during the period of my Higher Degree by Research candidature and is not subject to any obligations or contractual agreements with a third party that would constrain its inclusion in this thesis. I am the primary author of this paper.		
Signature		Date	17 January 2019

Co-Author Contributions

By signing the Statement of Authorship, each author certifies that:

i. the candidate's stated contribution to the publication is accurate (as detailed above);

ii. permission is granted for the candidate in include the publication in the thesis; and

iii. the sum of all co-author contributions is equal to 100% less the candidate's stated contribution.

Name of Co-Author	Rastko Živanović		
Contribution to the Paper	Supervised work development reviewed and assessed manuscript.		
Signature		Date	21 January 2019

Name of Co-Author	Said Al-Sarawi		
Contribution to the Paper	Supervised work development reviewed and assessed manuscript.		
Signature	Said Alsa	Date	17/1/2019

Please cut and paste additional co-author panels here as required.

5.1. Introduction

This chapter will show the detailed results obtained at the different steps of the process and discuss the method applicability options. Comparison with conventional Newton-Raphson, Holomorphic Embedding load-flow (HELM) and Continuation power-flow (CPF) approaches will also be discussed, as well as the D-P time performance and weakest bus determination.

- The application of the DFT-Padé method will be shown step by step through the IEEE 14-bus test system [103] for the analysis of bus No. 14. Each step is depicted with a graph.
- A 2-bus system is analysed through the use of different parameters, determination of stability limits and a comparison with HELM.
- The analysis of a weak bus is carried out by determining the voltage stability limits and a comparison with plain N-R and HELM using the IEEE 30-bus test system.
- The analysis of a load bus voltage as a function of a generator bus active power is used to show the different behaviour of plain N-R and DFT-Padé, and the results of a comparison with CPF [84] are also shown.
- A DFT-Padé comparison with a HELM formulation that scales load buses by different amounts [104] is undertaken to obtain the HV branch solutions and the approximation to the voltage stability limits for the IEEE 14 and 118-bus test systems [103].
- D-P, plain N-R and CPF time performance comparison is carried out on five different test systems.
- A D-P critical bus determination is presented on two different test networks, and the results are confirmed with CPF.
- D-P applicability on networks containing FACTS equipment and HVDC links is analysed and the conclusions presented.

5.1.1. Application to 14-bus system

The following simulation study, based on trigonometric coefficients to determine a load bus stability limit, is applied on the IEEE 14-bus test system [103]. Bus 14 of the system

is selected to determine its voltage stability limit and the results are shown in Figures 5-1 to 5-7.

The complex active power is calculated using $\mathrm{P}(\theta_l)$ (4.14) for each sampling point, and $P_c = -0.149$ (sign as per load convention). The bus base-line active power is shown in Figure 5-1. $N = 32$ gives the total amount of points used. It implies that the N-R method ran 32 times to obtain the voltage complex absolute values, as per Figure 5-2.

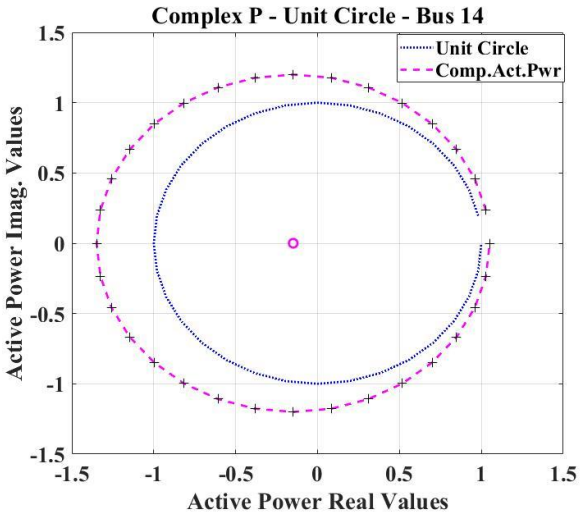

Figure 5-1. Circle of complex active power values.
$N = 32$ sampling points of radius $r = 1.2$ centred at $P_c = -0.149\ [pu]$

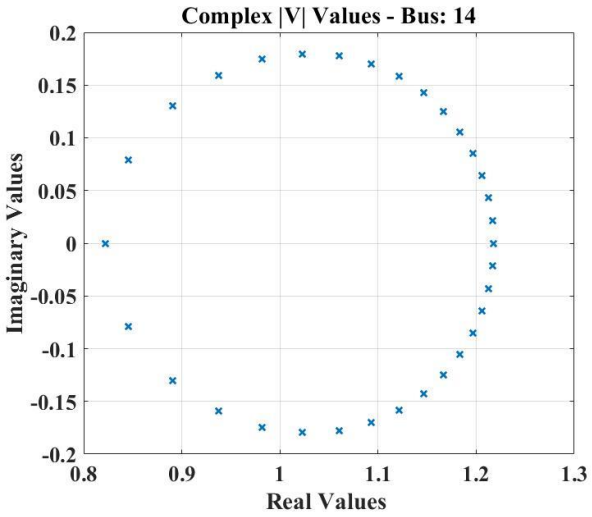

Figure 5-2. Voltage complex absolute values.
Obtained via N-R for each complex $\mathrm{P}(\theta_l)$.

It is to be noted that the smaller density of voltage values, as the real part of $|V(\mathrm{P}(\theta_l))| < 1\ [pu]$, indicates the increasing change of slope in the P-V curve, given that the sampling points are equally spaced. When there is no convergence, the points do not close the circle. It then becomes an indication of voltage collapse.

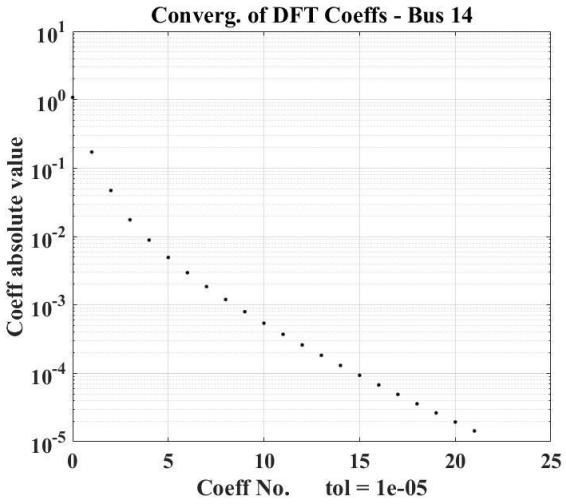

Figure 5-3. Fourier series coefficients. Twenty-two coefficients for tolerance $\mathbf{10^{-05}}$

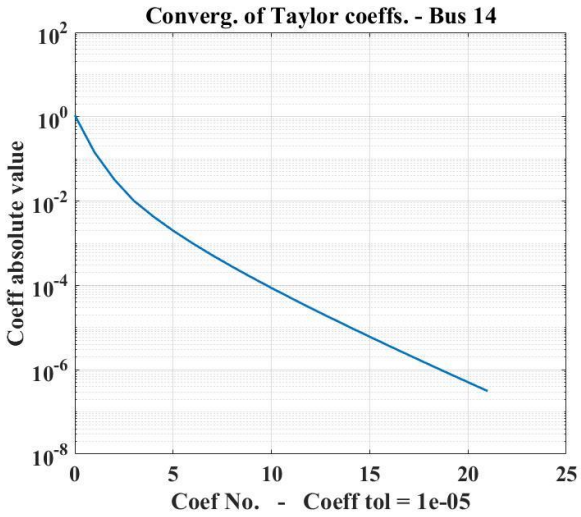

Figure 5-4. Taylor series coefficients. Coefficients scaled by $r = 1.2$

DFT coefficients, are considered in geometrically increasing amounts given $N = 4, 8, 16, 32$, by (4.16) and calculated using the trapezoidal rule (the expression between brackets in (4.17). They converged in 22 terms for a tolerance of 10^{-5}; the remaining 10 below tolerance were discarded. Their absolute values are shown in Figure 5-3. While Figure 5-4 represents the Taylor series coefficients (4.17), with a scaling factor of $\frac{1}{r^k}$ $(r = 1.2)$, making their absolute value decrease faster. It is interesting to estimate the radius of convergence of the Taylor series using the formula $R = \lim_{n\to\infty} \frac{|c(n)|}{|c(n+1)|}$ [105]. Figure 5-5 illustrates the process. The choice of $r = 1.2$ is well within that estimation of $R = 1.62$. Values of $r > R$ would have compromised the calculation of $|V(\mathrm{P}(\theta_l))|$ by the Newton-Raphson method. A value of $r = 1$ would have yielded the same results.

Having defined the polynomial representing the Taylor series, the next step is to obtain the Padé approximant rational function that will represent the HV branch of bus 14 as a function of the active power P. As explained above, the method of choice is Robust Padé. The results are shown in Figure 5-6.

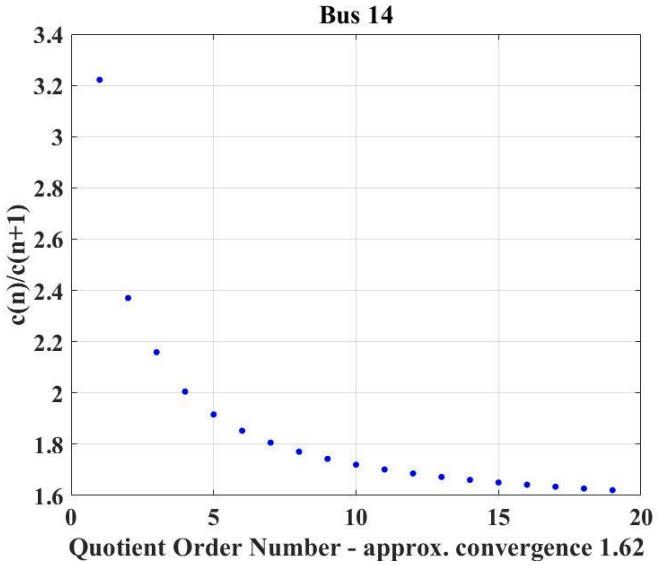

Figure 5-5. Estimation of series' convergence radius.
Determined by the ratio test for the given Taylor coefficients.

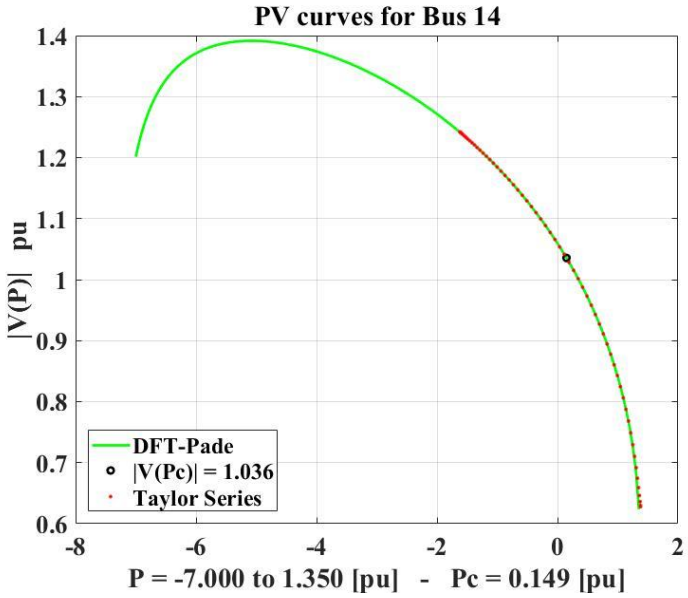

Figure 5-6. Padé and Taylor approximations to branch solutions.
Taylor within radius of convergence (red dots) overlaps the Padé approximant curve. Both approximations yield the same voltage at loading point $\boldsymbol{P_c}$ of bus 14.

The active power range P was taken from the intersections with the LV curve: [-6.812 pu left and 1.3657 pu right]. The LV curve was obtained through the same procedure, except that the first guess for the N-R iteration process was 0.45 $[pu]$. Both curves extend over the negative values of active power P. This can be assimilated to a fixed speed induction generator [106]. Any larger active power outside that range will cause instability

and voltage collapse (to either side). It is also to be noted that for practical purposes the Taylor approximation covers the voltage values with the same accuracy given that its convergence radius is large enough.

The inner singularities of the Padé approximants also give a very good approximation to the voltage stability limits, as shown in Figure 5-7 and Table 5-1.

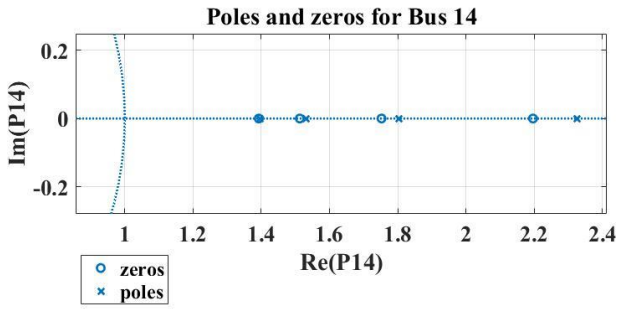

Figure 5-7. Singularities of the Padé rational function.
N.B. The negative singularities are not shown.

Table 5-1. Rational function singularities.
VSLs highlighted in yellow.
Values in [pu] of active power.

Zeros	Poles
12.5176	22.0154
-12.2251	-13.5039
-7.4768	-7.583
5.0734	6.2345
3.0632	3.4055
2.1968	2.3254
1.7526	1.8032
1.5128	1.5305
1.3926	1.3965

The voltage stability limit for bus 14 was found to be $1.356\ [pu]$, given by MATPOWER CPF [84]. The difference with the intersection method above is $-0.72\ \%$, and -2.7% with respect to the inner singularities (poles & zeros) method.

5.1.2. Two-bus system study

The 2-bus system has a closed-form algebraic solution to which the approximation methods can be compared. The algebraic solution is well known and is, for example, derived in [27]. This can represent a distributed generation system, where the generator and transmission line are the Thévenin equivalent. The generator can also be thought of as the infinite bus of constant voltage and reference angle. The energy can flow both ways provided the load bus can also act as a generator. When performing load sweep, the bus will acquire negative values, as well. This negative load can be thought of as a fixed speed induction generator or wind turbine [106]. The base-load values are as shown in Figure

5-8. The circuit parameters are: $V1 = 1\ [pu]$, transmission line, $0.001 + \mathrm{j}0.1\ [\mathrm{pu}]$, and the load at bus 2 is $1 + \mathrm{j}0.2506\ [\mathrm{pu}]$.

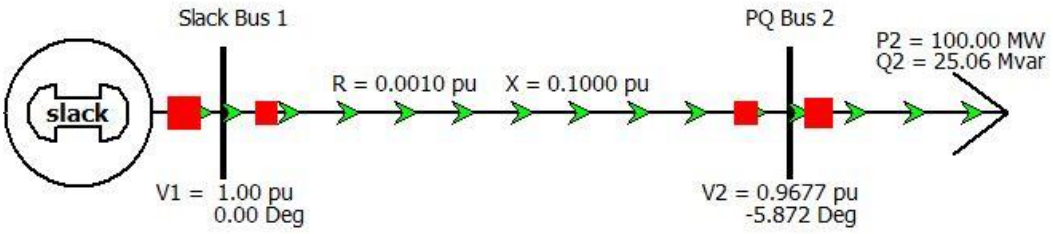

Figure 5-8. Two bus system: load base-line values in MW and Mvar. Generator or Thévenin equivalent. Load sweep will range from positive to negative values. Energy can flow in both directions. Graph obtained using PowerWorld software [81].

The DFT-Padé solution was obtained using exploring radii and tolerances according to Table 5-2. The radius has been termed "exploring", in this context, since it will fetch complex absolute voltage values according to its size as per (4.15).

Table 5-2. Comparison of Voltage Stability Limits. They are given by HV and LV curve intersections, inner singularities and algebraic solutions for two different "exploring" radii and coefficient tolerances using the DFT-Padé method.

Radius R	No. of Tolerances	No. of Coefficients	Active Power for Voltage Stability Limits		
			Intersections [pu]	Singularities [pu]	Branching Points [pu]
2	10^{-08}	16	-6.6878 3.8923	-6.9687 3.9310	-6.4905 3.8712
4	10^{-12}	32	-6.6152 3.8783	-6.9686 3.9311	

The positive VSL is of practical interest. It is shown in Figure 5-9. There may be some differences in the VSLs when using two different radii and tolerances: a bigger radius, $\mathrm{r} = 4$, and a smaller tolerance, $\mathrm{tol} = 10^{-12}$, will have greater "exploring" capabilities, and will bring more information from the voltage function than a small radius, $r = 2$, and a bigger tolerance $\mathrm{tol} = 10^{-8}$. If the algebraic branching point is taken as the true value, then the difference with the curves' two intersection points is 0.18% and 0.55% respectively. If the comparison is now made using the inner singularities of the rational function that characterise the HV branch of the voltage V_2, the differences with the algebraic branching point are 1.546% and 1.545% respectively, Figure 5-10. These singularities are less

accurate, as they both are the zeros of the rational function approximant and, as such, they are further away than the curves' intersection points. In general, if the exploring radius can take a large number, implying that the load bus is not a weak bus, there is a potential for reducing errors in the Fourier coefficients, see eq. (4.17). There is one complex absolute voltage for each Fourier coefficient, as seen from (4.16). This implies

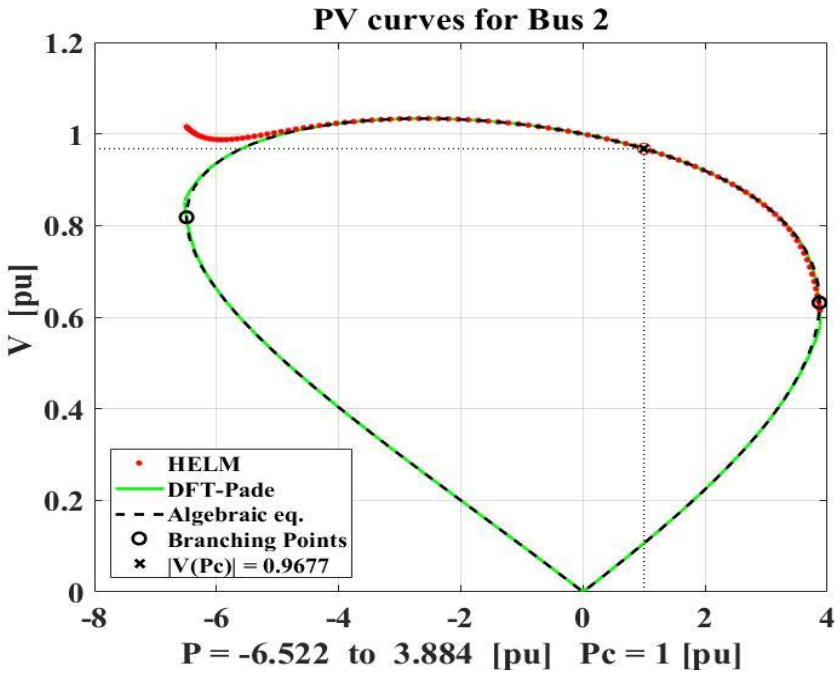

Figure 5-9. Two-bus branch solutions.
Exact solution, dashed. HELM, red curve, and DFT-Padé approximation, HV and LV, green curve. Pc is the base-line active power with corresponding voltage |V(Pc)|.

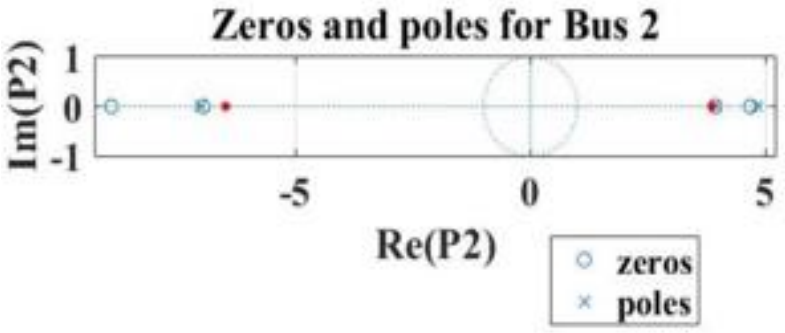

Figure 5-10. Zeros and poles of the Padé rational function (3.9).
True branching points from the algebraic solution are in red.

that the more coefficients that are required for the series to converge, the longer the processing time, i.e., there are as many N-R algorithms to execute as coefficients in the

series, hence the interest in keeping the series to a minimum to avoid unnecessary, expensive computational time. The number of N-R executions, or coefficients, cannot be known before the bus HV branch has been solved at least once. The LV branch approximation requires running DFT-Padé, where the starting voltage of the bus in question is $0.4\ [\mathrm{pu}]$, which will guarantee that the rational function will yield the LV instead of the HV branch. This LV approximation is more demanding than that of the HV. The series convergence radius is smaller, and the possible tolerances are larger. It may fail to converge in very difficult cases.

The HELM solution (the red curve) was derived from the convolution process implied by (3.7) and (3.8) to form the truncated Taylor series of coefficients $\mathbf{c}_s^{[2]}$ for PQ bus 2. The coefficients were calculated until the difference between the two consecutive ones was smaller than the tolerance 10^{-14}, see Table 5-2. Twenty-one of them were required. Robust Padé approximants were derived from the series $\sum_{s=0}^{20} \mathbf{c}_s^{[2]}\, \mathbf{z}^s$. The inner singularities of that rational function approximate the VSLs. A pole is the closest singularity from the left, which explains the upwards trend of the curve. Both HELM and DFT-Padé have similar approaches from the right. The three methods, including the algebraic solution, yield the same base-line voltage for bus 2.

Table 5-3. Voltage stability limits via HELM and DFT-Padé methods.
Tolerances and number of coefficients can be compared. Right-hand side singularities for both methods can be compared with the true branching point. Values are in [pu] of active power.

	Voltage Stability Limits			No. of Coefficients	Tolerances	Radius r
	by Intersection [pu]	by Singularities [pu]	Branching Points [pu]			
HELM	N/A	-7.3127 4.0793	-6.4905 3.8712	21	10^{-14}	N/A
DFT-Padé	-6.6152 3.8783	-6.9686 3.9311		16	10^{-08}	2

For the HELM case there is no radius involved, hence the N/A abbreviation. However, the intersection case could be resolved by using the equations of the LV as explained in [25]. Alternatively, the Padé approximants for the voltages must be evaluated until the function's domain boundary is reached, which is indicated by high bus-power mismatches [13]. The accuracy of both methods is very similar, as seen in Fig. 5-9.

5.1.3. IEEE 30-bus system test case

Voltage collapse starts at the weakest bus and then spreads out to other weak buses. Therefore, the weakest bus is the most important in the voltage collapse analysis [107]. Bus 30 is a weak bus for the present network, as identified by contingency ranking in the power system using a fuzzy-based load flow [108] and fast voltage stability index [109]. Also, after numerous DFT-Padé studies were conducted on different systems, this bus is of interest, given its small power series radius of convergence, manifesting its weak load bus characteristics.

The following tests were carried out on bus 30 of the IEEE test case using the base-line loads. The assumption is that all loads remain at those values except for bus 30, which is subjected to a load sweep (exposed to a range of loads) from and to the stability limits, or very close to them when using N-R. The generators' reactive power limits are not enforced. As already mentioned, the plain N-R MATLAB algorithm presented in [110] was used to solve the system of successive loads at bus 30 within the limits given by the DFT-Padé intersection points.

The HELM solution, a rational function approximant for bus 30 that allows extrapolation of the load within the stability limits, was obtained by applying the direction-of-change scaling formulation [104]. The DFT-Padé approximation, is also a rational function (3.9), that allows scaling of the load in the same range. A constant power factor is implicit in the load scaling of both rational functions, while it has been designed that way for the N-R load sweep.

The N-R power sweep range applied is [-1.562, 0.4816] pu, the red trace, as can be seen in Figure 5-11. Negative active power has been used under the same concept as in the 2-bus example. The HELM method, the blue trace, and the DFT-Padé, the green trace, are more accurate near the VSL, the generation side, where N-R solutions start to diverge, as shown in Figure 5-11. From this figure the following points can be noted:

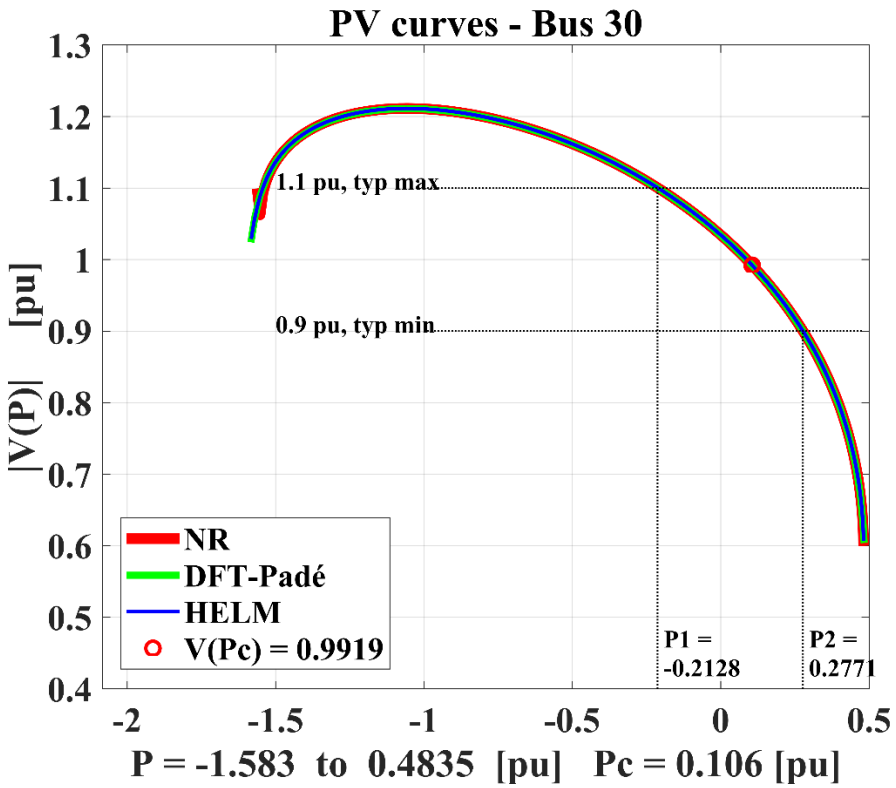

Figure 5-11. Bus No. 30 comparison of three methods.
Conventional NR, holomorphic embedding load flow (HELM) and DFT-Padé. Negative loads correspond to generation [39].

- The positive end of the load range was taken from CPF [84], but not the range left end, since it is a feature not documented and perhaps not programmed. Instead, the approximated value was obtained from the intersection of the HV and LV curves, from the DFT-Padé method.
- The HELM LV solution is investigated in [25] but no specific mention of its use to find voltage stability limits is made. The stability limit here is found by checking if the power balance equation, the difference between the actual and calculated power, is within a specified tolerance. Based on experience, the bus voltage solution may take somewhere between 21 and 41 terms. A fixed number of terms is used, as in this case. For buses or systems close to the voltage stability limit, the number of terms of the power series can be between 61 and 81 [104].
- The 3 curves overlap over nearly the whole range, except near the branching point or voltage stability limit on the negative load's side. The three methods yield the same $|V(Pc)|$ at the base load. The DFT-Padé method obtains the stability limit for bus 30 very close to the continuation power flow (CPF) value, with a difference of

-1.18%. The N-R voltage values, on the left, start to depart from the other two curves at -1.562 pu, where the Jacobian matrix yields very large increases in the condition number. Both, the HELM and DFT-Padé traces overlap the whole range. As expected, the inner singularities are a bit further away from the CPF, or the intersection values, hence they can provide a coarse approximation to the stability limit.

Bus 30 is of relevance for the DFT-Padé method, as the coefficients of its Taylor power series are divergent, unlike the DFT coefficients, providing an indication as to the bus' weakness. The small radius of convergence, approximately 0.6 pu, as per the ratio test: $\lim_{k\to\infty} \frac{h_k}{h_{k+1}}$ [111], when applied to the last two coefficients of the series as given by (4.17), is also an indication of the bus' weakness. To ensure convergence, the exploring radius, r, given in (4.15) should be less than 0.6. In this case, $r = 0.5$ has been chosen. Despite these limitations of the Taylor series, the Padé rational function coefficients are convergent.

5.2. Improvements over the plain N-R method and comparison with the continuation power flow approach

As the bus voltage approaches its stability limit, the accuracy of the Jacobian matrix deteriorates until it becomes singular [112], [63]. Consequently, conventional power flow algorithms are prone to convergence problems when operating near the stability limit. The continuation power-flow analysis overcomes this limitation by reformulating the power-flow equation, so that the equations remain well-conditioned at all possible load states [77]. Continuation methods or branching tracing methods are used to trace a curve given an initial point on the curve and can also be called a predictor-corrector method. Continuation power flow (CPF) [79] is an N-R based tool that traces the solution branches and therefore determines the voltage stability limit for power system buses. The limit is determined from a nose curve where the nose represents the maximum power transfer that the system can handle given a power transfer schedule. This is characterised by equations (2.17-19), as applied to MATPOWER [84] implementation.

5.2.1. Application to a 7-bus network

A study based on a 7-bus network, see Figure 5-12, involving HELM, Semidefinite Relaxation, and N-R methods, is already presented in [12]. It will now serve the purpose of showing the applicability of DFT-Padé and a comparison with CPF. It entails the analyses of load-bus 3 voltage behaviour as a function of generator bus 6 active power variations.

The DFT-Padé method was set with an exploring radius of 0.25 to obtain 16 coefficients (only 10 are used) of the discrete Fourier transform power series, with 10^{-05} tolerance.

Table 5-4. Bus No. 3 characteristic parameters, DFT-Padé method.
Seven-bus network. Voltage $|V_3|$ vs power P_6.

Radius r	Tolerance	No of Coefficients.	Inner Singularities	
			Left	Right
0.25	10^{-05}	10	-0.1945	1.1296

The inner singularities, corresponding to zeros of the Padé rational function, approximate the VSLs. They have been taken as the basis to set the generator bus 6 active power range. In this case, the negative active power corresponds to the generator acting as a load. Bus 3 voltage, as a function of bus 6 generator active power, is shown in Figure 5-13. It is worth noting that $P_6 = 0.3\ pu$ has been set as a base power to ensure N-R convergence, for which the bus 3 voltage, as per the given network, is $0.9897\ [pu]$. DFT-Padé LV approximation did not converge for this bus. The inner singularities range (both zeros of the rational function) are $[-0.194,\ 1.129]\ [pu]$, which served as a first approximation to determine the power range, see Table 5-4.

The MATPOWER continuation power flow options are based on the example given in the manual [84] and are listed in Table 5-5. One point of interest is that the generator base power in this case was given as the near-end range on the negative side (-100 MW) and the scaling factor is less than one. This allows the mechanisms of the predictor and corrector steps to work through most of the HV branch of the PV curve. MATPOWER CPF found the VSL at $P_6 = 1.0569\ [pu]$. The voltage stability limits for bus 3 was found to be $[-0.114,\ 1.057][\mathrm{pu}]$ of bus 6's active power, in the insightful work by Baghsorkhi and Suetin [12].

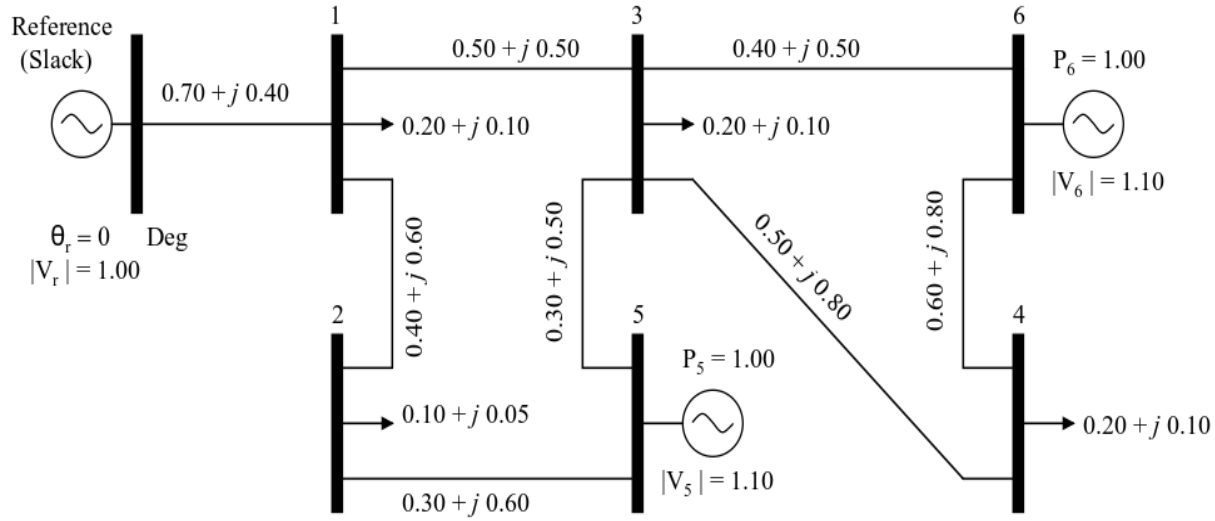

Figure 5-12. 7-bus network.

Monitoring of PQ bus 3 absolute voltage, while varying PV bus 6 generator's active power within bus 3's stability limits

Table 5-5. MATPOWER continuation power flow parameters and values

CPF Options	
cpf.stop_at	NOSE
cpf.step	0.05
cpf.plot.bus	3
cpf.adapt_step	1
P6 base	-100 [MW]
P6 target	-0.1 [MW]

The N-R power sweep on the bus 6 generator was conducted over the same range. However, it converged to the wrong values, or did not converge for the generator's active power greater than $0.97\ [pu]$, as shown in Figure 5-13. Both, CPF and DFT-Padé obtained the correct absolute voltage value for PQ bus 3 within the given range; and both yield $|V_3| = 0.8363\ [pu]$ when $P_6 = 1\ [pu]$, which is the generator active power according to Figure 5-12.

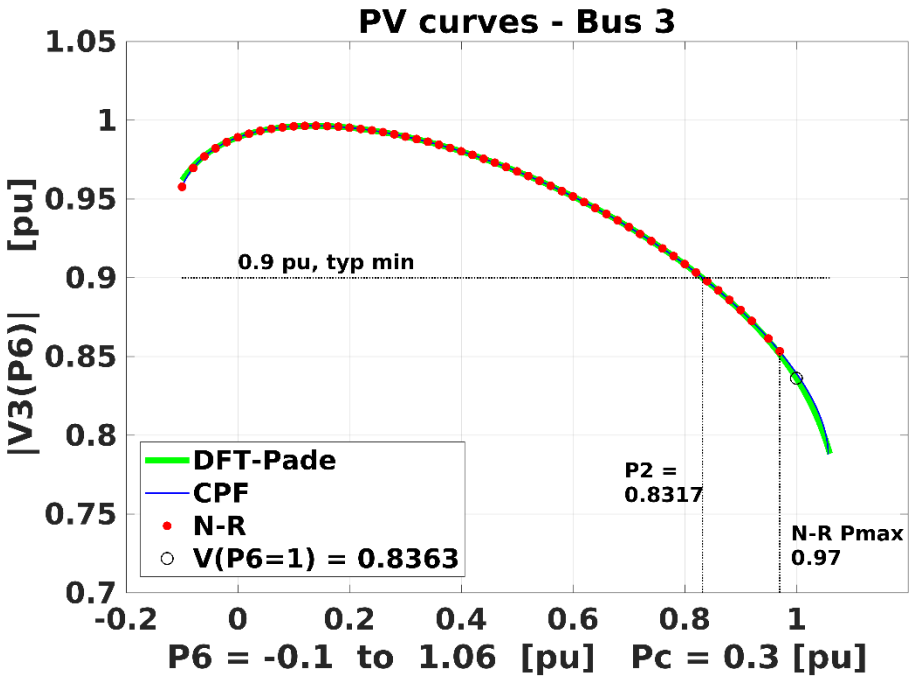

Figure 5-13. 7-Bus network – |V3| vs P6.
Bus No. 3 comparison by three methods. High voltage branch: N-R, CPF and DFT-Padé.

5.2.2. Performance comparison

Five networks were tested in order to determine the time performances of plain D-P, N-R and CPF namely, 2-bus – Figure 5-8, IEEE 14, 30, 57 and 118-bus test systems. The last bus of each network was tested, except for the 30-bus system where bus number 24 was used so 16 coefficients were obtained instead of 32. The conditions set for each system were as follows.

Sixteen coefficients were necessary to characterise those buses using the D-P method. Their tolerance was 10^{-05} in all cases. The radii for each network were 3, 1, 1, 0.4 and 3 respectively. D-P needed to run the load flow program once for each coefficient. Elapsed times were recorded for each case.

To make the comparison possible, sixteen points where calculated spanning through their allowable load range using a plain N-R solver [110]. As the load points got closer to the feasibility limits, the number of iterations increased. The time elapsed to run the load sweep for each case was recorded.

For CPF [84] the number of steps were determined by the options shown in Table 5-6. The base load was the starting point to reach the voltage stability limit for each one of the

buses under the test. Execution times and the number of steps required to reach the voltage stability limits were recorded. The execution times were taken from the elapsed time clock returned by the "runcpf.m" MATPOWER script, while the target loads were the voltage stability limits obtained through D-P, previously.

Table 5-6. Continuation Power Flow time performance parameters

CPF Options	
cpf.stop_at	NOSE
cpf.step	0.2
cpf.plot.level	0
cpf.adapt_step	1
cpf.plot.bus	bus under study
P base	base value
P target	bus VSL

Tests have been carried out with a computer running with a processor Intel Core™ i7-2630QM CPU @ 2.00 GHz, operating system Windows 10 Home, and simulation software based on MATLAB R2017a.

The results can be seen in Table 5-7. The run times are comparable and given as a guide only.

Table 5-7. Time performance comparison: D-P, N-R and CPF.
D-P and N-R calculated over 16 points, CPF steps as per option parameters.

System	D-P		N-R		CPF	
	Time (sec)	Iterations (Avg)	Time (sec)	Iterations (Avg)	Time (sec)	No. of Steps
2-bus	0.030	5.8	0.008	5.1	0.052	20
14-bus	0.045	5.5	0.025	5.3	0.079	24
30-bus	0.056	5.0	0.041	5.2	0.070	17
57-bus	0.087	5.2	0.079	4.8	0.116	23
118-bus	0.149	5.0	0.218	5.4	0.181	28

5.2.2.1 Contingencies

Contingency is better understood within the framework of Security Analysis which is about examining the system's ability to undergo disturbances. The power system is said

to be “secure” if it can withstand each specified disturbance without entering an emergency state. In practice, power grids are checked against a set of “credible incidents” (N), that is the ones which have a realistic chance of happening. They are called “contingencies”, and refer to the outage of generators, transmission lines, transformers, etc. For the long-term stability analysis, the well-known criterion is N-1 security, according to which the system must be able to withstand any single transmission or generation outage without entering an emergency state. It may also be required that no generator operates under reactive power limit after a contingency. The impact of a contingency is assessed by calculating the post-contingency long-term network stability. Multiple contingencies may also be taken into account to determine security criteria, especially when they are caused by a credible event [17].

It is necessary to know how far the system can deviate from the present operating condition and continue to be safe. The distance to that limit (in terms of MW or MVA) is called Security Margin. Contingencies generally decrease or even eliminate the security margin. Direct P-V curve computation can be used to determine post-contingency margins. Detailed analysis needs to be carried out to identify critical contingencies [113]. In other words, if a contingency is characterized by a maximum loading smaller than the specified margin (typically set by the network operator), that contingency is critical. Stability limits are generally determined in terms of active power and are computed off-line based on N-1 contingency criterion [41].

The following findings on the IEEE 118-bus network single contingency analysis were revealed in [114]. Two-line outages caused voltage collapse out of the of the 177 possible line outages, due to the fact that they isolated a critical generator. The majority of these outages did not cause an important effect: 126 of them had less than 10 MW decrease in loading margins. Twenty-five of the worst cases caused no less than 50 MW margin decrease, and fifteen of them involved lines terminating at transformer buses. Four cases out of the 25 could be attributed to generator VAR limits. Multiple contingencies were estimated by summing up two single line contingencies. The average margin reduction in twenty-one double line outages was 63 MW. Eleven of those 21 outages caused loading margin reductions larger than 50 MW.

The following contingency cases were also simulated, timed and recorded in Table 5-8 using the same conditions as the above example in Table 5-7.

- IEEE 14-bus test system: 1) Outage of line between bus 7 and bus 9. 2) Outage of transformer between bus 5 and bus 6.
- IEEE 30-bus test system: 1) Outage of line between bus 4 and bus 6. 2) Outage of transformer between bus 4 and bus 12.
- IEEE 118-bus test system: 1) Outage of lines between buses 37-49, 41-42, and 42-49. 2) Outage of generator at bus 12.

Table 5-8. Time performances using systems contingencies.
The same three load flow algorithms and conditions were used as in Table 5-7.

System	Contingency	D-P		N-R		CPF	
		Time (sec)	Iterations (Avg)	Time (sec)	Iterations (Avg)	Time (sec)	No. of Steps
14-bus	Line 7-9	0.050	5.4	0.021	5.1	0.042	17
	Transformer 5-6	0.054	5.3	0.02	4.6	0.043	15
30-bus	Line 4-6	0.054	5.2	0.04	5.2	0.048	15
	Transformer 4-12	0.054	5.3	0.046	5.3	0.049	14
118-bus	Lines 37-40, 41-42, 42-49	0.152	5.0	0.224	5.4	0.083	15
	Generator G12	0.158	5.0	0.229	5.4	0.083	15

Sixteen voltage points were sampled to approximate the HV branch rational function of D-P, and sixteen voltage points were obtained spanning the boundary limit for the buses under study for N-R. The number of steps achieved in MATPOWER CPF were obtained using target values much greater than the active power boundary limit. However, precise VSLs were calculated by the load flow algorithm. Contingency examples were taken from [115, 116].

5.2.3. Critical bus determination

A method to determine the critical bus (also referred to as the weakest bus) of a network is presented in this section through the features of the Taylor series bus-voltage representation (4.13) and (4.17), and the rational function (3.9) of the HV solution branch given by the DFT-Padé method. The approach is tested using the IEEE-14 and 30-bus systems and the results are presented in Tables 5-9 to 5-12.

To ensure the network's stability, it is required to identify critical network components. There are diverse methods presented by different authors [35] to that end. Voltage collapse starts at the weakest bus and extends to the other weak buses of the grid. For this reason, the critical (or weakest) bus is the most relevant determination in voltage collapse analysis [107]. The objective of the voltage security assessment is to find the weakest bus for the operating point under study [108, 117]. As a consequence, network stability can then be enhanced, taking appropriate action [118].

Transmission lines are characterised by their inductive and capacitive reactances. When the line is lightly loaded capacitive reactance is prevalent, injecting reactive power to the network and increasing the line voltage. Conversely, when the transmission line is heavily loaded, it takes reactive power from the network and its voltage drops [21]. There are two well-known methods, among others, that make use of this power transmission characteristic to point out the weakest bus of the grid, namely: modal analysis [41, 119], and the V-Q curve technique [107, 120].

It is convenient to use the P-V curve to identify the weakest bus given by the closest proximity of the working point to the "knee" of the curve [121], or branching point, see Figure 4-1. It can also be said that the weakest bus is the one that will have the greatest $\Delta V/\Delta P$ gradient according to [35]. The P-V curve is used in operation planning to determine weak buses [107].

The radius of convergence of the power series bus-voltage representation (4-1) is a parameter that closely reflects the voltage strength, as used by D-P. This became apparent through the countless network tests using the method, and it is also intuitively coherent. Tables 5-9 and 5-10 show the PQ buses for the IEEE 14 and 30-bus systems, sorted according to their criticality.

Table 5-9. 14-bus network - PQ buses ordered by criticality

IEEE 14-BUS TEST SYSTEM		
Bus No (PQ)	Radius of Convergence	Inner Singularity Right
14	1.620	1.366
10	1.970	1.749
12	1.980	1.899
11	2.020	1.941
9	2.920	2.665
13	2.990	2.840
7	3.940	3.792
5	7.010	6.480
4	7.850	8.036

Table 5-10. 30-bus network - PQ buses ordered by criticality.

IEEE 30-BUS TEST SYSTEM		
Bus No (PQ)	Radius of Convergence	Inner Singularity Right
26	0.350	0.304
29	0.460	0.452
30	0.620	0.490
25	0.870	0.798
23	1.090	1.045
24	1.120	1.017
18	1.280	1.199
19	1.340	1.180
20	1.340	1.256
27	1.340	1.288
14	1.520	1.361
16	1.540	1.485
17	1.750	1.608
21	1.890	1.709
15	2.180	2.003
22	2.490	2.443
12	2.840	2.672
10	2.950	2.807
9	4.120	4.091
3	4.600	4.410
7	4.820	4.443
28	5.570	5.668
4	6.980	6.906
6	7.520	7.949

Table 5-11. Weakest buses in14-bus system.
Comparison with CPF VSLs.

IEEE 14-BUS TEST SYSTEM			
Bus No (PQ)	Radius of Convergence	Inner Singularity Right	CPF [pu]
14	1.620	1.366	1.356
10	1.970	1.749	1.670
12	1.980	1.899	1.830
11	2.020	1.941	1.870

Table 5-12. Weakest buses in 30-bus system.
Comparison with CPF VSLs.

IEEE 30-BUS TEST SYSTEM			
Bus No (PQ)	Radius of Convergence	Inner Singularity Right	CPF [pu]
26	0.350	0.304	0.294
29	0.460	0.452	0.418
30	0.620	0.490	0.482
25	0.870	0.798	0.756
23	1.090	1.045	1.028
24	1.120	1.017	1.001

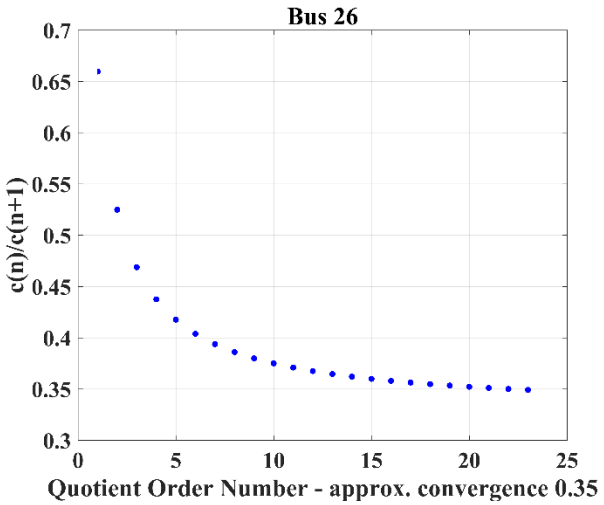

Figure 5-14. Radius of Convergence.
Approximation to the radius of convergence through the Taylor series coefficients, where n is the coefficient number applied to subsequent coefficients.

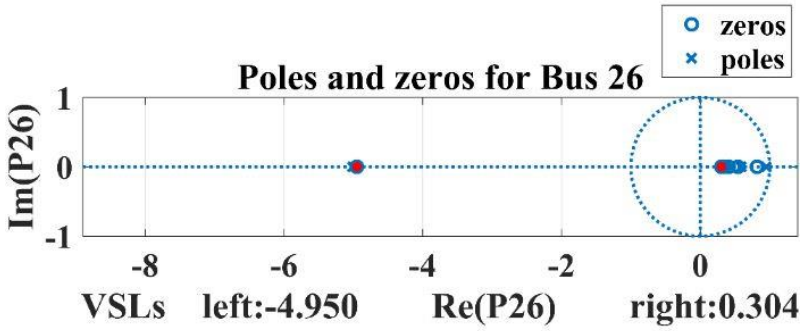

Figure 5-15. Poles and zeros of the Padé rational function.
Inner singularities, red dots, approach the voltage stability limit for bus 26.

They are approximate values to the maximum loadability of each bus for the systems' base loading, that is, while the bus in question is stressed, the rest remain at the base load condition. The inner singularities (those closest to the origin in the complex plane) also reflect the same hierarchy in terms of bus weakness. These singularities are given by the Padé approximants (PA) derived from the Taylor power series, as explained in Section 3.2 and equations (3.2) and (3.9).

Tables 5-10 and 5-11 show the comparison between the weakest buses and the active power stability limit obtained through continuation power flow [84]. All figures correspond to the level of active power per unit. Figures 5-14 and 5-15 show the radius of convergence of the Taylor coefficients' ratio test [111] and the right inner singularity (the red dot) for the weakest bus in the IEEE 30-bus test case.

Apart from the discrepancy in the sorting order between buses 23 and 24 due to possible numerical problems when generating the Taylor series but straightened out with the rational approximation, the HV branch of the DFT-Padé conveys this valuable additional information about the bus under study.

5.3. Comparison with the holomorphic embedding load-flow method (HELM)

A HELM formulation for scaling loads at buses by different amounts, as described in [13], is used for comparison with the proposed DFT-Padé method. This HELM formulation allows the researcher to scale one bus at a time, while the rest of the system remains at

the base load. It is worth noting that loads can also be scaled uniformly [13], the formulation will do so when individual buses are scaled, and behaves as if the whole system were scaled simultaneously, i.e. the rational function, representing the voltage for the bus in question, can achieve this remarkable feat. Further information and discussion about HELM can also be found in [87, 88].

5.3.1. IEEE 14-bus system

The basis for obtaining the DFT-Padé HV branch of bus No. 14, was to sample the complex active power in a radius $\mathrm{r} = 1.2$, with a tolerance of 10^{-5}, to obtain 32 DFT coefficients. The bus active load and variable P range are the same as in the previous section. Forty-three coefficients were calculated for the HELM Taylor series to determine its Padé approximation [104]. The limits of the curves have been set based on the intersection of the HV and LV curves using DFT-Padé, as explained in the Section 5.1.1 above. Figure 5-16 shows the HELM curve, red dots, and the DFT-Padé curve, using the green trace.

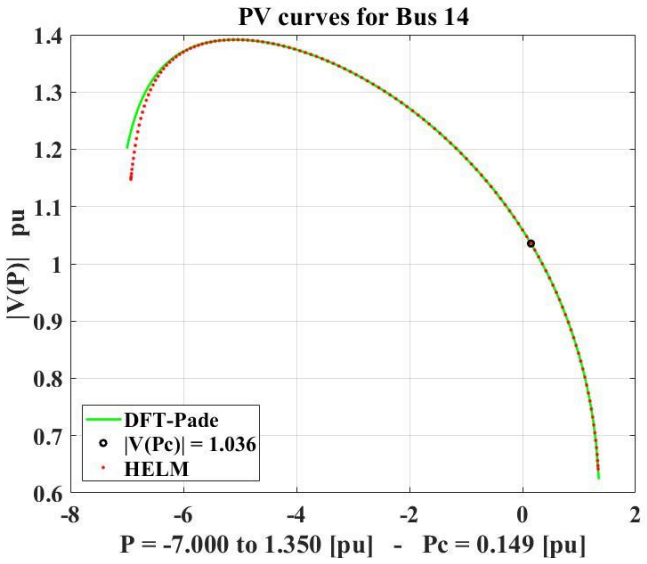

Figure 5-16. Bus 14: HELM and DFT-Padé methods, HV branch comparison.
Both find the same solution to the base-load voltage $V(P_c)$.

Both curves overlap for most of the active power range where the voltages are calculated; and both voltage values, $V(P_c)$, at the actual loading point, P_c, also match that of the N-R's. Table 5-12 shows the difference between the singularities that approximate the voltage stability limits by both methods, DFT-Padé and HELM.

Table 5-13. Bus 14 HELM and DFT-Padé voltage stability limits comparison.
Active power in [pu]

Load flow algorithm	Inner Singularities	
	Pl (left)	Pr (right)
HELM:	-7.343	1.2182
DFT-Padé:	-7.476	1.3657

The difference between both singularities on the RHS, positive active power, is $0.1475\ [\mathrm{pu}]$, where Pl and Pr are the left and right active power VSLs. There are no voltages associated with these P values, as they are zeros of the rational function $\therefore\ V = 0$. While the base-line load is $P_c = 0.149\ pu$, the VSL is $\sim 1.4\ pu$. This base load could still increase ~ 9 times before reaching the bus VSL.

5.3.2. IEEE 118-bus system .

The comparison of both methods on bus 118 can be seen in Figure 5-17. In this case, the DFT-Padé HV branch was obtained with a radius $\mathrm{r} = 3$ and a coefficients tolerance of 10^{-08}. 15 coefficients were needed to reach the desired tolerance. As in previous case, the HELM Padé rational function was built from a Taylor expansion of 43 coefficients [104].

Table 5-13 shows the difference between the singularities that approximate the voltage stability limits by both methods. The difference at the VSL (positive load) is 8.8%.

It can be seen that there is a large margin between the actual load, $P_c = 0.33\ pu$, and VSL ~ $7\ pu$ of the active power for bus 118. This bus is far from being stressed at the present system loading conditions.

Table 5-14. Bus 118 HELM and DFT-Padé voltage stability limits comparison.
Active power in [pu]

Load flow solution	Inner Singularities	
	Pl (left)	Pr (right)
HELM:	-28.01	6.5887
DFT-Padé:	-35.03	7.2249

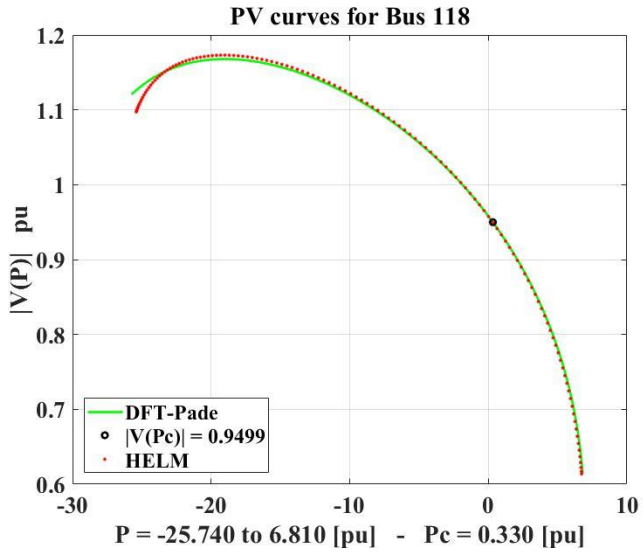

Figure 5-17. Bus 118: HELM and DFT-Padé methods HV branch comparison. Both find the same solution to the base-load voltage $V(P_c)$.

5.4. Flexible AC transmission system (FACTS) and high voltage direct current transmission (HVDC)

An introduction to FACTS and HVDC technologies follows to highlight their relevance to power system transmission. This will help frame their load flow algorithm characteristics and how they relate to DFT-Padé requirements.

The motivation is to find out how the FACTS and HVDC-link Jacobians will work with the split active and reactive powers' derivatives demanded by the D-P N-R based method. The derivatives' decoupled power is the definition of the Jacobian matrix, as can be seen from the power system design textbooks [20, 21].

FACTS and HDC have come to resolve serious power transmission issues stemming from low infrastructure investment, increasing demand, environmental concerns in the United States (US) and many parts of the world [122, 123]. Power systems have become highly integrated to keep track of the increasing energy consumption. The need to lower costs and environmental concerns is a worldwide phenomenon. These constraints have given rise to the more efficient direct current (DC) power transmission, aided by new developments in power electronics, instead of investing in conventional AC transmission lines [124].

FACTS technologies are based in highly engineered power semiconductor converters and advanced control software. Among other applications, they are used to increase transmission capacity, enhance voltage stability, stabilise voltages at transmission lines, and reduce reactive power consumption, etc. FACTS can take many forms, namely, static var compensators (SVC), thyristor-controlled series capacitors (TCSC), and voltage source converter (VSC)-based systems. VSC systems include static reactive compensators (STATCOMs), static series synchronous compensators (SSSCs), unified power controllers (UPFCs), and back-to-back (BTB) converters. SVCs and STATCOMs are shunt connected devices that provide reactive power compensation for voltage control, power quality improvements and system stability. TCSCs and SSSCs deliver control of real power flows. UPFCs are a combination of SSSC and STATCOM designs that allow for increased active power flow and voltage stability controls from the same device. BTBs interconnect two systems to improve inter-tie reliability and control [122, 123].

HVDC has certain advantages over long distance transmission, as well as submarine cable crossing. The core HVDC technologies are current-sourced converters (CSC) and voltage-sourced converters (VSC). CSC are based on conventional thyristors and require a synchronous voltage source in order to operate. VCSs are based in self-commutated devices and dominated by IGBTs. VSC technology is developing fast and overcoming problems associated with CSCs. CSC-HVDCs have reached distances of 2400 km and transmission capacities of 8000 MW [123, 125].

When compared with conventional solutions in US transmission infrastructure upgrades, FACTS could become 30% less expensive, as estimated in [122]. Also, similar savings can be expected for long distance HVDC lines, where 500 km is a typical “break even” value [125]. Another study found the distance to be over 600 km [126]. It was found in [123] that the “break-even” distance for overhead lines is 500 km, or 40 km for underground cables. These comparisons are indicative guidelines, since each installation would have its own specific requirements.

An SVC advanced model is presented in [127], where the equations to determine the susceptance that maintains the specified voltage level in the N-R iteration process are

purely reactive. The second partial derivative matrix to determine the optimal power flow shows separate active and reactive power derivatives.

There are nine control modes to the STATCOM model presented in [128]. The load flow solution uses an extended Jacobian with two additional rows and columns for each STATCOM. The first additional row corresponds to the active power constraint at the STATCOM bus, and the second one to the variable constraints of each one of the control modes: voltage magnitudes and voltage angles. The derivatives of active and reactive powers are shown separately in the extended Jacobian (eq. 2-24) of [128].

The SSSC is characterised by four control modes in [128]: namely, active and reactive powers' flow through the line (branch) in question, with voltages at either bus, and transmission line impedance. The extended Jacobian has the same structure as the STATCOM: two additional lines and columns for each SSSC line. Likewise, the active and reactive power derivatives are shown separately.

SVC and TCSC are represented by STATCOM and SSSC models respectively in [128].

UPFC can control bus voltage as well as line power flow simultaneously. Direct voltage injection and shifting of phase angle and impedance control are also used in practice. Power flow equations follow similar strategies as STATCOMs and SSSCs. They represent thirteen control modes and two degrees of freedom, involving two variables of the bus under study and two variables of the UPFC controls. Two variables of each of the two interconnected buses are also possible. The Jacobian includes the information regarding variables for each control mode, plus the conventional active and reactive power derivatives [128]. Other UPFC variants follow the same Jacobian arrangement, where active and reactive power derivatives are shown separately.

The load flow in mixed HVAC and HVDC systems is presented in [123]. The power mismatch equations contain the expression of the active and reactive power with the rectifier and inverter components. The resulting Jacobian is expressed as a function of split active and reactive power derivatives.

DFT-Padé forms the power series voltage representation using voltage values obtained from the N-R method. The Jacobian modifications discussed for the different FACTS arrangements and HVDC transmission have shown formats compatible with DFT-Padé

method requirements, therefore it is straightforward to conclude that this method will be able to obtain the voltage values to construct the bus-voltage representations. It is worth mentioning that the software implantation of these Jacobians should follow the formulation presented; that is, the active and reactive powers should be calculated separately. In general, this is true for any voltage regulation strategy and should be considered under those merits to ascertain its D-P compatibility.

FACTS were recommended by Electrical Power Research Institute (EPRI) of U.S in 1998 to maximise power networks functionality when they are placed in suitable locations. Many methods have been devised to find the locations that optimises the network loadability. Modal analysis near the point of collapse, heuristic methods e.g., particle swarm optimization and genetic algorithms, sensitivity-based approaches, and mixed integer dynamic optimization are extensively employed. FACTS can improve existing networks performance by re-dispatching power flows to avoid exceeding thermal limits while satisfying contractual obligations [129, 130].

There has been a surge of interest in HVDC transmission lines since the middle of the last century. Lately, they have gained momentum by the development of voltage converters and the need to connect offshore wind turbines in Europe. The interconnection of HVDC lines with existing AC grids has aroused interest in the research and engineering communities. Some sources argue that HVDC technologies are preferable to the conventional AC power transmission [131].

A tool for optimal placement of multiple FACTS devices that maximises networks loadability using genetic algorithm is presented in [130]. The software that applies the algorithm, termed FACTS Placement Toolbox, requires a grid (network) definition, settings for the genetic algorithm, and the number and type of FACTS to be allocated to the grid. The algorithm then identifies places for the static loadability of the power system will to maximised. It does so by analysing transmission line loading and bus voltage violations in a considerable number of possible network stress levels. It makes use of continuation power flow to solve the optimisation problem and standard power flow to enforce security (power and voltage) constrains. As an application example on the IEEE 57-bus test case, the algorithm allocates one SVC, two TCSC, one UPFC and one thyristor-controlled phase shifting transformer (TCPST) to maintain acceptable voltage

levels when maximum loading factors are applied to the network. When the FACTS were not used, some of the buses had unacceptable low voltages for the same loading conditions.

An analysis of three different FACTS and HVDC when applied to the IEEE 14-bus and IEEE 30-bus system and a comparison of resulting voltage stability boundaries are carried out in [129]. Static var compensator (SVC), static compensator (STATCOM) and thyristor-controlled series capacitor (TCSC) are the three FACTS. The HVDC comprises two voltage source converters (VSC), one acting as rectifier and the other as inverter, and a DC line, with the same resistance as the original line, between the two (VSC). The weakest buses of both networks are the locations for the SVC and STATCOM. They are determined using three different indices: modal analysis, VQ-sensitivity and minimum distance to voltage collapse. Voltage stability boundaries for the three cases: base load, SVC and STATCOM are obtained for each network. The voltage stability boundary improved 18% with the SVC and 20% with the STATCOM, both connected as shunt devices to bus 14 of the IEEE 14-bus system. While for bus 30 of the IEEE 30-bus system, the improvements over the system without FACTS were 51% and 56% respectively.

The locations of the series devices, TCSC and HVDC, were determined using four different indices to find the weakest line connected to the weakest bus for both networks. They were line stability index ($\mathrm{L_{mn}}$), fast voltage stability index ($\mathbf{FSVI}$), line stability factor (LQP), and line collapse proximity index ($\mathbf{LCPI}$). The TCSC and the HVDC improved the voltage stability boundary of the bus 14 by 26% and 79% respectively, while the improvements in the bus 30 voltage stability boundary were 43% and 134% respectively. Noting that TCSC provided 50% of line compensation for both networks. The impact of the HVDC is unrivalled with respect to the FACTS performances.

5.5. Conclusions

The DFT-Padé method workings were shown in detail with the 14-bus system. Two key aspects of the algorithm are the radius of convergence of the power series (or truncated polynomial) and the tolerance with which the bus under study is to be analysed. There is no a priori way to know what those two values are, so the default is to use a unity radius and a rather large tolerance between consecutive series coefficients: 10^{-5}. This will return

the minimum required number of coefficients to characterise the solution branch of the PQ bus. However, if the bus in question is lightly loaded in a context of low system demand, then those minimum requirements may have to be adjusted to produce the correct results, and a fast converging polynomial with few terms will result.

Little difference is found by increasing the radius and decreasing the tolerance to obtain the bus voltage and VSLs in the 2-bus system. However, the number of coefficients is halved when using the default values, which implies a reduction in the N-R solutions by the same amount.

Bus 30 of the 30-bus system shows the signs of a weak bus, characterized by its small radius of convergence, $0.6[pu]$, where the Fourier Series coefficients are convergent, the Taylor coefficients are not, but the PA can characterise the bus-voltage between the stability limits.

D-P method's improvement over conventional N-R is shown in the 7-bus test, where plain N-R fails to converge for values close to the stability limit. In this case, DFT-Padé can still find the solution by working with a smaller generator active power P_6, avoiding N-R non-convergence, and taking advantage of the maximal analytic continuation provided by the Padé approximant, proving the robust nature of the method.

D-P's execution time is shown to be comparable to that of plain N-R when both systems resolve the same quantity of active power loads within the allowable range. This comparison is not so direct with CPF, since it adjusts the number of steps to reach the stability limit. This comparison is a guide to indicate the D-P processing speed for different networks.

PQ buses were classified according to their smallest load range, not the safe load margin to the VSL. Network structural weakness conditions were key considerations for the given loading level. Tests were done at constant power factors. The weakest buses were confirmed using CPF methods for the IEEE 14-bus and IEEE 30 bus test systems.

CPF and HELM comparisons with D-P showed a near exact match for all the networks tested.

Lastly, it was shown through the analysis of FACTS equipment and HVDC links that D-P can resolve any network that can be processed through an N-R based algorithm, as long as the Jacobian active and reactive power derivatives are separate.

It was also shown that the correct location of FACTS equipment and HVDC links is critical to improve the voltage collapse limits of power networks. Some of the location methods were presented.

Chapter 6: Conclusion and future work

This thesis presented an augmentation to the conventional N-R algorithm, based on the superior convergence properties of harmonic interpolations in the complex domain and Robust Padé approximations. As a result, PQ Buses are characterised by their HV values in the whole stable load range. The thesis can be summarised as follows.

The introductory discussion in the first chapter of this thesis aims to frame the current condition of the power grid, and its likelihood to function close to the stability limit is one of its salient aspects. Regulatory policies, together with market conditions, technological disruptions, and investment trends, play in the medium to long term timeframe, and they result in stretching existing infrastructures to their maximum capacity.

The literature review in the second chapter has highlighted the importance of a reliable power-flow methodology that gives planners and operators dependable tools for best performance when applied to demanding processes. For about five decades, innumerable contributions from researchers and practitioners all over the world have resulted in not only framing the problems of conventional power-flow methods, but also giving more accurate responses for improved algorithm performances.

The third chapter exposes a methodology to make Padé approximants more reliable. This fits in the context of non-iterative load flow techniques that represent bus-voltages through Taylor series. They are also an important step in the DFT-Padé method that allow for the easy identification of voltage stability limit approximations.

The fourth chapter explores key mathematical formulations that are the bases of the proposed method: the convergence properties of functions resulting from interpolations around the roots of unity, the benefits of the trapezoidal rule in calculating the integrals, as well as the solid convergence properties of harmonic polynomials. This highlights the numerical applicability and validity of the mathematical instruments used. Finally, the algorithm is discussed and put together.

The fifth chapter shows the workings of the method, step by step, highlighting the salient aspects of its main parameters: Taylor series radius of convergence and coefficients' tolerance. The DFT-Padé approximants need to be calculated at operating points of the power system where the N-R method will converge. It will require as many points of the complex active power to be applied to N-R as coefficients of the Taylor series are needed, and then to compute the Padé approximants. Complex active power is a mathematical artifice, as shown in equations (4.14) and (4.15) and explained in subsection 4.3.1. These rational functions are used to extrapolate the bus voltages at any point within the allowable active power range for the bus under study. The voltage stability limits have been compared with HELM, N-R and Continuation Power Flow. The D-P's accuracy was tested and shown to be a reliable algorithm.

A summary of the load flow methods discussed in previous sections can be summarised in the following way:

- Newton-Raphson or some of its variations are widely used in industry today. It presents many advantages, it converges quickly and accurately in most cases as has been discussed in Chapter II. However, the complexity of interconnected power systems and their operation close to their capacity limit has brought to light inherent problems of N-R. the applicability, namely: initial guess far from the actual operating point, convergence problems close to the stability limit where it may converge to the wrong value, or it may diverge. The number of iterations increases as the systems approaches the stability limit increasing the solution time.
- HELM is a load flow method that has come to public knowledge in 2012. Many research contributions have appeared since then. It is a method based in complex analysis, it arrives at the solution by progressive convolution (recursive calculations) instead of iterations. It is dependent on the embedding method and the solution germ. It overcomes most of the iterative methods shortcomings, it is deterministic. The number of terms required for the power series voltage representation increases as the grid approaches its stability limit. It uses power binary search to determine the stability limit, which is computationally expensive, and it's been reported to lack accuracy in its determination. However, the problem seems to have been overcome in [132]. There is only one report of time comparison [133] known to the authors where it was found to be slower than N-R.

However, the HELM seminal paper states that 3,000 electrical nodes were solved within 10 to 20 milliseconds according to the loading using an Intel Xeon 5500 processor. One important HELM advantage is that it produces a rational function to represent the bus voltage, so each bus behaviour is fully characterised within its voltage stability limits, and the inner singularities of these rational functions are a rather accurate approximation to these stability limits.

- Continuation Power Flow (CPF) is an extension of N-R developed in the early 1990s. The technique used in this approach overcomes N-R problems [134]. It arrives to the voltage stability limit through solving N-R many times, this means that the P-V curve is represented by as many points as the required N-R solutions. The most relevant application of CPF is the contingency analysis [41]. It is commonly used as a benchmark. Possibly the most reliable technique for this purpose. Time comparisons with plain N-R and D-P methods were presented in Tables 5-7 and 5-8.
- DFT-Padé requires as many N-R solutions as terms of the voltage power series which normally varies between 16 and up to 32. Its final product, as in the HELM case, is a rational function of the Padé type that returns the bus voltage value within the allowable load range for the existing power network loading. It is suitable as a planning and simulation tool for PQ buses as it is the case in its present state of development. Its advantage is that it can be applied to N-R with minor software modifications and can deliver similar, if not the same results, as HELM. The stability limits can be obtained by the inner singularities of the rational function, or a more precise one given be the intersections of the HV and LV curves. Detailed comparisons with N-R, HELM and CPF can be seen in subsections 5.2 “Improvements over the plain N-R method and comparison with the continuation power flow approach”, and 5.3 “Comparison with the holomorphic embedding load-flow method (HELM)”.

The main advantage of the D-P method is that it can deliver similar results to a non-iterative method like HELM, that is, it will converge at all points within the load bus stability limits; and only minor additions to existing N-R load flow software will suffice to run D-P.

There is a minor advantage with respect to continuation power flow (CPF) which is the rational function that represents the load bus voltage will extrapolate the bus voltage for

any load within the feasibility range, while the high voltage solution obtained from CPF is a fixed set of P-V points.

It is the author's opinion that HELM is the algorithm of choice when weighing performance advantages, and disadvantages, in terms of accuracy and speed. Its disadvantage, otherwise, is that it is a relatively new development and not a mainstream application. However, in years to come, it may become widely used given its present amount of research interest.

Future work will include escalating the analysis of the whole network instead of just the bus under study, finalising the voltage angle curve for the allowable power range, and ensuring the LV solution branch can be determined in all cases. Also, D-P's possible adaptation for real time applications will be considered, as well as its application for large networks with voltage regulation and HVDC links.

Bibliography

[1] L. Trefethen, *Approximation Theory and Approximation Practice*. SIAM - Society of Industrial and Applied Mathematics, 2013.

[2] P. Kundur *et al.*, "Definition and classification of power system stability.(Author Abstract)," *IEEE Transactions on Power Systems,* vol. 19, no. 3, p. 1387, 2004.

[3] W. Cigré, "Modelling of voltage collapse including dynamic phenomena," p. 159. Accessed on: 2017, April 15Technical brochure. Available: https://e-cigre.org/publication/075-modelling-of-voltage-collapse-including-dynamic-phenomena

[4] W. Cigré, "Protection Against Voltage Collapse," pp. 35, 36. Accessed on: 2016, March 10.Technical brochure. Available: https://e-cigre.org/publication/128-protection-against-voltage-collapse

[5] Aemo. (2018, April 06). *Storms cause electricity supply disruptions across Victoria Energy Live*. Available: http://energylive.aemo.com.au/Latest-News/Storms-Cause-Electricity-Supply-Disruptions-Across-Victoria

[6] Aemo. (2018, April 06). *AEMO observations: operational and market challenges to reliability and security in the NEM – Australian Energy Market Operator*. Available: http://www.aemo.com.au/Media-Centre/AEMO-observations---operational-and-market-challenges

[7] Aemo. (2018, April 06). *Power system operating incident reports – Australian Energy Market Operator*. Available: http://www.aemo.com.au/Electricity/National-Electricity-Market-NEM/Market-notices-and-events/Power-System-Operating-Incident-Reports

[8] D. Jones and M. Hablutzel, "Can hydrogen be used to add stability to the electricity grid?," ed. AEMO Website, 2018.

[9] D. Jones, T. Lim, and A. Dodds, "Video: Tesla has built the world's largest battery in South Australia | Energy Live," D. Jones, Ed., ed. AEMO Website: AEMO, 2018.

[10] T. J. Overbye and J. D. Weber, "Visualizing the electric grid," *IEEE Spectrum,* vol. 38, no. 2, pp. 52-58, 2001.

[11] A. Trias, "The Holomorphic Embedding Load Flow method," in *2012 IEEE Power and Energy Society General Meeting*, 2012.

[12] S. S. Baghsorkhi and S. P. Suetin, "Embedding AC Power Flow with Voltage Control in the Complex Plane : The Case of Analytic Continuation via Pad\'e Approximants," *ArXiv e-prints,* vol. 1504, p. 9, 2015.

[13] S. D. Rao, D. J. Tylavsky, and Y. Feng, "Estimating the saddle-node bifurcation point of static power systems using the holomorphic embedding method," *International Journal of Electrical Power & Energy Systems,* vol. 84, pp. 1-12, 2017.

[14] W. Cigré, "Indices Predicting Voltage Collapse and Dynamic Phenomena," pp. 10, 21, 43, 54, 79-81, 1995, December. Accessed on: 2016, 15 April

[15] D. Vowles, "L1_PowerSystemOverview_Ver01b," in *Power Systems lectures*, T. U. o. Adelaide, Ed., Power System lecture ed. School of Electrical and Electronic Engineering, 2017, pp. 36-41.

[16] C. W. Taylor, *Power system voltage stability*. New York: McGraw-Hill, 1994.

[17] T. van Cutsem and C. Vournas, *Voltage Stability of Electric Power Systems*. Springer US, 2007.

[18] G. Ledwich, "Voltage Stability," in *Collaborative Power Engineering Centres of Excellence* vol. Dynamic Transient Stability, ed. School of Engineering System, QUT2009: Queensland University of Technology, 2009, p. 6.

[19] F. Dong, T. Kostyniak, and B. Lam, "Dealing with power flow solution difficulties," *PTI eNewsletters*, 2012, March. Accessed on: 20 December 2017Available: https://w3.usa.siemens.com/datapool/us/SmartGrid/docs/pti/2012March/PDFs/Dealing_with_power_flow_solution_difficulties.pdf

[20] H. Saadat, *Power System Analysis*. WCB/McGraw-Hill, 1999, p. 695.

[21] J. D. Glover, M. S. Sarma, and T. Overbye, Power System Analysis and Design, 6 ed. 200 First Stamford Place, Suite 400 Stamford, CT 06902 USA: Cengage Learning, 2011. [Online]. Available: https://books.google.com.au/books?id=U77A2C37QesC. Accessed on 2016, March 15.

[22] G. A. Baker, Jr. and P. R. Graves-Morris, G.-C. Rota, Ed. *Pade approximants*, 2nd ed. (Encyclopedia of Mathematics and Its Applications). Cambridge [England] New York: Cambridge University Press, 1996.

[23] P. Gonnet, S. Güttel, and L. Trefethen, "Robust Padé Approximation via SVD," *SIAM Review,* vol. 55, no. 1, pp. 101-117, 2013.

[24] W. Murray, T. T. De Rubira, and A. Wigington, "Improving the robustness of Newton-based power flow methods to cope with poor initial points," presented at the 2013 North American Power Symposium (NAPS) 2013.

[25] Y. Feng, "Solving for the Low-Voltage/Large-Angle Power-Flow Solutions by Using the Holomorphic Embedding Method," D. J.Tylavsky, D. Armbruster, K. Holbert, L. Sankar, J. Undrill, and V. Vittal, Eds., ed: ProQuest Dissertations Publishing, 2015.

[26] S. D. Rao, "Exploration of a Scalable Holomorphic Embedding Method Formulation for Power System Analysis Applications," D. J. Tylavsky, A. Pal, J. Undrill, and V. Vittal, Eds., ed: ProQuest Dissertations Publishing, 2017.

[27] R. Živanovič, "Continuation via quadratic approximation to reconstruct solution branches and locate singularities in the power flow problem," in *2016 24th Mediterranean Conference on Control and Automation (MED)*, 2016, pp. 866-870.

[28] V. A. Venikov, V. A. Stroev, V. I. Idelchick, and V. I. Tarasov, "Estimation of electrical power system steady-state stability in load flow calculations," *IEEE Transactions on Power Apparatus and Systems,* vol. 94, no. 3, pp. 1034-1041, 1975.

[29] K. M. Brown, "A Quadratically Convergent Newton-Like Method Based Upon Gaussian Elimination," *SIAM Journal on Numerical Analysis,* vol. 6, no. 4, pp. 560-569, 1969.

[30] S. C. Tripathy, G. Prasad, O. P. Malik, and G. S. Hope, "Load-Flow Solutions for Ill-Conditioned Power Systems by a Newton-Like Method," *Power Apparatus and Systems, IEEE Transactions on,* vol. PAS-101, no. 10, pp. 3648-3657, 1982.

[31] M. S. Sachdev and T. K. P. Medicherla, "A second order load flow technique," *Power Apparatus and Systems, IEEE Transactions on,* vol. 96, no. 1, pp. 189-197, 1977.

[32] S. Iwamoto and Y. Tamura, "A Load Flow Calculation Method for Ill-Conditioned Power Systems," *Power Apparatus and Systems, IEEE Transactions on,* vol. PAS-100, no. 4, pp. 1736-1743, 1981.

[33] G. Durga Prasad, A. K. Jana, and S. C. Tripathy, "Modifications to Newton-Raphson load flow for ill-conditioned power systems," *International Journal of Electrical Power and Energy Systems,* vol. 12, no. 3, pp. 192-196, 1990.

[34] H. Le Nguyen, "Newton-Raphson method in complex form [power system load flow analysis]," *Power Systems, IEEE Transactions on,* vol. 12, no. 3, pp. 1355-1359, 1997.

[35] V. Ajjarapu, *Computational Techniques for Voltage Stability Assessment and Control* (no. https://link-springer-com.proxy.library.adelaide.edu.au/bookseries/6403). Boston, MA: Springer US, Boston, MA, 2007.

[36] H. D. Chiang, A. J. Flueck, K. S. Shah, and N. Balu, "CPFLOW: a practical tool for tracing power system steady-state stationary behavior due to load and generation variations," *IEEE Transactions on Power Systems,* vol. 10, no. 2, pp. 623-634, 1995.

[37] W. F. Tinney and C. E. Hart, "Power Flow Solution by Newton's Method," *IEEE Transactions on Power Apparatus and Systems,* vol. PAS-86, no. 11, pp. 1449-1460, 1967.

[38] B. Stott, "Review of load-flow calculation methods," *Proceedings of the IEEE,* vol. 62, no. 7, pp. 916-929, 1974.

[39] M. R. G. Al-Shakarchi, "Nodal iterative load flow," M.Sc., Institute of Science and TEchnology University of manchester, 1973.

[40] A. Ralston, *A first course in numerical analysis*, 2d ed. ed. New York: McGraw-Hill, 1978.

[41] F. Milano, *Power System Modelling and Scripting*. Berlin, Heidelberg: Springer Berlin Heidelberg, Berlin, Heidelberg, 2010.

[42] R. Seydel, *From equilibrium to chaos : practical bifurcation and stability analysis*. New York: Elsevier, 1988.

[43] B. Stott, "Effective starting process for Newton-Raphson load flows," *Proceedings of the Institution of Electrical Engineers,* vol. 118, no. 8, pp. 983-987, 1971.

[44] W. Hubbi and A. Refsum, "Starting algorithm and modification for Newton-Raphson load-flow method," *International Journal of Electrical Power and Energy Systems,* vol. 5, no. 3, pp. 166-172, 1983.

[45] G. Leoniopoulos, "Efficient starting point of load-fow equations. ," *International Journal of Electrical Power and Energy Systems,* vol. 16, no. 6, pp. 419 -422, 1994.

[46] S. Cvijic, P. Feldmann, and M. Ilic, "Applications of Homotopy for Solving AC power flow and AC Optimal Power Flow," *Power and Energy Society General Meeting,2012 IEEE,,* pp. 1-8, 2012.

[47] D. C. Lay, *Linear algebra and its applications*, 3rd ed. update. ed. Boston: Pearson/Addison-Wesley, 2006.

[48] F. Milano, "Continuous Newton's Method for Power Flow Analysis," *IEEE Transactions on Power Systems,* vol. 24, no. 1, pp. 50-57, 2009.

[49] M. D. Schaffer and D. J. Tylavsky, "A nondiverging polar-form Newton-based power flow," *Industry Applications, IEEE Transactions on,* vol. 24, no. 5, pp. 870-877, 1988.

[50] S. Iwamoto and Y. Tamura, "A Fast Load Flow Method Retaining Nonlinearity," *IEEE Transactions on Power Apparatus and Systems, Sept/Oct 1978,* vol. PAS-97, no. 5, pp. 1586 - 1599, 1978.

[51] T. Kulworawanichpong, "Simplified Newton–Raphson power-flow solution method," *International Journal of Electrical Power and Energy Systems,* vol. 32, no. 6, pp. 551-558, 2010.

[52] J. E. Tate and T. J. Overbye, "A comparison of the optimal multiplier in polar and rectangular coordinates," *Power Systems, IEEE Transactions on,* vol. 20, no. 4, pp. 1667-1674, 2005.

[53] C. A. Castro and L. M. C. Braz, "A new approach to the polar Newton power flow using step size optimization," in *Proc. 29th North Amer. Power Symp*, WY, 1997: Laramie,.

[54] C. A. Castro, L. M. C. Braz, and C. A. F. Murari, "A critical evaluation of step size optimization based load flow methods," *IEEE Transaction on Power Systems,* Journal vol. 15, no. 1, pp. pp. 202–207,2000.

[55] V. H. Quintana and N. Muller, "Studies of Load Flow Methods in Polar and Rectangular Coordinates," *Electric Power Systems Research,,* Journal no. 20, pp. 225 - 235, 1991.

[56] A. Klos and A. Kerner, "The non-uniqueness of the load-flow solution," in *Power System Computation Conference*, Cambridge, 1975, vol. 1, pp. 3.1-8, Queen Mary College, University of London.

[57] T. Park and Y. Sekine, "A Method for Analyzing Multisolution in Power Flow Analysis," *Electrical Engineering in Japan, Translated from Denki Gakkai Ronbunshi,* vol. 99, no. 2, pp. 245-252, 1979.

[58] K. Iba and H. Suzuki, "A method for finding a pair of multiple load flow solutions in bulk power systems," *IEEE Transactions on Power Systems,* vol. 5, no. 2, pp. 582 - 591, 1990.

[59] T. J. Overbye and C. L. DeMarco, "Improved Techniques for Power System Voltage Satbility Assessment Using Energy Methods," *Transactions on Power Systems,* Journal vol. 6, no. 4, 1991.

[60] N. Yorino , S. Harada, and H. Cheng, "A method to approximate a closest loadability limit using multiple load flow solutions," *IEEE Transactions on Power Systems,* Journal vol. 12, no. 1, 1997.

[61] N. Yonno, S. Harada, and H. Sasaki, "Use of multiple load flow solutions to approximate a closest loadability limit," in *Voltage Stability, Securify and Control* Davos, Switzerfand, 1994.

[62] I. Dobson and L. Lu, "New methods for computing a closest saddle node bifurcation and worst case load power margin for voltage collapse," *IEEE Transactions on Power Systems,* vol. 8, no. 3, pp. 905-913, 1993.

[63] F. Alvarado, I. Dobson, and Y. Hu, "Computation of closest bifurcations in power systems," *IEEE Transactions on Power Systems,* vol. 9, no. 2, pp. 918 - 928, 1994.

[64] C. A. Castro, "Improved method for the calculation of power systems low voltage solutions," *International Journal of Electrical Power and Energy Systems,* vol. 24, no. 6, pp. 503-513, 2002.

[65] R. B. L. Guedes, L. F. C. Alberto, and N. G. Bretas, "Power System Low-Voltage Solutions Using an Auxiliary Gradient System for Voltage Collapse Purposes," *IEEE Transactions on Power Systems,* vol. 20, no. 3, p. 10, 2005, Art. no. TPWRS-00662-2003.

[66] H. Mokhlis, A. Shahriari, A. H. A. Bakar, H. A. Illias, and M. Karimi, "Improved Step Size Newton Raphson Method using quadratic equations properties in ill-conditioned power system," *International Transactions on Electrical Energy Systems,* vol. 24, no. 9, pp. 1323-1342, 2014.

[67] Y. Tamura, K. Sakamoto, and Y. Tayama, "Voltage instability proximity index (VIPI) based on multiple load flow solutions in ill-conditioned power systems," ed, pp. 2114-2119, 1988.

[68] J. Hashimoto, N. Yorino, and Y. Tamura, "On the Continuous Monitoring of Voltage Stability Margin in Electric Power Systems'," (in Japanese), *JIEE Transactions,* vol. 108, no. 2, pp. 65-72, 1988.

[69] I. Dobson and H.-D. Chiang, "Towards a theory of voltage collapse in electric power systems," *Systems & Control Letters,* vol. 13, no. 3, pp. 253-262, 1989.

[70] P. W. Sauer and M. A. Pai, "Power system steady-state stability and the load-flow Jacobian," *IEEE Transactions on Power Systems,* vol. 5, no. 4, 1990.

[71] C. L. DeMarco and T. J. Overbye, "An energy based security measure for assessing vulnerability to voltage collapse," *IEEE Transactions on Power Systems,* vol. 5, no. 2, 1990.

[72] Y. Sekine, "Cascaded voltage collapse," *IEEE Transactions on Power Systems,* vol. 5, no. 1, 1990.

[73] C. A. Canizares, F. L. Alvarado, C. L. DeMarco, I. Dobson, and W. F. Long, "Point of collapse methods applied to ac/dc power systems," *IEEE Transactions on Power Systems,* vol. 7, no. 2, 1992.

[74] C. Gómez-Quiles, A. Gómez-Expósito, and W. Vargas, "Computation of Maximum Loading Points via the Factored Load Flow," *IEEE Transactions on Power Systems,* vol. 31, no. 5, pp. 4128-4134, 2016.

[75] K. Iba, H. Suzuki, M. Egawa, and T. Watanabe, "Calculation of critical loading condition with nose curve using homotopy continuation method," *Power Systems, IEEE Transactions on,* vol. 6, no. 2, pp. 584-593, 1991.

[76] D. Mehta, H. Nguyen, and K. Turitsyn, "Numerical Polynomial Homotopy Continuation Method to Locate All The Power Flow Solutions," 2014.

[77] P. Kundur, *Power system stability and control*. New York: New York : McGraw-Hill, 1994.

[78] C. D. Christy, "Analysis of steady state voltage stability in large scale power systems," Master of Science, Electrical Engineering and Computer Engineering, Iowa State University, Ames, Iowa, 16819, 1990.

[79] V. Ajjarapu and C. D. Christy, "The continuation power flow: a tool for steady state voltage stability analysis," *IEEE Transactions on Power Systems,* vol. 7, no. 1, pp. 416-423, 1992.

[80] Siemens. (2018, 2016, June 10). *PSS®E – high-performance transmission planning and analysis software - PSS® power system simulation and modeling software - Siemens Global Website (34.02 ed.)* [newton_ps-detail]. Available: https://www.siemens.com/global/en/home/products/energy/services/transmission-distribution-smart-grid/consulting-and-planning/pss-software/pss-e.html

[81] P. Corporation. (2018, 2017, September 3). *PowerWorld v20 Released Â» PowerWorld (20 ed.)*. Available: https://www.powerworld.com/powerworld-v20-released

[82] F. Milano. (2017, 2017, October 7). *Power System Analysis Toolbox (PSAT) (2.1.10 ed.)*. Available: http://faraday1.ucd.ie/psat.html

[83] G. Rogers, J. H. Chow, and L. Vanfretti. (2018, 2017, November 8). *Power System Toolbox Webpage (3 ed.)*. Available: http://www.eps.ee.kth.se/personal/vanfretti/pst/Power_System_Toolbox_Webpage/PST.html

[84] R. D. Zimmerman, C. E. Murillo-Sanchez, and R. J. Thomas, "MATPOWER: Steady-State Operations, Planning, and Analysis Tools for Power Systems Research and Education," *IEEE Transactions on Power Systems,* vol. 26, no. 1, pp. 12-19, 2011.

[85] B. Wang, C. Liu, and K. Sun, "Multi-Stage Holomorphic Embedding Method for Calculating the Power-Voltage Curve," *Power Systems, IEEE Transactions on,* vol. 33, no. 1, pp. 1127-1129, 2018.

[86] M. K. Subramanian, "Application of Holomorphic Embedding to the Power Flow Problem," Master of Science, School of Electrical, Computer and Energy Engineering, Arizona State University, 2014

[87] A. Trias, "Fundamentals of the Holomorphic Embedding Load-Flow Method," *ArXiv e-prints*, vol. 1509*,* p. 17, 2015, September 8. Accessed on: 2016, February 17Available: http://adsabs.harvard.edu/abs/2015arXiv150902421T

[88] S. S. Baghsorkhi and S. P. Suetin, "Embedding AC Power Flow in the Complex Plane Part I: Modelling and Mathematical Foundation," *ArXiv e-prints*, vol. 1604*,* p. 13. Accessed on: March 1, 2016Available: http://adsabs.harvard.edu/abs/2016arXiv160403425S

[89] P. Gonnet, R. Pachón, and L. Trefethen, "Robust rational interpolation and least-squares," *Electronic Transactions on Numerical Analysis,* vol. 38, pp. 146-167, 2011.

[90] L. N. Trefethen, "Square blocks and equioscillation in the Padé, Walsh, and CF tables," in *Rational approximation and interpolation*: Springer, pp. 170-181, 1984.

[91] L. N. Trefethen and M. H. Gutknecht, "On convergence and degeneracy in rational Padé and Chebyshev approximation," *SIAM Journal on Mathematical Analysis,* vol. 16, no. 1, pp. 198-210, 1985.

[92] H. Stahl, "Spurious poles in Padé approximation," *Journal of Computational and Applied Mathematics,* vol. 99, pp. 511-527, 1998.

[93] J. Gilewicz and M. Pindor, "Padé approximants and noise: rational functions," *Journal of Computational and Applied Mathematics,* p. 285-297, 1999.

[94] I. Dobson and L. Lu, "Voltage collapse precipitated by the immediate change in stability when generator reactive power limits are encountered," *IEEE Transactions on Circuits and Systems I: Fundamental Theory and Applications,* vol. 39, no. 9, pp. 762-766, 1992.

[95] S. S. Baghsorkhi and S. P. Suetin, "Embedding AC Power Flow in the Complex Plane Part II: A Reliable Framework for Voltage Collapse Analysis," 2016.

[96] A. J. Sarnari and R. Živanović, "Robust Pade approximation for the holomorphic embedding load flow," in *Australasian Universities Power Engineering Conference (AUPEC)*, 2016.

[97] A. P. Austin, P. Kravanja, and L. N. Treffethen, "Numerical Algorithms Based on Analytic Function Values at Roots of Unity," p. 27, 2013.

[98] L. N. Trefethen and J. A. C. Weideman, "The Exponentially Convergent Trapezoidal Rule," *Society for Industrial and Applied Mathematics,* vol. 6, no. 3, pp. 385–458, 2014.

[99] J. H. Curtiss, "Interpolation by harmonic polynomials," Air Force Office of Scientific Research - Mathematical Science Directorate, ASTIA Document Service CenterDecember 1st, 1961.

[100] B. Osgood, The Fourier Transform and its Applications: Stanford University, Stanford, California 94305, 2007, p. 428. [Online]. Available: https://see.stanford.edu/materials/lsoftaee261/book-fall-07.pdf. Accessed on 2016, October 17.

[101] W. L. Briggs, *The DFT : an owner's manual for the discrete Fourier transform*. Philadelphia: Society for Industrial and Applied Mathematics, 1995.

[102] E. M. Stein and R. Shakarchi, *Complex Analysis*. 41 William Street, Princeton, New Jersey 08540: Princeton University Press, 2010.

[103] University of Washington. (2018, 2015, March 20). *Power systems test Case archive - UWEE*. Available: https://www2.ee.washington.edu/research/pstca/

[104] Q. Li, "Holomorphic Embedding Load Flow solutions for buses 14, 30 and 118 of IEEE test cases.," Q. Li, Ed., ed. Arizona State University, 2018.

[105] M. J. Ablowitz, *Complex variables : introduction and applications*, 2nd ed. ed. Cambridge, UK New York: Cambridge University Press, 2003.

[106] J. Machowski, J. W. Bialek, and J. R. Bumby, *Power system dynamics stability and control*, 2nd ed. ed. Chichester, U.K.: Wiley, 2008.

[107] A. M. Abed *et al.*, "WECC Voltage Stability Criteria, Undervoltage Load Shedding Strategy, and Reactive Power Reserve Monitoring Methodology," in "Final Report – May 1998," Western Electricity Coordinating CouncilMay1998.

[108] R. Kanimozhi and K. Selvi, "A Novel Line Stability Index for Voltage Stability Analysis and Contingency Ranking in Power System Using Fuzzy Based Load Flow," *Journl of Electrical Engineering and Technology,* vol. 8, no. 4, pp. 694-703, 2013.

[109] I. Musirin and T. K. Abdul Rahman, "Novel fast voltage stability index (FVSI) for voltage stability analysis in power transmission system," ed. USA, pp. 265-268, 2002.

[110] F. L. Alvarado, "Solving power flow problems with a Matlab implementation of the power system applications data dictionary," vol. Track3, ed, 1999.

[111] T. W. Gamelin, *Complex analysis*. New York: Springer, 2001.

[112] I. Dobson, "Observations on the geometry of saddle node bifurcation and voltage collapse in electrical power systems," *Circuits and Systems I: Fundamental Theory and Applications, IEEE Transactions on,* vol. 39, no. 3, pp. 240-243, 1992.

[113] Z. Feng and W. Xu, "Fast computation of post-contingency system margins for voltage stability assessments of large-scale power systems," *IEE Proceedings - Generation, Transmission and Distribution,* vol. 147, no. 2, pp. 76-80, 2000.

[114] S. Greene, I. Dobson, and F. L. Alvarado, "Contingency ranking for voltage collapse via sensitivities from a single nose curve," *IEEE Transactions on Power Systems,* vol. 14, no. 1, pp. 232-240, 1999.

[115] Z. Q. Wu, Z. Hao, and D. Yang, "A new MVA sensitivity method for fast accurate contingency evaluation," *International Journal of Electrical Power and Energy Systems,* vol. 38, no. 1, pp. 1-8, 2012.

[116] Y. C. Chen, A. D. Dominguez-Garcia, and P. W. Sauer, "Measurement-Based Estimation of Linear Sensitivity Distribution Factors and Applications," *IEEE Transactions on Power Systems,* vol. 29, no. 3, pp. 1372-1382, 2014.

[117] R. B. Prada, E. G. C. Palomino, L. A. S. Pilotto, and A. Bianco, "Weakest bus, most loaded transmission path and critical branch identification for voltage security reinforcement," *Electric Power Systems Research,* vol. 73, no. 2, pp. 217-226, 2005.

[118] K. Ramar and M. S. Raviprakasha, "Determination of weak bus ordering vector in multimachine power systems from voltage stability viewpoint.," *Electric Machines & Power Systems,* vol. 23, no. 5, pp. 597-609, 1995.

[119] B. Gao, G. K. Morison, and P. Kundur, "Voltage stability evaluation using modal analysis," *IEEE Transactions on Power Systems,* vol. 7, no. 4, 1992.

[120] CIGRE, "Planning Against Voltage Collapse," TF 38-01-03, 1986.

[121] C. D. Christy, "Analysis of steady state voltage stability in large scale power systems," Master of Science, Electrical Engineering and Computer Engineering, Iowa State University, 1990.

[122] G. Reed, J. Paserba, and P. Salavantis, "The FACTS on resolving transmission gridlock," *Power and Energy Magazine, IEEE,* vol. 99, no. 5, pp. 41-46, 2003.

[123] M. Eremia, C.-C. Liu, and A. Edris, *Advanced Solutions in Power Systems : HVDC, FACTS, and AI Techniques*. Somerset: Somerset: John Wiley & Sons, Incorporated, 2016.

[124] A. Pizano-Martinez, C. R. Fuerte-Esquivel, H. Ambriz-Perez, and E. Acha, "Modeling of VSC-Based HVDC Systems for a Newton-Raphson OPF Algorithm," *Power Systems, IEEE Transactions on,* vol. 22, no. 4, pp. 1794-1803, 2007.

[125] M. P. Bahrman and B. K. Johnson, "The ABCs of HVDC transmission technologies," *Power and Energy Magazine, IEEE,* vol. 5, no. 2, pp. 32-44, 2007.

[126] K. Meah and S. Ula, "Comparative Evaluation of HVDC and HVAC Transmission Systems," in *2007 IEEE Power Engineering Society General Meeting*, 2007.

[127] H. Ambriz-Pérez, E. Acha, and C. R. Fuerte-Esquivel, "Advanced SVC Models for Newton-Raphson Load Flow and Newton Optimal Power Flow Studies," *IEEE TRANSACTIONS ON POWER SYSTEMS.,* vol. 15., no. 1, pp. 129 - 136, 2000.

[128] X. Zhang, C. Rehtanz, and B. Pal, *Flexible AC Transmission Systems: Modelling and Control*. Berlin: Berlin, Heidelberg: Springer, 2012.

[129] P. Prabhakar and A. Kumar, "Voltage stability boundary and margin enhancement with FACTS and HVDC," *International Journal of Electrical Power & Energy Systems,* vol. 82, pp. 429-438, 2016.

[130] E. Ghahremani and I. Kamwa, "Optimal placement of multiple-type FACTS devices to maximize power system loadability using a generic graphical user interface," *IEEE Transactions on Power Systems,* vol. 28, no. 2, pp. 764-778, 2013.

[131] D. Van Hertem, O. Gomis-Bellmunt, and J. Liang, HVDC GRIDS. For Offshore and Supergrid of the Future., I. Press, ed., Hoboken, New Jersey.: John Wiley & Sons, Inc., 2016, p. 513. [Online]. Available. Accessed on April 2019.

[132] A. Trias and J. L. Marín, "A Padé-Weierstrass technique for the rigorous enforcement of control limits in power flow studies," *International Journal of Electrical Power and Energy Systems,* vol. 99, pp. 404-418, 2018.

[133] P. S. Sauter, C. A. Braun, M. Kluwe, and S. Hohmann, "Comparison of the Holomorphic Embedding Load Flow Method with Established Power Flow Algorithms and a New Hybrid Approach," ed, pp. 203-210, 2017.

[134] Z. Jinquan and Z. Boming, "Reasons and countermeasures for computation failures of continuation power flow," ed, 2006.